TIMING SYNCHRONIZATION AND ICI MITIGATION FOR PILOT-AIDED OFDM MOBILE SYSTEMS

A DISSERTATION
SUBMITTED TO THE DEPARTMENT OF ELECTRICAL ENGINEERING
AND THE COMMITTEE ON GRADUATE STUDIES
OF STANFORD UNIVERSITY
IN PARTIAL FULFILLMENT OF THE REQUIREMENTS
FOR THE DEGREE OF
DOCTOR OF PHILOSOPHY

Yasamin Mostofi

November 2003

I certify that I have read this dissertation and that, in my opinion, it is fully adequate in scope and quality as a dissertation for the degree of Doctor of Philosophy.

Donald C. Cox
(Principal Adviser)

I certify that I have read this dissertation and that, in my opinion, it is fully adequate in scope and quality as a dissertation for the degree of Doctor of Philosophy.

Ahmad Bahai

I certify that I have read this dissertation and that, in my opinion, it is fully adequate in scope and quality as a dissertation for the degree of Doctor of Philosophy.

John C. Cioffi

Approved for the University Committee on Graduate Studies:

Abstract

Robust high date rate mobile communications have several challenges. Transmission of high rate information typically experiences higher delay spread in mobile environments. Furthermore, high mobility introduces time-variations which can make the link less reliable.

Orthogonal Frequency Division Multiplexing (OFDM) is suitable for high delay spread applications. However, performance of OFDM systems, is affected by channel estimation, timing synchronization and mobility. Timing synchronization becomes challenging in high mobility applications as power delay profile of the channel can change rapidly due to the sporadic birth and death of the paths. Furthermore, timing synchronization errors introduce Inter-Carrier-Interference (ICI) in OFDM systems. Due to the expansion of symbol length, OFDM systems are very sensitive to ICI. Furthermore, for mobile applications time-variations in one OFDM symbol introduce ICI as well which further degrades the performance. This becomes more severe as mobile speed, carrier frequency or OFDM symbol duration increases. Therefore to have an acceptable reception quality for the applications that experience high delay and Doppler spread, design of robust timing synchronizer, channel estimator and ICI mitigator is essential. This thesis takes an overall look at these issues. While each of them has been looked at separately by other researchers, an overall look allows for better understanding and design of more robust algorithms. Based on mathematical analysis of the overall performance, a new cross-block design is proposed and implemented that uses channel estimation information to improve timing synchronization. After robust timing synchronization is achieved, two mitigation methods are proposed and analyzed to remove the effect of ICI introduced by high mobility. All the algorithms are tested against high delay and Doppler spread channels.

Results of simulation and analysis show considerable performance improvement without a need to increase the training overhead.

Acknowledgments

First of all, I would like to thank my advisor, Professor Cox. It has been a privilege working with him at Stanford. He has been a great mentor and friend to me and I learned a lot from our technical discussions. Moreover, he always gave me fatherly support, especially during my first year at Stanford when he did his best to make me feel at home.

I thank Dr. Bahai and Dr. Cioffi for accepting to be in my defense and reading committee and for providing helpful suggestions. I would also like to thank Dr. Hashemi, my professor at Sharif University of Technology who introduced me to the area of communications. His deep academic grasp and noble manner have always been a great inspiration to me. I would like to thank Dr. Anthony Fraser-smith for being such a great friend and a source of positive energy in the third floor of Packard. I enjoyed having my first Thanksgiving turkey with his family. Also, I would like to thank Dr. Thomas Lee for giving me a teaching assistantship the second quarter that I was at Stanford. This gave me the freedom to explore research opportunities early on.

I thank the members of my wireless communications research group for all the helpful discussions, friendships and the yummy food they brought to the group meetings. Also, I thank the administrative assistant of our group, Jenny Xu, and the assistants of Dr. Cioffi's group, Joice Debolt and Pat Oshiro, for all their help and support.

I would like to thank all my friends. Stanford gave me the opportunity of meeting some wonderful people both in Iranian community (PSA) and outside of it. Their support has made the difficult times easier to deal with and made the past few years much more memorable.

I owe a lot to Pradeep Sen, my fiance, who always sees the best in me. He has been a great source of encouragement, support and joy and made the journey of the past few

years much more fun. I would also like to thank his family for all their kindness and support.

It is impossible to put in words how much I owe to my parents. I am so grateful for all that they did for me and I thank them in every possible way. Their kindness, love and selflessness have always nurtured me throughout my life. Also, I would like to thank my brother, Shahram, my sister, Nazanin, all my family and friends back home, especially my cousins. Although far away, they have always been close to my heart.

Contents

Abstract **iv**

Acknowledgments **vi**

1 Introduction **1**

1.1 Dissertation Outline 3

1.2 Contributions 4

2 Mobile Communications **5**

2.1 Free-Space Propagation 5

2.2 Spatial Variations and Doppler Effect 6

2.3 Narrowband multipath propagation: small scale fading 7

2.4 Large-scale fading 9

2.5 Wideband Channels 10

2.6 Summary 11

3 OFDM Systems **12**

3.1 History 12

3.2 System Model 13

3.3 Number of subcarriers 15

3.4 Length of the guard interval 15

4 Pilot-aided Channel Estimation **16**

4.1 Introduction 16

4.2 Average error rate analysis 17
4.3 Pilot-aided channel estimation 19
4.4 A Trigonometric Interpolator 20
4.5 A Linear Interpolator 22
4.6 Analysis and Simulation Results 25
4.7 Summary 26

5 Timing Synchronization for Low-Mobility Cases 29

5.1 Introduction 30
5.2 Effect of Timing Synchronization Errors 31
5.2.1 Case of timing errors to the right ($m > 0$) 31
5.2.2 Case of timing errors to the left ($m < 0$) 34
5.2.3 Simulation Results 35
5.2.4 Effect of timing errors on the trigonometric interpolator, case of $m > 0$ 37
5.2.5 Effect of timing errors on the trigonometric interpolator, case of $m < 0$ 44
5.2.6 Analytical and Simulation Results of the effect of timing errors on channel estimation 45
5.3 Timing Synchronization Error Correction 46
5.4 Simulation Results 47
5.5 Summary 49

6 Timing Synchronization for High-Mobility Cases 56

6.1 Introduction 57
6.2 Effect of timing Synchronization Errors in a high-mobility environment . 58
6.3 Effect of timing errors on the triogonometric interpolator in the presence of high mobility, case of $m > 0$ 66
6.4 Effect of timing errors on the triogonometric interpolator in the presence of high mobility, case of $m < 0$ 70
6.5 Timing synchronization error correction 71

6.6 Simulation Results 72
6.7 Summary 73

7 Mobility Mitigation **76**
7.1 Introduction 76
7.2 System Model in a mobile environment 78
7.3 Pilot Extraction 79
7.4 Piece-wise Linear Approximation 80
7.4.1 Method I: ICI mitigation using cyclic prefix 83
7.4.2 Method II: ICI mitigation utilizing adjacent symbols 84
7.4.3 Complexity Analysis 86
7.5 Mathematical Analysis of the effect of linearization 87
7.6 Noise/Interference Reduction 90
7.7 Simulation Results 91
7.8 Conclusion 92

8 Conclusions **98**
8.1 Thesis Summary 98
8.2 Future Work 100

A Piecewise Linearization's Impact on Correlation **102**

B Finding $\sigma^2_{e_i}$,$\sigma^2_{\hat{h}^{(i)}} and \rho_{e_i,\hat{h}^{(i)}}$ **106**
B.0.1 The Case of ICI Mitigation 106
B.0.2 The Case of No Mitigation 107

Bibliography **108**

List of Tables

7.1 Procedure for Method I 84

List of Figures

2.1 Two-ray model 6

2.2 One path arriving at angle Θ with respect to the motion of the receiver . 7

3.1 Discrete baseband equivalent system model 14

4.1 $\overline{P_e}$ vs. SNR_{ave} for channel c4.1 27

4.2 $\overline{P_e}$ vs. SNR_{ave} for channel c4.2 28

5.1 Errors of m sampling periods to the right side (top figure) and left side (bottom figure) 32

5.2 Average SIR vs. m (analysis and simulation) for channel c5.1 36

5.3 Average SIR vs. m (analysis and simulation) for channel c5.2 37

5.4 Effect of rotation 50

5.5 Normalized channel estimation error vs. sub-carrier for channel c5.3 . . . 51

5.6 Power-Delay profile of channel c5.4 52

5.7 Performance for channel c5.4 in the absence of noise 53

5.8 Performance for channel c5.5 in the absence of noise 54

5.9 Average P_b for channel c5.4 in the presence of noise 55

6.1 Normalized channel estimation error vs. normalized m for channel c5.3 (G is as defined in Section 3.2) 74

6.2 Performance in the presence of mobility for channel c5.4 at $\frac{\sigma_X^2 \sigma_H^2}{\sigma_W^2} = 20dB$ 75

7.1 Piece-wise linear model in one received OFDM symbol 80

7.2 Piece-wise linear model for method II 80

7.3 Average SIR vs. % of $f_{d,norm}$ for a narrowband channel 93
7.4 Power-Delay profile of channel c7.2 (same as channel c5.4 of Fig. 5.6) . . 94
7.5 Error floor vs. maximum normalized Doppler 95
7.6 Average bit error rate vs. average received SNR for $f_{d,norm} = 6.5\%$ 96
7.7 Required average received SNR to achieve average $P_b = .02$ 97

A.1 Piece-wise linear approximation of a random process h 104
A.2 $\Delta PW_{normalized}$ vs. % of $f_d \times T$ 105

Chapter 1

Introduction

There has been an increasing demand for high date rate wireless applications in recent years. Digital Audio Broadcasting (DAB) [8], Digital Video Broadcasting (DVB) [23] and Wireless Local Area Networks (WLAN) [16] are a few examples of such applications. The first two applications, while sharing challenges of high speed communications, also require transmission over high mobility links.

Robust high date rate mobile communications have several challenges. Transmission of high rate information typically experiences higher delay spread in mobile environments. Furthermore, high mobility introduces time-variations which can make the link less reliable.

While current wireless data applications like 802.11a and b are used with limited mobility, ongoing research is working towards making the vision of multimedia high mobility communications a reality. Therefore, a robust design is required to ensure reliable communication in high mobility high delay spread environments as channel estimation, synchronization and data recovery become more challenging.

Orthogonal Frequency Division Multiplexing (OFDM) is robust in high delay spread environments and eliminates the need to equalize the effect of delay spread. This feature allows for higher data rates and has resulted in the selection of OFDM as a standard for DAB, DVB and some Wireless Local Area Networks (802.11a). Also, it is being considered as a potential technology for 4th generation mobile communications.

Performance of OFDM systems, however, is affected by channel estimation, timing synchronization and mobility. Timing synchronization errors introduce Inter-Carrier-Interference (ICI). Due to the expansion of symbol length, OFDM systems are very sensitive to ICI. Depending on the choice of the channel estimator, OFDM systems can become even more sensitive to timing synchronization errors, as this thesis shows. Furthermore, for mobile applications time-variations in one OFDM symbol introduce ICI as well which further degrades the performance. This becomes more severe as mobile speed, carrier frequency or OFDM symbol duration increases. Therefore to have an acceptable reception quality for the applications that experience high delay and Doppler spread, design of a robust timing synchronizer, channel estimator and ICI mitigator is essential.

This thesis takes an overall look at issues of channel estimation, timing synchronization and ICI mitigation. Timing synchronization in this thesis refers to the detection of the start of an OFDM symbol. It becomes of great importance and challenge in high mobility applications as the power delay profile of the channel can change rapidly due to the sporadic birth and death of the paths[1]. While each of the three aforementioned issues has been looked at separately by other researchers, an overall look allows for better understanding and design of more robust algorithms. Based on mathematical analysis of the overall performance, a new cross-block design is proposed and implemented that uses channel estimation information to improve timing synchronization. After robust timing synchronization is achieved, two mitigation methods are proposed and analyzed to remove the effect of ICI introduced by high mobility. All the algorithms are tested against high delay and Doppler spread channels. Results of simulation and analysis show considerable performance improvement without a need to increase the training overhead.

[1]In wireline applications, OFDM symbol alignment is not as challenging and does not need to be done as often. Therefore, training information can be used. For high mobility applications, however, due to the sporadic and frequent nature of birth and death of the paths, applying wireline timing synchronization methods can increase the overhead considerably.

1.1 Dissertation Outline

Chapter 2 discusses some of the key issues of mobile communications. It includes channel modeling and describes some of the characteristics of the received signal, which will be used in the remainder of the thesis.

Chapter 3 gives a brief overview of communications using OFDM technology. It shows how OFDM systems can handle delay spread without a need for equalization. The choice of the length of the guard interval and number of sub-carriers is also discussed.

Chapter 4 discusses pilot-aided channel estimation in OFDM systems. It explains the choice of number of frequency-domain pilot tones. Then it looks at different possible frequency-domain interpolators to estimate the channel at all the sub-carriers. It derives probability of error formulas for pilot-aided OFDM systems. Then it compares the performance of two specific interpolators: a linear interpolator and a trigonometric one. The trigonometric interpolator will be used for channel estimation in the subsequent chapters.

Chapter 5 first explores the effect of timing synchronization errors on the performance of pilot-aided OFDM systems in the absence of mobility (mobility is added in Chapter 6). It includes extensive mathematical analysis and derivations, which are used to design robust algorithms. After showing that a pilot-aided channel estimator is supersensitive to timing synchronization errors, a robust timing synchronizer is proposed. This synchronizer is a cross-block design and uses channel estimation information to improve timing synchronization with no additional training overhead. Finally, this chapter shows the performance of the proposed algorithm in high delay spread environments.

Chapter 6 extends the analysis of Chapter 5 to mobile applications. The whole analysis is done in the presence of mobility. The proposed algorithm is shown to work robustly in high mobility high delay spread environments.

Once timing synchronization is achieved, the effect of mobility still degrades the performance of OFDM systems. Chapter 7 then explores the effect of mobility on OFDM

systems that already achieved accurate timing synchronization. Two methods to mitigate the resulting ICI are proposed. To evaluate performance improvement after applying these methods, Signal to Interference Ratio, SIR, formulas are derived analytically. Simulation results also show the performance improvement in high delay spread and Doppler spread environments.

Finally, Chapter 8 contains a summary of the thesis and suggestions for potential future work.

1.2 Contributions

In Chapter 4, formulas for probability of error for pilot-aided OFDM systems have been derived. Also, a comparison of linear and trigonometric interpolators, using analysis and simulation results, is presented. Chapter 5 derives channel estimation error formulas in the presence of timing synchronization errors. Based on this analysis, a new algorithm is proposed for fine timing synchronization, which requires no additional training overhead. The algorithm works robustly in high delay spread environments. It can reduce the error profile to a level very close to that of no synchronization error. Chapter 6 extends the whole analysis to mobile environments. The proposed algorithm is shown to work robustly in high mobility environments as well and is hence suitable for high delay and Doppler spread applications. Finally Chapter 7 proposes two new mobility mitigation methods for pilot-aided OFDM systems. Performance improvement is first shown analytically by deriving SIR_{ave} formulas in a narrowband mobile environment. Then, for high delay and Doppler spread applications, simulation results show considerable performance improvement. They illustrate that applying these methods reduces average bit error rate, P_b, or the required received SNR to values close to those for no Doppler. The power savings become considerable as mobility increases.

Chapter 2

Mobile Communications

Communication in a mobile environment poses several challenges. To increase the probability of a reliable transmission, an understanding of this environment and appropriate modeling are essential. In general, different models should be used to describe transmission in different environments and a single model can not be applied everywhere. For instance, transmission characteristics in a city like Manhattan, with tall buildings, can be very different from those in a rural area. Furthermore, such characteristics depend on the system parameters like carrier frequency, mobile speed, base station location and data rate. This chapter provides a brief overview of key characteristics of a mobile environment. For a more detailed discussion, refer to [7], [10] and [20].

2.1 Free-Space Propagation

Consider a transmitter and a receiver that are separated by a distance D. In case of a Line of Sight (LOS) free space transmission, the received signal power, Π_r, is related to the transmitted power, Π_t, as follows:

$$\frac{\Pi_r}{\Pi_t} = g_t g_r \frac{\lambda^2}{(4\pi D)^2} \tag{2.1}$$

where g_t and g_r refer to the gain of the the transmitter and receiver antennas respectively. λ is the wavelength of the transmitted signal. The simple relationship of Eq. 2.1 will not

hold in case of arrival of more than one path, with different angles of arrivals, at the receiver. For instance, consider the case of reflection from earth, as is shown in Fig. 2.1. Then for a large enough D, we will have the following approximate relationship:

$$\frac{\Pi_r}{\Pi_t} \approx \frac{g_t g_r h_r^2 h_t^2}{D^4} \tag{2.2}$$

where h_t and h_r refer to the heights of the transmitter and receiver. As can be seen from Eq. 2.2, received power drops faster as the distance increases in this case.

In general, power falls off in a general form of D^{-n}, where n depends on the number of

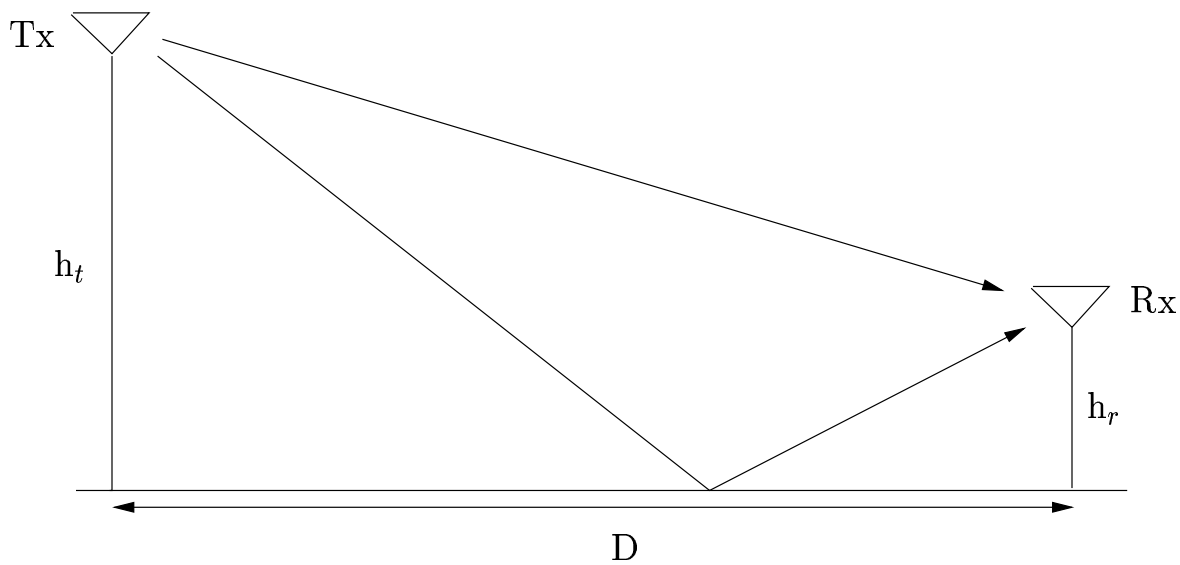

Figure 2.1: Two-ray model

received paths, their angles of arrivals and properties and locations of the reflectors and shadowing objects.

2.2 Spatial Variations and Doppler Effect

For a mobile receiver, the frequency of the received signal is different from that of the transmitted signal due to the Doppler effect. Consider an incoming wave that makes an angle of Θ with the direction of the mobile, as shown in Fig. 2.2. Then for a mobile speed of vel_m and transmitted signal (unmodulated) of $s(t) = cos(2\pi f_c t)$, the received signal,

$y(t)$, will be as follows:

$$y(t) = cos(2\pi f_c(1 + \frac{vel_m}{c} cos\Theta)t - \Phi_0) \tag{2.3}$$

where Φ_0 is a phase shift introduced due to the distance between the transmitter and receiver, c is the speed of light and f_c is the carrier frequency.

2.3 Narrowband multipath propagation: small scale fading

The example in Fig. 2.2 shows only one wave arriving at the receiver. Due to the presence of scatterers and reflectors, however, more than one wave would arrive at the mobile. These waves can have different angles of arrivals. Consider the case of N_r arriving paths and the modulated transmitted signal of $s(t) = Re\{x(t)e^{j2\pi f_c t}\}$, where $x(t)$ is the data carrying signal.

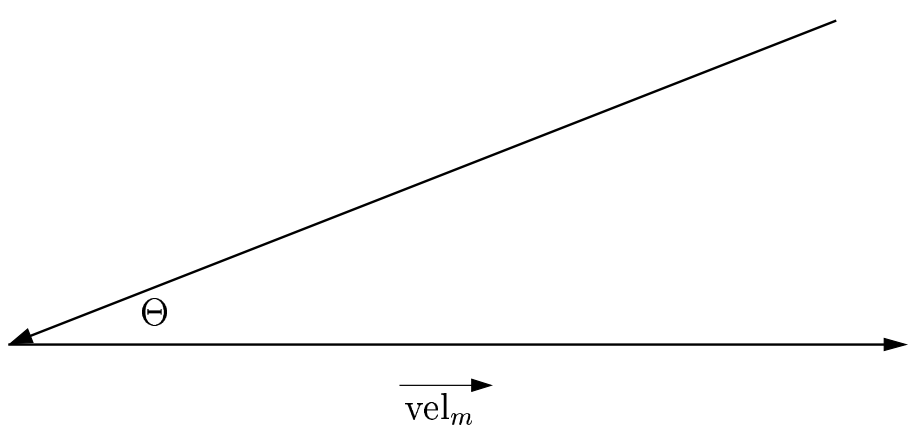

Figure 2.2: One path arriving at angle Θ with respect to the motion of the receiver

In this section we assume that the difference between the arrival times of these paths is negligible. The case with distinguishable arrival times is considered in section 2.5. The

received signal will be the sum of these paths, as follows:

$$y(t) = \sum_{i=0}^{N_r(t)-1} AMP_i(t) Re\{e^{j2\pi f_c(1+\frac{vel_m}{c}cos\Theta_i(t))t-\Phi_{0,i}(t)} x(t)\} \tag{2.4}$$

where Θ_i represents the angle of arrival of the ith path. AMP_i and $\Phi_{0,i}$ denote the amplitude and phase shift respectively. The baseband equivalent signal, $y_{bb}(t)$, will be

$$\begin{gathered} y_{bb}(t) = h_{bb}(t) \times x(t) \\ h_{bb}(t) = \sum_{i=0}^{N_r(t)-1} AMP_i(t) e^{j2\pi f_c \frac{vel_m}{c} cos\Theta_i(t)t-\Phi_{0,i}(t)} = h_{inphase}(t) + j h_{quad}(t) \\ h_{inphase}(t) = \sum_{i=0}^{N_r(t)-1} AMP_i(t) cos(2\pi f_c \frac{vel_m}{c} cos\Theta_i(t)t - \Phi_{0,i}) \\ h_{quad}(t) = \sum_{i=0}^{N_r(t)-1} AMP_i(t) sin(2\pi f_c \frac{vel_m}{c} cos\Theta_i(t)t - \Phi_{0,i}) \\ h_{amp}(t) = \sqrt{h_{inphase}^2(t) + h_{quad}^2(t)} \\ h_\phi(t) = tan^{-1} \frac{h_{quad}(t)}{h_{inphase}(t)} \end{gathered} \tag{2.5}$$

For a large enough N_r, $h_{inphase}$ and h_{quad} can be modeled as Gaussian processes. In the absence of a LOS path, they will have zero means. Therefore, h_{amp} will have a Rayleigh distribution with the following pdf:

$$pdf(h_{amp}) = \frac{h_{amp}}{\sigma_{amp}^2} e^{-\frac{h_{amp}^2}{2\sigma_{amp}^2}} \quad h_{amp} \geq 0 \tag{2.6}$$

where $\sigma_{amp}^2 = \frac{E(h_{amp}^2)}{2}$. $h_{bb}(t)$ is referred to as a *Narrowband Channel* since the time difference between arrivals of different paths is considered negligible in Eq. 2.4. As the mobile moves, the envelope of the received signal changes rapidly in accordance with the time-varying random process of Eq. 2.5. The rates of change depend on angles of arrival, mobile speed and carrier frequency. For instance if the angles of arrival are uniformly distributed in a horizontal plane, the correlation characteristics, $R_{h_{bb}}(\tau)$ and power spectrum of the baseband channel, $PS_{bb}(f)$, will be as follows [10]

$$\begin{gathered} R_{h_{bb}}(\tau) = E(h_{bb}(t) h_{bb}(t-\tau)^*) = 2\sigma_{amp}^2 J_0(2\pi f_d \tau) \\ PS_{bb}(f) = \int_{-\infty}^{\infty} R_{h_{bb}}(\tau) e^{-j2\pi f\tau} d\tau = \frac{2\sigma_{amp}^2}{\sqrt{1-(\frac{f}{f_m})^2}} \quad for \quad |\frac{f}{f_m}| \leq 1 \end{gathered} \tag{2.7}$$

J_0 represents the zeroth order Bessel function. f_d is the maximum Doppler shift: $f_d = \frac{vel_m}{c} f_c$.

The coherence time CT is defined as the time duration over which the channel is correlated. One approximation of it is given in [20] as

$$CT = \frac{.423}{f_d} \tag{2.8}$$

For instance for carrier frequency of $f_c = 1GHz$ and mobile speed of $vel_m = 60miles/hr$, $f_d = 89Hz$ and $CT = 4.8ms$. As this thesis will show, a lot of applications may require much higher time-domain correlation, compared to the CT of Eq. 2.8 (which is defined as the time that the signal becomes uncorrelated), for an acceptable performance. In the presence of a LOS path, $h_{inphase}$ will have a non-zero mean. Then h_{amp} will have a Rician distribution.

2.4 Large-scale fading

The process $h_{bb}(t)$ can be considered wide-sense stationary within distances on the order of the size of the buildings. When the reflecting environment changes, different paths arrive at the receiver. Then the characteristics of this process changes (σ^2_{amp} will change). This is referred to as "shadowing effect" or large-scale variations. From analyzing empirical data, the distribution of σ^2_{amp} can be best approximated by log-normal, as follows:

$$z = log(\sigma^2_{amp})$$
$$pdf(z) = \frac{1}{\sqrt{2\pi\sigma^2_{ls}}} e^{-\frac{(z-mean_{ls})^2}{2\sigma^2_{ls}}} \tag{2.9}$$

Where σ^2_{ls} and $mean_{ls}$ are the variance and average of the large-scale variations. Furthermore, $mean_{ls} = log_{10}(\kappa \times D^{-prf})$ for a power roll-off factor of prf. κ is the attenuation factor and includes effects of antenna heights and gains and frequency of operation, as discussed at the beginning of this chapter.

2.5 Wideband Channels

In a mobile communication environment, multiple copies of the transmitted signal may arrive at the receiver due to the presence of the reflectors and scatterers. In section 2.3, it was assumed that the time difference between arrival of these copies is negligible. Depending on the environment and the rate of transmission, however, this may not be the case. If τ_0, τ_1, ..., τ_{N_p-1} denote distinguishable arrival times of the paths (distinguishable with respect to the sampling period), the received signal for the transmitted signal of $s(t) = Re\{x(t)e^{j2\pi f_c t}\}$ at location R will be as follows[1]:

$$y(t;R) = \sum_{i=0}^{N_p(R)-1} \sum_{k=0}^{N_r(i;R)-1} AMP_{i,k}(R) Re\{e^{j2\pi f_c(1+\frac{vel_m}{c}cos\Theta_{i,k}(R))t-\Phi_{0,i,k}(R)} x(t-\tau_i(R))\} \tag{2.10}$$

$N_p(R)$ refers to the number of clusters of received paths with distinguishable delays and $N_r(i;R)$ is the number of paths that are non-distinguishable in i^{th} cluster. $AMP_{i,k}$, $\Theta_{i,k}$ and $\Phi_{0,i,k}$ denote the gain, angle of arrival and phase of the kth path in the ith cluster respectively. The baseband equivalent signal will be as follows:

$$\begin{aligned} y_{bb}(t;R) = h_{bb}(t;R) * x(t) &= \sum_{i=0}^{N_p(R)-1} \iota_i(R) x(t-\tau_i(R)) \\ \iota_i(R) &= \sum_{k=0}^{N_r(i;R)-1} AMP_{i,k}(R) e^{j2\pi f_c \frac{vel_m}{c} cos\Theta_{i,k}(R)t-\Phi_{0,i,k}(R)} \\ h_{bb}(t;R) &= \sum_{i=0}^{N_p(R)-1} \iota_i(R)\delta(t-\tau_i(R)) \end{aligned} \tag{2.11}$$

Taking Fourier transform of the baseband equivalent channel, $h_{bb}(t;R)$, with respect to t will give the following frequency spectrum:

$$H_{bb}(f;R) = \int_{-\infty}^{\infty} h_{bb}(t;R) e^{-j2\pi ft} dt \tag{2.12}$$

[1]Note that R is related to time as the mobile moves through $\Delta R = vel_m t$. Therefore, the expressions of the previous sections can be expressed in terms of R as well. In this section due to the presence of a delay-dispersive channel, notation R will be used to avoid confusion.

2.6 Summary

This chapter discussed propagation in mobile environments. It started with free-space and two-ray propagation models. Then it explained Doppler effect and its impact in a multipath environment. First narrowband channels were discussed and baseband equivalent models were derived. A definition of coherence time was presented as a function of maximum Doppler shift for a case of uniform angle of arrivals. Finally, wideband channels were presented and corresponding baseband models were derived.

Chapter 3

OFDM Systems

3.1 History

OFDM systems are based on the idea of dividing the available bandwidth into narrow sub-channels and sending low data rate signals in parallel on them. This idea was first implemented in the Collin's Kineplex system [2]. The early multi-carrier modems used filters to separate the individual sub-carriers. Later a more efficient way to modulate and demodulate data on the sub-carriers using Fast Fourier Transform operations was introduced. Discrete Multitone (DMT) [5] systems use OFDM for transmission over a twisted-pair copper lines. DMT can achieve high rates by using the "water filling" algorithm [2]. This algorithm uses knowledge of the channel at each subcarrier and sends more information on the sub-channels with highest signal to noise ratio. Despite its considerable performance improvement for wireline applications, applying the "water filling" algorithm for high mobility applications poses some challenges. Due to rapid time-variations, there may not be enough time to estimate the channel and feed back the estimate before the channel changes. Therefore, currently DMT is not deployed in such applications. Still mobile applications can benefit from using OFDM to improve performance in delay spread channels. OFDM systems handle frequency selective fading resulting from delay spread by expanding the symbol duration [6]-[30]. By adding a guard interval to the beginning of each OFDM symbol, the effect of delay spread (provided that there is perfect synchronization) would appear as a multiplication in the frequency domain

for a time-invariant channel[1]. In the presence of mobility and synchronization errors, the carrier orthogonality of OFDM systems is ruined. This thesis will examine such effects and present algorithms to improve the performance. This chapter explains the bases of an OFDM system in the ideal case of no mobility and no synchronization errors. It lays the foundations for the subsequent chapters, where mobility and synchronization errors are added to the system.

3.2 System Model

Fig. 3.1 shows the discrete baseband equivalent system model. The available bandwidth is divided into N sub-channels. X_i represents the transmitted data point in the ith frequency sub-band and is related to the time domain sequence, x_k, as follows:

$$X_i = \sum_{k=0}^{N-1} x_k e^{-\frac{j2\pi ki}{N}} \quad 0 \leq i \leq N-1 \tag{3.1}$$

The guard interval spans G sampling periods. This thesis assumes that the normalized length of the channel is always less than or equal to G. $\vec{x}_p$ is the cyclic prefix vector with length G and is related to x as follows:

$$\vec{x}_{pf}(i) = x_{N-G+i} \quad 0 \leq i \leq G-1 \tag{3.2}$$

$T_s = \frac{T}{N+G}$ is the sampling period where T is the time duration of one OFDM symbol after adding the guard interval. Let h_k represent the kth sample of channel delay profile. h_k has Rayleigh fading amplitude and uniformly distributed phase. In this chapter, the channel is assumed to be constant over one OFDM symbol. A sample of channel output, y_i, can then be expressed as follows:

$$y_i = \overbrace{\sum_{k=0}^{G} h_k x_{((i-k))_N}}^{\vartheta_i} + w_i \quad 0 \leq i \leq N-1 \tag{3.3}$$

[1]Adding the guard interval will also prevent Inter-OFDM Symbol-Interference

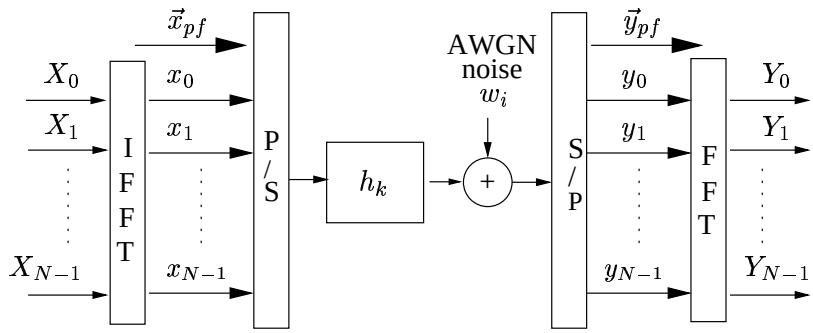

Figure 3.1: Discrete baseband equivalent system model

$((\quad))_N$ represents a cyclic shift in the base of N and w_i represents a sample of additive white Gaussian noise. Then Y, the FFT of sequence y, will be as follows:

$$Y_i = H_i X_i + W_i \quad 0 \leq i \leq N-1 \tag{3.4}$$

H and W denote the FFTs of the sequences h and w. As can be seen from Eq. 3.4, the effect of delay spread appears as a multiplication in frequency domain. Thus to remove the effect of the channel in this case, only gain and phase equalization is required at each sub-carrier. This feature is very attractive for high delay spread applications as it removes the need to perform complex time domain equalization. To retrieve the transmitted data points from Eq. 3.4, the gain and phase of channel should be estimated and removed. Frequency-domain pilot tones or differential modulation can be used to mitigate channel frequency-variations. As the delay spread increases, differential modulation across adjacent sub-bands degrades the performance. As mobility and/or the length of the OFDM symbol increase, differential modulation across adjacent symbols leads to performance loss as well. Therefore, in this thesis frequency-domain pilot tones are used because this thesis deals with high delay and Doppler spread environments. Chapter 4 will discuss

how channel estimates can be acquired using pilot tones.

3.3 Number of subcarriers

For a given bandwidth of BW, N should be chosen such that channel gain and phase can be considered approximately constant over each sub-carrier. If this criteria is not met, multi-tap equalization is required in each sub-band as Eq. 3.4 will not be valid anymore. This thesis does not consider such cases.

To achieve a nearly-constant channel in each sub-band, the bandwidth of each sub-band should be considerably smaller than the channel coherence bandwidth:

$$\begin{aligned} \frac{BW}{N} &<< CB \\ BW &= \frac{1}{T_s} \\ N &>> \frac{1}{CB \times T_s} \end{aligned} \tag{3.5}$$

where CB, the coherence bandwidth, is the frequency interval over which channel is correlated.

3.4 Length of the guard interval

Addition of the guard interval to the beginning of each OFDM symbol serves two purposes. First, if chosen sufficiently long, it prevents interference from previous OFDM symbols, i.e. Inter-OFDM Symbol-Interference. The length of the guard interval should be chosen longer than the maximum expected channel delay spread. Second, if chosen as the replica of the data points at the end of the OFDM symbol, it results in the simple multiplication relationship of Eq. 3.4.

Chapter 4

Pilot-aided Channel Estimation

4.1 Introduction

In OFDM receivers, pilot tones should be inserted among the sub-carriers in order to estimate the channel in high delay spread environments. To estimate the channel at all the sub-carriers, using the pilot tones, different interpolators can be used. This chapter first finds an analytical average error rate formula for a pilot-aided OFDM receiver in a fading environment. Then, to see the effect of interpolation, it evaluates and compares the performance of two interpolators with different levels of complexity: a trigonometric interpolator and a linear one. The average error rate formulas of the interpolators are derived. It is shown that the former one has a considerably better performance as delay spread increases. However, for flat fading channels, it is shown that the linear interpolator has a 3dB gain compared to the trigonometric interpolator. Finally, simulation results support the mathematical analysis and comparison. It should be noted that the analysis in this chapter is carried out under the assumption of ideal synchronization and no mobility. Timing synchronization errors and mobility are added in the subsequent chapters.

The minimum number of pilot tones required in each OFDM symbol exceeds normalized channel delay spread by one[1][15]. These pilot tones should be equally spaced in the

[1]Normalized channel delay spread refers to the channel delay spread (the difference between the arrival times of the first and last paths of the channel) divided by the sampling period.

frequency domain to minimize noise enhancement. To estimate the channel in the sub-bands between the pilot tones, different interpolators with different levels of complexity can be used.

In this chapter, first a general formula for the average error rate of an OFDM system is found in the presence of channel estimation error[2]. Then the error rate for two specific interpolators are found. The first one is based on an IFFT, zero padding and an FFT operation. The equivalent of these operations in the form of an interpolation in the frequency domain is derived and a mathematical analysis of the average error rate is provided. The second interpolator is a linear one. A complete mathematical analysis is then provided for this interpolator, which allows for a comparison of the two. Finally, simulation results confirm the analysis.

4.2 Average error rate analysis

Let $H_i = \xi_i e^{j\theta_i}$ and $\hat{H}_i = \hat{\xi}_i e^{j\hat{\theta}_i}$ where ξ_i and $\hat{\xi}_i$ are Rayleigh fading amplitudes and θ_i and $\hat{\theta}_i$ are uniformly distributed phases. $\hat{H}_i$ is the estimated channel at the ith sub-carrier. To estimate the transmitted data from Eq. 3.4,

$$\hat{X}_i = \frac{\xi_i}{\hat{\xi}_i} e^{j\phi_i} X_i + \frac{\Xi_i}{\hat{\xi}_i} \tag{4.1}$$

where $\phi_i = \theta_i - \hat{\theta}_i$ and $\Xi_i = \Xi_R(i) + j\Xi_I(i) = W_i e^{-j\hat{\theta}_i}$ is Gaussian noise with the same statistics as W_i. In this chapter, it is assumed that X_i is a 4PSK modulated signal with power of σ_X^2. Then for one realization of ϕ_i and ξ_i, the instantaneous probability of receiving the correct symbol of the constellation at the ith sub-carrier will be,

$$P_{c,inst.}(i) = Prob\{\frac{\sigma_X \xi_i (cos\phi_i - sin\phi_i)}{\sqrt{2}\hat{\xi}_i} + \frac{\Xi_R(i)}{\hat{\xi}_i} > 0 \quad \& \quad \frac{\sigma_X \xi_i (cos\phi_i + sin\phi_i)}{\sqrt{2}\hat{\xi}_i} + \frac{\Xi_I(i)}{\hat{\xi}_i} > 0\} \tag{4.2}$$

[2]Authors in reference [4] found a formula for the error rate in the case that pilot tones have been inserted in all the sub-carriers. Therefore, the effect of interpolation was not studied in their work. Furthermore, extending their work to the case of interpolation does not produce good results since they made a limiting assumption that the channel estimation error is independent of the channel at each sub-carrier, which may not be the case depending on the interpolator. Hence, this chapter takes a different approach and will perform the analysis without a need to make this assumption.

where $\Xi_R(i)$ and $\Xi_I(i)$ are uncorrelated and have Gaussian distributions (hence they are independent) with zero means and variances of $\sigma^2_{\Xi_R} = \sigma^2_{\Xi_I} = .5\sigma^2_{\Xi}$, where $\sigma^2_{\Xi} = \overline{|\Xi_i^2|} = \overline{|W_i^2|}$. Then, $P_{c,inst.}$ will be as follows:

$$P_{c,inst.}(i) = Q(\frac{-\sigma_X \xi_i(cos\phi_i - sin\phi_i)}{\sigma_\Xi}) \times Q(\frac{-\sigma_X \xi_i(cos\phi_i + sin\phi_i)}{\sigma_\Xi}) \quad \Rightarrow$$
$$P_{e,inst.}(i) = 1 - P_{c,inst.}(i) =$$
$$Q(\frac{\sigma_X \xi_i(cos\phi_i - sin\phi_i)}{\sigma_\Xi}) + Q(\frac{\sigma_X \xi_i(cos\phi_i + sin\phi_i)}{\sigma_\Xi}) - Q(\frac{\sigma_X \xi_i(cos\phi_i - sin\phi_i)}{\sigma_\Xi}) \times Q(\frac{\sigma_X \xi_i(cos\phi_i + sin\phi_i)}{\sigma_\Xi}) \tag{4.3}$$

where $Q(g) = \frac{1}{\sqrt{2\pi}} \int_g^\infty e^{-\frac{z^2}{2}} dz$ for an arbitrary g. To evaluate the average error rate, $\overline{P_e}$, $P_{e,inst.}$ is averaged over the distributions of ξ_i and ϕ_i. First an averaging is performed over ξ_i, which has a Rayleigh distribution. Since the last term of Eq. 4.3 has a considerably smaller value than other terms (as long as the error rate is not too high), $P_{e,inst.}$ is approximated with the first two terms. $\overline{P_e}$ evaluated through this approximation is slightly larger than the exact value at high error rates but matches well otherwise. It can be shown that for an arbitrary g,

$$\begin{aligned}
\overline{Q(\xi_i g)} &= \frac{2}{\overline{\xi_i^2}} \int_0^\infty Q(\xi_i g)\xi_i e^{-\frac{\xi_i^2}{\overline{\xi_i^2}}} d\xi_i \\
&= \frac{1}{2} - \frac{g}{\sqrt{2\pi}} \int_0^\infty e^{-\frac{\xi_i^2}{2}(g^2 + \frac{2}{\overline{\xi_i^2}})} d\xi_i \\
&= \frac{1}{2} \times (1 - \frac{g}{\sqrt{g^2 + \frac{2}{\Omega_i}}})
\end{aligned} \tag{4.4}$$

where,

$$\Omega_i = \overline{\xi_i^2} = \overline{H_i H_i^*} = \sum_n \sum_{n'} \overline{h_n h_n'^*} e^{-\frac{j2\pi i(n-n')}{N}} \tag{4.5}$$

Since $\overline{h_n h_{n'}^*} = \sigma^2_{h_n} \delta_{n,n'}$, where $\sigma^2_{h_n} = \overline{|h_n|^2}$ ($\delta_{n,n'}$ is one for $n = n'$ and zero otherwise), then

$$\Omega_i = \sum_n \sigma^2_{h_n} \tag{4.6}$$

The index i of Ω_i is dropped since it is not a function of i so $\Omega = \sum_n \sigma^2_{h_n}$. Using Eq. 4.3-4.6, the average error rate will be as follows,

$$\begin{aligned}\overline{P_e}(i) &= 1 - .5\sqrt{\frac{SNR_{ave}}{2}} \times E_{\phi_i}\left\{\frac{cos(\phi_i) - sin(\phi_i)}{\sqrt{1 + \frac{SNR_{ave}(1-sin(2\phi_i))}{2}}}\right\} - \\ &\quad .5\sqrt{\frac{SNR_{ave}}{2}} \times E_{\phi_i}\left\{\frac{cos(\phi_i) + sin(\phi_i)}{\sqrt{1 + \frac{SNR_{ave}(1+sin(2\phi_i))}{2}}}\right\}\end{aligned} \tag{4.7}$$

SNR_{ave}, the average received Signal to Noise Ratio, is defined as $SNR_{ave} = \frac{\Omega\sigma^2_X}{\sigma^2_\Xi}$ and $E_{z_1}\{z_2\}$ represents average of z_2 with respect to z_1 for arbitrary z_1 and z_2. The distribution of ϕ_i is as follows [28]:

$$pdf(\phi_i) = \left[\frac{\sqrt{1-\rho_i cos^2(\phi_i)} + \sqrt{\rho_i} cos(\phi_i)(\pi - cos^{-1}(\sqrt{\rho_i} cos(\phi_i)))}{(1-\rho_i cos^2(\phi_i))^{1.5}}\right] \frac{(1-\rho_i)\times(2\pi - |\phi_i|)}{4\pi^2} \quad |\phi_i| \leq 2\pi \tag{4.8}$$

where $\rho_i = \frac{cov(\xi_i^2, \hat{\xi}_i^2)}{\sqrt{var(\xi_i^2) var(\hat{\xi}_i^2)}}$ with $cov(\xi_i^2, \hat{\xi}_i^2) = \overline{\xi_i^2 \hat{\xi}_i^2} - \overline{\xi_i^2} \times \overline{\hat{\xi}_i^2}$ and $var(\xi_i^2) = \overline{\xi_i^4} - (\overline{\xi_i^2})^2$. Then[3],

$$\overline{P_e}(i) = 1 - .5\sqrt{\frac{SNR_{ave}}{2}} \int_{\phi_i} \left[\frac{cos(\phi_i) - sin(\phi_i)}{\sqrt{1 + \frac{SNR_{ave}(1-sin(2\phi_i))}{2}}} + \frac{cos(\phi_i) + sin(\phi_i)}{\sqrt{1 + \frac{SNR_{ave}(1+sin(2\phi_i))}{2}}}\right] \times pdf(\phi_i) d\phi_i \tag{4.9}$$

4.3 Pilot-aided channel estimation

Let $\nu \leq G$ be the maximum predicted normalized length of the channel. It can be shown that $L \geq \nu + 1$ equally spaced frequency-domain pilot tones are required for channel estimation [15]. These L pilot tones, $X_{pilot}(l_i)$, are inserted at sub-channels $l_i = \frac{i \times N}{L}$ for $0 \leq i \leq L - 1$. An estimate of the channel at pilot tones can then be acquired as follows:

$$\hat{H}_{l_i} = \frac{Y_{l_i}}{X_{pilot}(l_i)} = H_{l_i} + \frac{W_{l_i}}{X_{pilot}(l_i)} \quad 0 \leq i \leq L - 1 \tag{4.10}$$

[3]Note that $\overline{P_e}(i)$ of Eq. 4.9 is a function of i through ρ_i.

To estimate the channel at sub-carriers in between the pilot tones, different interpolators can be used. The complexity of these interpolators varies depending on the number of pilot tones used to estimate the channel at each sub-carrier. In this chapter two extreme cases are analyzed. The first interpolator uses all the pilot tones to estimate the channel at each sub-band. The second one, on the other hand, only uses the two adjacent pilot tones. Therefore the former is expected to have superior performance in environments where delay spread is the main cause of performance degradation (as opposed to noise) at the cost of an increase in the complexity, as will be seen from the results of this chapter.

4.4 A Trigonometric Interpolator

To find the time domain channel from Eq. 4.10, an IFFT of length L is performed. The time-domain channel estimate, $\hat{h}_k$, is:

$$\hat{h}_k = \frac{1}{L}\sum_{i=0}^{L-1} \hat{H}_{l_i} e^{\frac{j2\pi ik}{L}} \quad 0 \leq k \leq L-1 \tag{4.11}$$

Through an FFT of length N, the estimate of the channel at all the sub-carriers is:

$$\hat{H}_i = \sum_{k=0}^{L-1} \hat{h}_k e^{\frac{-j2\pi ik}{N}} \quad 0 \leq i \leq N-1 \tag{4.12}$$

It is also possible to find $\hat{H}_i$ directly from the pilot tones. Using Eq. 4.11 and 4.12,

$$\begin{aligned}
\hat{H}_i &= \frac{1}{L}\sum_{z=0}^{L-1}\sum_{k=0}^{L-1} \hat{H}_{l_z} e^{-j2\pi k(\frac{i}{N}-\frac{z}{L})} \quad 0 \leq i \leq N-1 \\
&= \frac{1}{L}\sum_{z=0}^{L-1} \hat{H}_{l_z} \frac{1-e^{-\frac{j2\pi i}{r}}}{1-e^{-j2\pi(\frac{i}{N}-\frac{z}{L})}} \\
&= \sum_{z=0}^{L-1} \underbrace{\frac{1-e^{-\frac{j2\pi i}{r}}}{2Lj}(cot(\frac{\pi i}{N}-\frac{\pi z}{L})+j)}_{\alpha_{i,z}} \times \hat{H}_{l_z}
\end{aligned} \tag{4.13}$$

where $r = \frac{N}{L}$ and $cot(s) = \frac{cos(s)}{sin(s)}$ for an arbitrary s. From Eq. 4.13, it can be seen that to estimate the channel at any sub-carrier, all the L pilots have been used. This

interpolator is referred to as a "trigonometric interpolator" since the coefficient of $\hat{H}_{l_z}$ is a trigonometric function of i in Eq. 4.13. Inserting Eq. 4.10 in Eq. 4.13,

$$\hat{H}_i = H_i + \sum_{z=0}^{L-1} \alpha_{i,z} \frac{W_{l_z}}{X_{pilot}(l_z)} \tag{4.14}$$

Therefore:

$$\hat{\Omega}_{i,Tri} = \overline{\hat{\xi}_i^2} = \overline{|\hat{H}_i|^2} = \Omega + \frac{\sigma_\Xi^2}{\sigma_X^2} \sum_{z=0}^{L-1} |\alpha_{i,z}^2| \quad 0 \leq i \leq N-1 \tag{4.15}$$

The subscript Tri in $\hat{\Omega}_{i,Tri}$ refers to the trigonometric interpolator. It can be easily shown that $\sum_{z=0}^{L-1} |\alpha_{i,z}^2| = 1$ for any i. Therefore,

$$\hat{\Omega}_{i,Tri} = \Omega + \frac{\sigma_\Xi^2}{\sigma_X^2} \quad 0 \leq i \leq N-1 \tag{4.16}$$

The index i of $\hat{\Omega}_{i,Tri}$ is dropped since $\hat{\Omega}_{i,Tri}$ is not a function of i as can be seen from Eq. 4.16. It is easy to show that for a Rayleigh distributed variable g, $\overline{g^4} = 2(\overline{g^2})^2$ and hence $var(g^2) = (\overline{g^2})^2$. Thus, $var(\xi_i^2) = \Omega^2$ and $var(\hat{\xi}_i^2) = \hat{\Omega}_{Tri}^2$. Using these equalities, $\overline{\xi_i^2 \hat{\xi}_i^2}$ is:

$$\overline{\xi_i^2 \hat{\xi}_i^2} = \overline{|H_i|^2 |\hat{H}_i|^2} = 2\Omega^2 + \frac{\sigma_\Xi^2}{\sigma_X^2}\Omega \tag{4.17}$$

Finally, ρ_i for this interpolator is,

$$\rho_{i,Tri} = \frac{\overline{\xi_i^2 \hat{\xi}_i^2} - \Omega\hat{\Omega}_{Tri}}{\Omega\hat{\Omega}_{Tri}} = \frac{\Omega}{\hat{\Omega}_{Tri}} = \frac{SNR_{ave}}{1 + SNR_{ave}} \tag{4.18}$$

As can be seen from Eq. 4.18, for this interpolator, ρ_i and therefore $\overline{P_e(i)}$ are neither functions of i nor functions of the shape of the channel delay profile and are solely functions of SNR_{ave}.

4.5 A Linear Interpolator

It is also possible to estimate the channel at all the sub-carriers by linear interpolation. In this case, the channel is estimated at each sub-carrier using only the two adjacent pilots. Therefore, this interpolator will be less computationally complex than the one of the previous section. The channel estimate will be as follows for this interpolator,

$$\hat{H}_i = \varrho_i \hat{H}_{d_i} + \eta_i \hat{H}_{d_i+r} \quad 0 \leq i \leq N-1 \tag{4.19}$$

$d_i = floor(\frac{i}{r}) \times r$ refers to the sub-carriers with pilot tones, $\eta_i = \frac{i-d_i}{r}$ and $\varrho_i = 1 - \eta_i$. Using Eq. 4.10,

$$\hat{H}_{d_i} = H_{d_i} + \frac{W_{d_i}}{X_{pilot}(d_i)} \tag{4.20}$$

Therefore,

$$\hat{H}_i = \varrho_i H_{d_i} + \varrho_i \frac{W_{d_i}}{X_{pilot}(d_i)} + \eta_i H_{d_i+r} + \eta_i \frac{W_{d_i+r}}{X_{pilot}(d_i+r)} \quad 0 \leq i \leq N-1 \tag{4.21}$$

Using Eq. 4.21, $\hat{\Omega}_{i,Lin}$ is found, where the subscript Lin refers to the linear interpolator,

$$\hat{\Omega}_{i,Lin} = \overline{\hat{\xi}_i^2} = (\varrho_i^2 + \eta_i^2) \times (\Omega + \frac{\sigma_\Xi^2}{\sigma_X^2}) + 2\varrho_i\eta_i \times real(R_H(r)) \tag{4.22}$$

$R_H(g)$, the auto-correlation function of the wide-sense stationary process H, is defined as $R_H(g) = \overline{H_{g+t}H_t^*} = \sum_z \sigma_{h_z}^2 e^{-\frac{j2\pi zg}{N}}$ and $\Omega = R_H(0)$ is as defined in the previous section. Next, the covariance is calculated. Using Eq. 4.21,

$$\begin{aligned}
\overline{\xi_i^2 \hat{\xi}_i^2} &= \overline{H_i H_i^* \hat{H}_i \hat{H}_i^*} \\
&= \varrho_i^2 \overline{H_i H_i^* H_{d_i} H_{d_i}^*} + \eta_i^2 \overline{H_i H_i^* H_{d_i+r} H_{d_i+r}^*} + \\
&\quad 2\varrho_i\eta_i \times real(\overline{H_i H_i^* H_{d_i} H_{d_i+r}^*}) + (\varrho_i^2 + \eta_i^2)\frac{\Omega\sigma_\Xi^2}{\sigma_X^2}
\end{aligned} \tag{4.23}$$

To evaluate the terms in Eq. 4.23, $\overline{H_i H_i^* H_z H_n^*}$ is calculated for an arbitrary z and n:

$$\begin{aligned}
\overline{H_i H_i^* H_z H_n^*} &= \sum_k \sum_{k'} \sum_{k''} \sum_{k'''} \overline{h_k h_{k'}^* h_{k''} h_{k'''}^*} e^{-\frac{j2\pi((k-k')i+zk''-nk''')}{N}} \\
&= \sum_k \overline{|h_k|^4} e^{\frac{-j2\pi k(z-n)}{N}} + \underbrace{\sum_{k=k'} \sum_{k''=k'''}}_{k\neq k''} \sigma_{h_k}^2 \sigma_{h_{k''}}^2 e^{-\frac{j2\pi(z-n)k''}{N}} + \\
&\quad \underbrace{\sum_{k=k'''} \sum_{k'=k''}}_{k\neq k'} \sigma_{h_k}^2 \sigma_{h_{k'}}^2 e^{-\frac{j2\pi((k-k')i+zk'-nk)}{N}} + \\
&\quad \underbrace{\sum_{k=k''} \sum_{k'=k'''}}_{k\neq k'} \overline{h_k^2 h_{k'}^{*2}} e^{-\frac{j2\pi((k-k')i+zk-nk')}{N}}
\end{aligned} \tag{4.24}$$

For an h_k with Rayleigh fading amplitude and uniformly distributed phase, $\overline{h_k^2} = 0$. Therefore, the last term on the right hand side of Eq. 4.24 is zero. Evaluating the other terms,

$$\begin{aligned}
\overline{H_i H_i^* H_z H_n^*} &= 2R_{4H}(z-n) + \Omega R_H(z-n) - \\
&\quad R_{4H}(z-n) + R_H(i-n)R_H(z-i) - R_{4H}(z-n) \\
&= \Omega R_H(z-n) + R_H(i-n)R_H(z-i)
\end{aligned} \tag{4.25}$$

where $R_{4H}(g) = \sum_k \sigma_{h_k}^4 e^{-\frac{j2\pi kg}{N}}$. Using Eq. 4.25, Eq. 4.23 can be written as follows,

$$\begin{aligned}
\overline{\xi_i^2 \hat{\xi}_i^2} &= \varrho_i^2(\Omega^2 + |R_H(i-d_i)|^2) + \eta_i^2(\Omega^2 + |R_H(i-d_i-r)|^2) + \\
&\quad 2\varrho_i\eta_i \times real(\Omega R_H(r) + R_H(i-d_i)R_H(d_i+r-i)) + \\
&\quad (\varrho_i^2 + \eta_i^2)\frac{\Omega\sigma_\Xi^2}{\sigma_X^2}
\end{aligned} \tag{4.26}$$

Then,

$$\begin{aligned}
cov(\xi_i^2, \hat{\xi}_i^2) &= \overline{\xi_i^2 \hat{\xi}_i^2} - \Omega\hat{\Omega}_{Lin} \\
&= \varrho_i^2|R_H(i-d_i)|^2 + \eta_i^2|R_H(i-d_i-r)|^2 + \\
&\quad 2\varrho_i\eta_i \times real(R_H(i-d_i)R_H(d_i+r-i))
\end{aligned} \tag{4.27}$$

Therefore,

$$\rho_{i,Lin} = \frac{\varrho_i^2|R_H(i-d_i)|^2+\eta_i^2|R_H(i-d_i-r)|^2+2\varrho_i\eta_i\times real(R_H(i-d_i)R_H(d_i+r-i))}{\Omega\times\hat{\Omega}_{i,Lin}} \tag{4.28}$$

To write Eq. 4.28 as a function of SNR_{ave}, the power of the channel is normalized: $\sigma^2_{h_{k,norm.}} = \frac{\sigma^2_{h_k}}{\Omega}$. Let $R_{H,norm.}(g) = \sum_k \sigma^2_{h_{k,norm.}} e^{-\frac{j2\pi kg}{N}}$ for an arbitrary g. Then, Eq. 4.28 can be written as follows:

$$\rho_{i,Lin} = \frac{\varrho_i^2|R_{H,norm.}(i-d_i)|^2+\eta_i^2|R_{H,norm.}(i-d_i-r)|^2+2\varrho_i\eta_i\times real(R_{H,norm.}(i-d_i)R_{H,norm.}(d_i+r-i))}{(\varrho_i^2+\eta_i^2)\times(\frac{SNR_{ave}+1}{SNR_{ave}})+2\varrho_i\eta_i\times real(R_{H,norm.}(r))} \tag{4.29}$$

As can be seen from Eq. 4.29, ρ_i and therefore $\overline{P_e(i)}$ of the linear interpolator are functions of i. There are $\lfloor\frac{r}{2}\rfloor+1$ different error rates that each sub-carrier may experience depending on its location. For example, pilot carrying sub-carriers are those with $\eta_i = 0$. From Eq. 4.29, it can be seen that for these sub-carriers $\rho_{i,Lin} = \frac{SNR_{ave}}{1+SNR_{ave}}$ which is the same as $\rho_{i,Tri}$. In general, there are two factors determining the performance of a linear interpolator: noise and delay spread. For a sub-carrier farther from the pilots, $R_{H,norm.}$ decreases for non-flat channels[4]. However, the amount of added noise decreases as well. To see this, take the noisy terms, $\varrho_i\frac{W_{d_i}}{X_{pilot}(d_i)} + \eta_i\frac{W_{d_i+r}}{X_{pilot}(d_i+r)}$, of Eq. 4.21. It can be easily shown that the power of these terms is minimized for $\varrho_i = \eta_i = .5$, which refers to the sub-carriers in the middle of every two consecutive tones. At high delay spreads, delay spread becomes the dominant factor. Then, $R_{H,norm.}$ decreases and the linear interpolator will have worse performance than the trigonometric one. However, for nearly-flat fading channels, noise becomes the dominant factor. Then the linear interpolator will have better performance than the trigonometric one. For instance, consider the sub-carriers with $\varrho_i = \eta_i = .5$. Inserting $R_{H,norm.} = 1$ (flat fading) in Eq. 4.29 for these carriers would result in the following:

$$\varrho_i = \eta_i = .5 \quad \& \quad R_{H,norm.} = 1 \Rightarrow \rho_{i,Lin} = \frac{2SNR_{ave}}{2SNR_{ave}+1} \tag{4.30}$$

Comparing Eq. 4.30 with Eq. 4.18 shows that the linear interpolator has a 3dB gain in this specific case. This is due to the fact that the trigonometric interpolator uses

[4] the sub-carrier in the middle of every two consecutive pilot tones has the least correlation.

all the pilots for channel estimation at each sub-carrier, which adds more noise than the linear one that uses solely the adjacent pilots. Despite the superiority of the linear interpolator in the flat fading case, since these interpolators are to be used in delay spread environments, the trigonometric interpolator will outperform the linear one. Therefore, this thesis will use the trigonometric interpolator in the subsequent chapters as part of the channel estimation process.

4.6 Analysis and Simulation Results

This section finds $\overline{P_e}(i)$ of Eq. 4.9 for two channels, channels c4.1 and c4.2, using the correlation coefficients of the interpolators[5]. Also, the whole system is simulated for both channels to compare the results of analysis and simulation. The power delay profile of both channels has two non-zero samples with relative powers of $\frac{2}{3}$ and $\frac{1}{3}$ respectively. The delay between the two samples is[6] $5\mu s$ for channel c4.1 and $26\mu s$ for channel c4.2. Therefore, the frequency response of channel c4.2 is less correlated, i.e. $R_{H,norm.}$ has smaller values for this channel since it is the FFT of the power-delay profile with a longer delay. Input modulation is 4PSK, $r = 4$, $N = 892$ and the total bandwidth is $3.9MHz$. Since $r = 4$, there are three sub-carriers in between every two consecutive pilots. Therefore for the linear interpolator, there will be three sets of error rates. Set#1 refers to the pilot sub-carriers[7]. Set#2 refers to the sub-carriers that are adjacent to one pilot carrier and set#3 denotes the remaining sub-carriers. Fig. 4.1 shows $\overline{P_e}$ of channel c4.1 as a function of SNR_{ave} for both interpolators. For this channel, the trigonometric and linear interpolators have very similar performance due to low delay spread. It can be seen that, the error rate of set#1 of the linear interpolator is the same as that of the trigonometric one, as was shown in the previous section. Since the delay spread of this channel is low,

[5]This thesis would refer to the simulated channels in the following format: c*.*, where the first * refers to the Chapter in which the channel is used and the second * distinguishes that channel in the Chapter.

[6]In both cases, the channel delay spread is less than the cyclic prefix length.

[7]In the OFDM symbols with training, pilots are transmitted on these sub-carriers. However, when considering the error rates at these sub-carrier frequencies, it refers to the subsequent symbols, without training, that use the estimate of the channel from the training symbols. For the remaining sub-carriers, error rate analysis applies to both training and non-training symbols.

at low SNR_{ave}, noise is the dominant factor. Therefore, for set#2 and 3, the performance of the linear interpolator is slightly better than the trigonometric one at low SNR_{ave}, as can be seen. On the other hand, at very high SNR_{ave}, delay spread becomes the dominant factor and the trigonometric interpolator slightly outperforms the linear one at set#2 and 3. This is more pronounced for set#3 since channel values at those subcarriers are less correlated with those at the pilot carrying ones. Fig. 4.2 shows the error rates for channel c4.2. The performance of the linear interpolator degrades considerably at set#2 and 3 for this channel due to higher delay spread. However, the performance of the trigonometric interpolator stays independent of the shape of the channel. As can be seen, the results of the mathematical analysis and simulation match well in both Fig. 4.2 and 4.3. At very high $\overline{P_e}$, the results of the analysis are slightly higher than those of the simulation, which is due to the omission of the last term of Eq. 4.3.

4.7 Summary

In this chapter average probability of error formulas are derived for an OFDM receiver that uses frequency-domain pilot-aided channel estimation. In particular, the performance of a trigonometric interpolator and a linear interpolator was analyzed. It was shown mathematically that the average error rate of the trigonometric interpolator is independent of the shape of the channel and is solely a function of SNR_{ave}. Furthermore, it was shown that as delay spread increases, the performance of the linear interpolator degrades considerably. In the case of a flat fading channel, however, the linear interpolator has a 3dB gain over the trigonometric one due to the smaller contribution of noise sources. Finally, the simulation results confirmed the mathematical analysis.

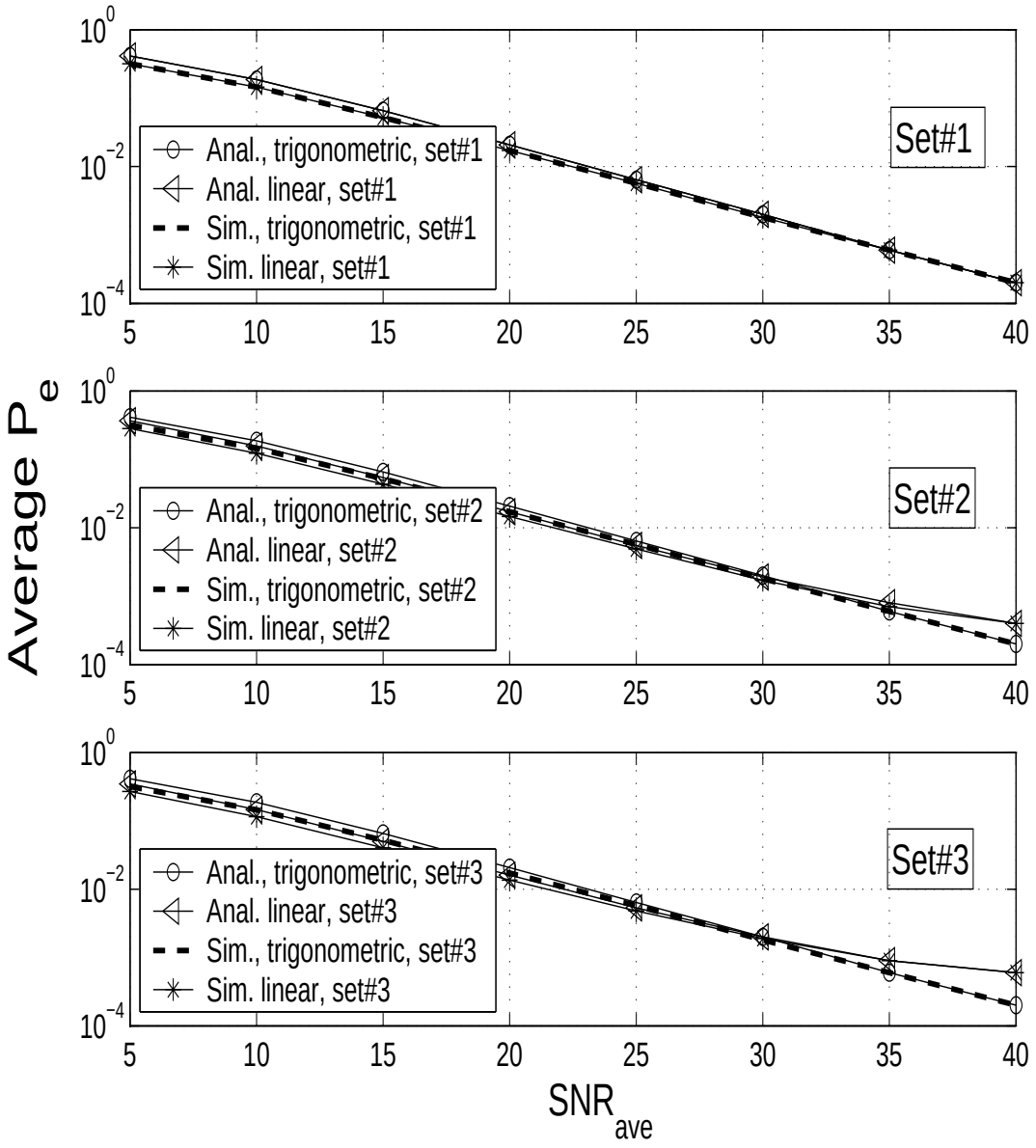

Figure 4.1: $\overline{P_e}$ vs. SNR_{ave} for channel c4.1

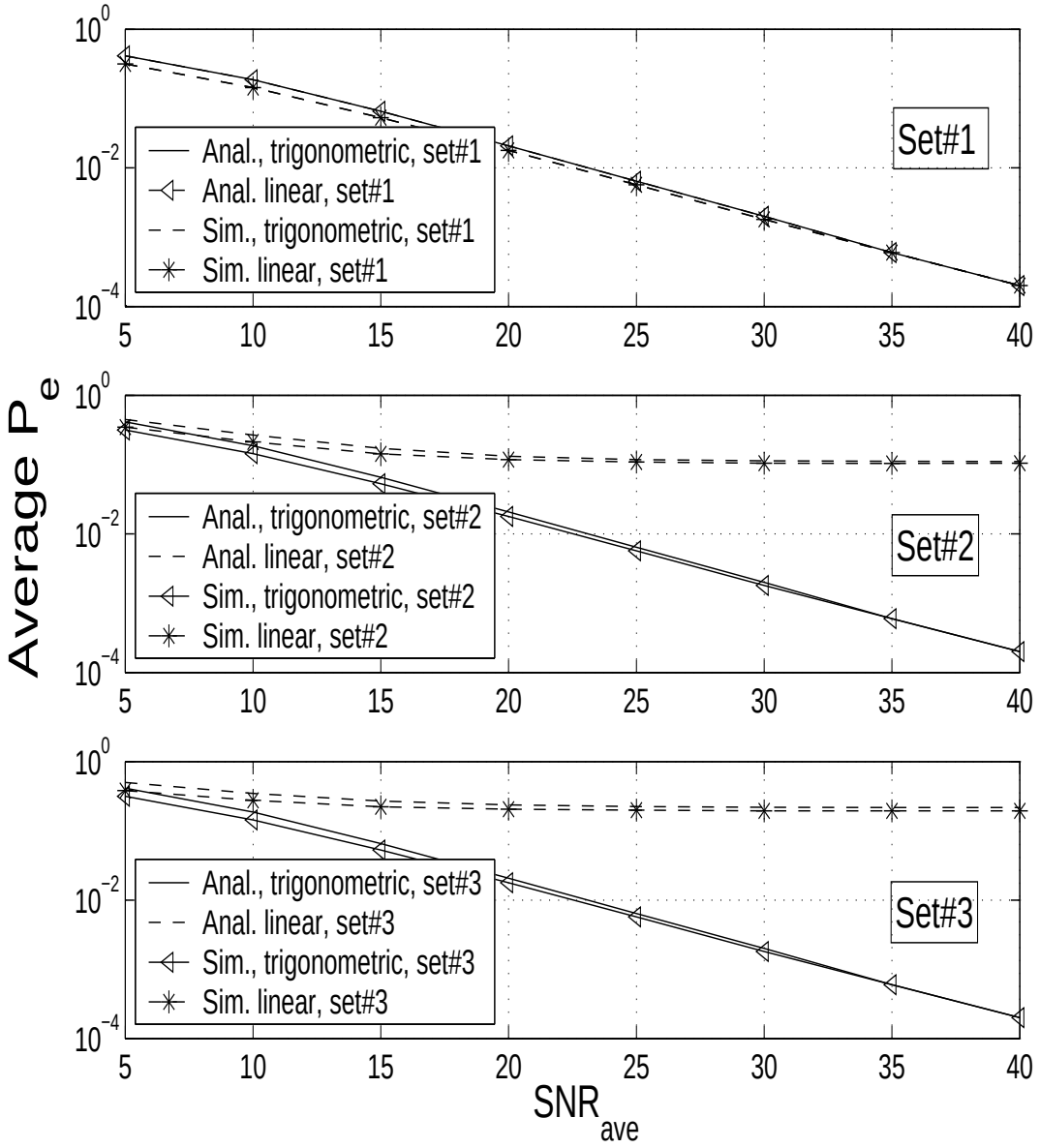

Figure 4.2: $\overline{P_e}$ vs. SNR_{ave} for channel c4.2

Chapter 5

Timing Synchronization for Low-Mobility Cases

The goals of this chapter are as follows: to analyze the impact of timing synchronization errors on the performance of pilot-aided OFDM systems and to design a robust timing synchronization algorithm without additional training overhead. This chapter will focus on low-mobility environments and the effect of high mobility is introduced in the next chapter.

The first part of the chapter provides a mathematical analysis of the effect of timing synchronization errors on the performance of an OFDM receiver in a frequency selective fading environment. Exact formulas for the average Signal to Interference Ratio (SIR_{ave}) are derived. The effect of these errors on a pilot-aided channel estimator is then studied. Channel estimation error expressions are derived in the presence of timing synchronization errors.

The second part of the chapter introduces a new timing synchronization algorithm based on the analysis of the first part.

5.1 Introduction

In this thesis, timing synchronization refers to the correct detection of the start of the OFDM symbol (symbol alignment). Timing synchronization errors degrade the performance of an OFDM receiver by introducing Inter-Carrier-Interference (ICI) and Inter-Symbol-Interference (ISI). Timing synchronization algorithms can be categorized mainly into two groups: training-based and correlation-based. The first group is based on transmitting two identical symbols [24]. Muller [14] has provided a good survey and comparison of such algorithms. The performance of these methods are good but there is a waste of bandwidth in transmitting the training information. The waste can become considerable in high mobility environments for the following reason. As mobility increases, OFDM symbol alignment can become obsolete more rapidly due to the frequent changes of the power-delay profile of the channel. This requires more frequent update of the symbol alignment. Therefore, using training-based methods could result in a considerable waste of the bandwidth.

The second category is based on using the redundancy of the cyclic prefix [29]. Then the start of the symbol is where the correlation of the start and end data points is maximized. In the absence of delay spread, this would work fine. However, in the presence of delay spread, the cyclic prefix is affected by the previous symbol resulting in performance degradation. There are other methods that use the cyclic prefix for coarse synchronization followed by a fine tuning [32]. However, Yang in [32] makes the assumption that the first sample of the channel-delay profile is the strongest, which is not always true in environments with no line of sight path.

While the effect of timing errors on OFDM systems has been extensively studied by researchers in this field, the effect of these errors on a pilot-aided channel estimator has not been investigated before. In order to design a robust timing synchronization algorithm, this chapter takes an overall look at timing synchronization and channel estimation. It provides a complete mathematical analysis of the effect of timing errors on a pilot-aided OFDM system to provide the following:

1) Understanding the effect of such errors on an OFDM system in general and characterizing the introduced interference terms;
2) Understanding the effect of such errors on a pilot-aided channel estimator in particular.
In reference [25], authors have worked on the first category. They have provided an *approximate* formula with limited applications for the interference caused by timing errors. However, no work has so far been published in the second category. It is the goal of this chapter to first provide an *exact* derivation of the effect of timing errors on an OFDM system in general. Once this is done, the effect of these errors on a pilot-aided channel estimator is studied and channel estimation error formulas are derived. Based on this analysis, a new timing synchronization algorithm is proposed.

5.2 Effect of Timing Synchronization Errors

Consider a case of timing errors of m sampling periods. $m > 0$ and $m < 0$ denote timing errors of m to the right and left side respectively, as is shown in Fig. 5.1.

5.2.1 Case of timing errors to the right $(m > 0)$

In this case, an error of m sampling periods to the right side has occurred. Then, the terms $y_0, y_1, \ldots, y_{m-1}$ are missed and instead m data points of the next OFDM symbol are erroneously selected. The received signal can thus be written as follows[1]:

$$y_i^r = \vartheta_{((i+m))_N} \times \gamma_i^r + s_i + w_i^r \quad 0 \leq i \leq N-1 \tag{5.1}$$

where y_i^r is a sample of the received signal for $m > 0$, ϑ is as defined in Eq. 3.3, $s_i = \begin{cases} 0 & 0 \leq i \leq N-m-1 \\ y_{pf}^{next}(i-N+m) & else \end{cases}$, with $y_{pf}^{next}(i)$ representing the ith sample of the output cyclic prefix of the next OFDM symbol (excluding the effect of AWGN), $\gamma_i^r = \begin{cases} 1 & 0 \leq i \leq N-m-1 \\ 0 & N-m \leq i \leq N-1 \end{cases}$ and w_i^r is a sample of AWGN. Then Y_i^r, the FFT of y_i^r,

[1]Since this chapter assumes a low mobility environment, the channel is considered constant over one OFDM symbol.

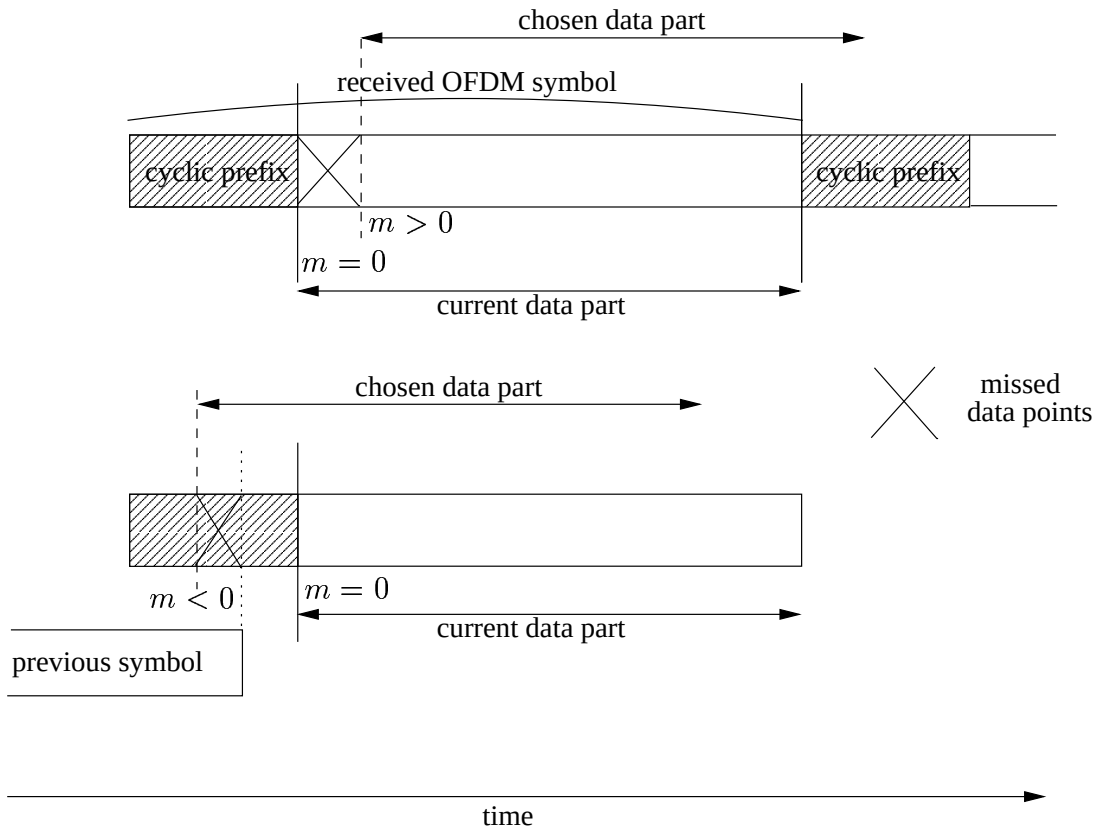

Figure 5.1: Errors of m sampling periods to the right side (top figure) and left side (bottom figure)

will be,

$$Y_i^r = \frac{\Gamma_0^r}{N} H_i X_i e^{\frac{j2\pi mi}{N}} + \underbrace{\overbrace{\sum_{k=1}^{N-1} \frac{\Gamma_k^r}{N} H_{((i-k))_N} X_{((i-k))_N} e^{\frac{j2\pi m(i-k)}{N}}}^{I_i^r} + S_i}_{ICI \quad \& \quad ISI} + W_i^r \quad 0 \leq i \leq N-1 \quad (5.2)$$

Where S_i is the FFT of s_i and Γ_i^r, the FFT of γ_i^r, is $\Gamma_i^r = \begin{cases} \frac{1-e^{\frac{j2\pi im}{N}}}{1-e^{-\frac{j2\pi i}{N}}} & i \neq 0 \\ N-m & i = 0 \end{cases}$.

I_i^r represents the ICI resulting from multiplication of $\vartheta_{((i+m))_N}$ by γ_i^r in Eq. 5.1. The power of I_i^r can then be calculated as follows:

$$\begin{aligned} \sigma_{I^r}^2 &= \frac{1}{N^2} \sum_{k=1}^{N-1} \sum_{k'=1}^{N-1} \Gamma_k^r \Gamma_{k'}^{r*} \overline{H_{((i-k))_N} H_{((i-k'))_N}^*} \times \overline{X_{((i-k))_N} X_{((i-k'))_N}^*} e^{-\frac{j2\pi m(k-k')}{N}} \\ &= \frac{(N-m)m}{N^2} \sigma_X^2 \sigma_H^2 \end{aligned} \quad (5.3)$$

Let $C \leq \nu$ represent the normalized length of the channel delay spread. In Eq. 5.3, $\overline{X_i X_j^*} = \sigma_X^2 \delta_{i,j}$, $\overline{H_i H_j^*} = \sigma_H^2 \delta_{i,j}$, with $\sigma_H^2 = \sum_{i=0}^{C} \sigma_{h_i}^2$, and $\sum_{k=1}^{N-1} |\Gamma_k^r|^2 = N \sum_{k=0}^{N-1} |\gamma_k^r|^2 - \Gamma_0^2 = m \times (N-m)$. δ is as defined in Chapter 4. Next, σ_S^2, the power of S_i, is calculated. Since y_{pf}^{next} includes delayed replicas of the current OFDM symbol from the delayed paths, S_i has an ICI term in addition to an ISI term. $S_i = \sum_{k=0}^{m-1} s_{N-m+k} e^{-\frac{j2\pi i(k-m)}{N}}$, where s_{N-m+k} can be written as follows:

$$s_{N-m+k} = y_{pf}^{next}(k) = \overbrace{\sum_{k'=k+1}^{C} h_{k'} x_{N-k'+k}}^{ICI} + \overbrace{\sum_{k'=0}^{k} h_{k'} x_{N-G+k-k'}^{next}}^{ISI} \quad 0 \leq k \leq m-1 \tag{5.4}$$

where x_i^{next} represents the ith time-domain transmitted data point of the next OFDM symbol. Since x and x^{next} are independent, σ_S^2 will be as follows:

$$\sigma_S^2 = \frac{\sigma_X^2}{N} \sum_{k=0}^{m-1} \sum_{k'=k+1}^{C} \sigma_{h_{k'}}^2 + \frac{\sigma_X^2}{N} \sum_{k=0}^{m-1} \sum_{k'=0}^{k} \sigma_{h_{k'}}^2 = \frac{m \sigma_X^2 \sigma_H^2}{N} \tag{5.5}$$

To evaluate the power of interference terms, $\overline{I_i^r S_i^*}$ need to be calculated. Using the definition of I_i^r and S_i,

$$\overline{I_i^r S_i^*} = \frac{1}{N} \sum_{k=0}^{m-1} \sum_{k'=k+1}^{C} \sum_{k''=1}^{N-1} \Gamma_{k''}^r \overline{h_{k'}^* H_{((i-k''))_N}} \times \overline{x_{N-k'+k}^* X_{((i-k''))_N}} e^{-\frac{j2\pi(mk''-ik)}{N}} \tag{5.6}$$

Using $\overline{h_{k'}^* H_{((i-k''))_N}} = \sigma_{h_{k'}}^2 e^{-\frac{j2\pi k'(i-k'')}{N}}$ and $\overline{x_{N-k'+k}^* X_{((i-k''))_N}} = \frac{\sigma_X^2}{N} e^{-\frac{j2\pi(k-k')(i-k'')}{N}}$, Eq. 5.6 can be simplified as follows:

$$\begin{aligned}
\overline{I_i^r S_i^*} &= \frac{\sigma_X^2}{N^2} \sum_{k=0}^{m-1} \sum_{k'=k+1}^{C} \sigma_{h_{k'}}^2 \sum_{k''=1}^{N-1} \Gamma_{k''}^r e^{\frac{j2\pi k''(k-m)}{N}} \\
&= \frac{\sigma_X^2}{N^2} \sum_{k=0}^{m-1} \sum_{k'=k+1}^{C} \sigma_{h_{k'}}^2 (N \gamma_{((k-m))_N}^r - \Gamma_0^r) \\
&= -\frac{N-m}{N^2} \sigma_X^2 \sum_{k=0}^{m-1} \sum_{k'=k+1}^{C} \sigma_{h_{k'}}^2
\end{aligned} \tag{5.7}$$

$\gamma^r_{((k-m))_N}$ is zero for the given range of k. Therefore, the total interference power and average Signal-to-Interference Ratio for $m > 0$ (SIR^r_{ave}) will be as follows:

$$\begin{aligned} \overline{|I^r_i + S_i|^2} &= \tfrac{(2N-m)m}{N^2}\sigma^2_X\sigma^2_H - 2\tfrac{N-m}{N^2}\sigma^2_X \textstyle\sum_{k=0}^{m-1}\sum_{k'=k+1}^{C}\sigma^2_{h_{k'}} \Rightarrow \\ SIR^r_{ave} &= \frac{(N-m)^2}{(2N-m)m - 2\frac{N-m}{\sigma^2_H}\sum_{k=0}^{m-1}\sum_{k'=k+1}^{C}\sigma^2_{h_{k'}}} \end{aligned} \tag{5.8}$$

5.2.2 Case of timing errors to the left $(m < 0)$

In this case, due to the presence of the cyclic prefix, the number of data points that are missed can be less than $-m$. If the length of the channel delay spread spans C sampling periods, only $d = max(C - (G + m), 0)$ data points are corrupted due to the interference from the previous symbol. Therefore,

$$y^l_i = \vartheta_{((i+m))_N} \times \gamma^l_i + \psi_i + w^l_i \quad 0 \le i \le N-1 \tag{5.9}$$

Where y^l_i is a sample of the received signal for $m < 0$, $\psi_i = \begin{cases} y_{pf}(G+m+i) & 0 \le i \le d-1 \\ 0 & d \le i \le N-1 \end{cases}$ with $y_{pf}(i)$ representing the ith sample of the output cyclic prefix of the current OFDM symbol (excluding the effect of AWGN), $\gamma^l_i = \begin{cases} 0 & 0 \le i \le d-1 \\ 1 & d \le i \le N-1 \end{cases}$ and w^l_i is a sample of AWGN. Then Y^l_i, the FFT of y^l_i, will be,

$$Y^l_i = \frac{\Gamma^l_0}{N} H_i X_i e^{\frac{j2\pi mi}{N}} + \underbrace{\overbrace{\sum_{k=1}^{N-1}\frac{\Gamma^l_k}{N} H_{((i-k))_N} X_{((i-k))_N} e^{\frac{j2\pi m(i-k)}{N}}}^{I^l_i} + \Psi_i}_{ICI \quad \& \quad ISI} + W^l_i \tag{5.10}$$

where Ψ_i is the FFT of ψ_i and Γ^l_i, the FFT of γ^l_i, is $\Gamma^l_i = \begin{cases} \frac{e^{-\frac{j2\pi id}{N}}-1}{1-e^{-\frac{j2\pi i}{N}}} & i \ne 0 \\ N-d & i = 0 \end{cases}$. Then, similar to the $m > 0$ case, the power of I^l_i will be $\sigma^2_{I^l} = \frac{(N-d)d}{N^2}\sigma^2_X\sigma^2_H$. Next, the power of

$\Psi_i = \sum_{k=0}^{d-1} \psi_k e^{-\frac{j2\pi ki}{N}}$, σ_Ψ^2, is calculated. ψ_k can be written as follows:

$$\psi_k = \sum_{k'=0}^{G+m+k} h_{k'} x_{N+m+k-k'} + \sum_{k'=G+m+k+1}^{C} h_{k'} x_{N-k'+G+m+k}^{prev} \quad 0 \leq k \leq d-1 \tag{5.11}$$

where x_i^{prev} represents the ith time-domain transmitted data point of the previous OFDM symbol. Then σ_Ψ^2 will be as follows:

$$\sigma_\Psi^2 = \frac{\sigma_X^2}{N} \sum_{k=0}^{d-1} \sum_{k'=0}^{G+m+k} \sigma_{h_{k'}}^2 + \frac{\sigma_X^2}{N} \sum_{k=0}^{d-1} \sum_{k'=G+m+k+1}^{C} \sigma_{h_{k'}}^2 = \frac{d\sigma_X^2 \sigma_H^2}{N} \tag{5.12}$$

Similar to the case of $m > 0$, $\overline{I_i^l \Psi_i^*}$ will be as follows:

$$\overline{I_i^l \Psi_i^*} = -\frac{N-d}{N^2} \sigma_X^2 \sum_{k=0}^{d-1} \sum_{k'=0}^{G+m+k} \sigma_{h_{k'}}^2 \tag{5.13}$$

Therefore, the total interference power and SIR_{ave}^l for $m < 0$ are as follows:

$$\begin{aligned} \overline{|I_i^l + \Psi_i|^2} &= \tfrac{(2N-d)d}{N^2} \sigma_X^2 \sigma_H^2 - 2\tfrac{N-d}{N^2} \sigma_X^2 \textstyle\sum_{k=0}^{d-1} \sum_{k'=0}^{G+m+k} \sigma_{h_{k'}}^2 \Rightarrow \\ SIR_{ave}^l &= \frac{(N-d)^2}{(2N-d)d - 2\frac{N-d}{\sigma_H^2} \sum_{k=0}^{d-1} \sum_{k'=0}^{G+m+k} \sigma_{h_{k'}}^2} \end{aligned} \tag{5.14}$$

5.2.3 Simulation Results

The effect of timing errors on the performance of an OFDM system for both $m > 0$ and $m < 0$ cases is simulated. In this simulation $N = 512$ and $G = 52$. The power-delay profile of channel c5.1 is as follows:

Power-delay profile of channel c5.1:

[0.1214 0.1529 0 0 0.1924 0.1529 0 0.1160 0.0965 0.0766 0.0609 0.0305]

where the numbers are the fractioned received power at increasing delays in sampling period[2]. Fig. 5.2 shows average SIR resulting from the analysis (Eq. 5.8 and 5.14) and simulation for this channel. Since the length of channel c5.1 spans only 21% of the guard

[2]These fractioned received power values at different delays spaced at sampling period are sometimes called "channel taps".

interval, the interference power will be zero ($d = 0$) for $-42 < m < 0$. Furthermore, the level of interference for $m > 0$ and $m < 0$ is different. This non-symmetric effect of the timing errors can be seen from Fig. 5.2. Furthermore, the results of the analysis and simulation match well. To see the effect of $m < 0$ more prominently, the effect of timing errors is simulated for channel c5.2. This channel has the same power delay profile as channel c5.1 but the last five delay-profile samples are delayed such that the total delay spread spans 48% of the guard interval. Fig. 5.3 has plots of simulation and analysis for channel c5.2. Increasing the delay spread does not have a significant effect for $m > 0$. However, for $m < 0$, the interference power is only zero for the reduced range of $-28 < m < 0$. The match of simulation and analysis results can be seen in Fig. 5.3.

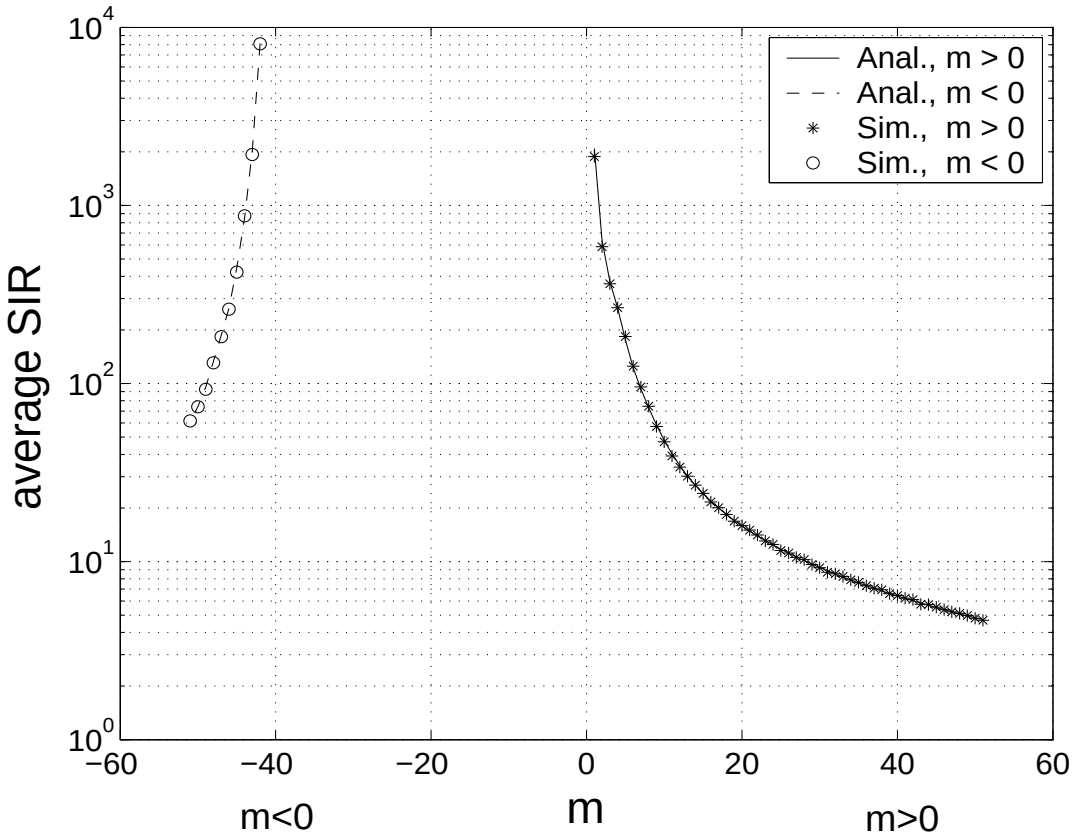

Figure 5.2: Average SIR vs. m (analysis and simulation) for channel c5.1

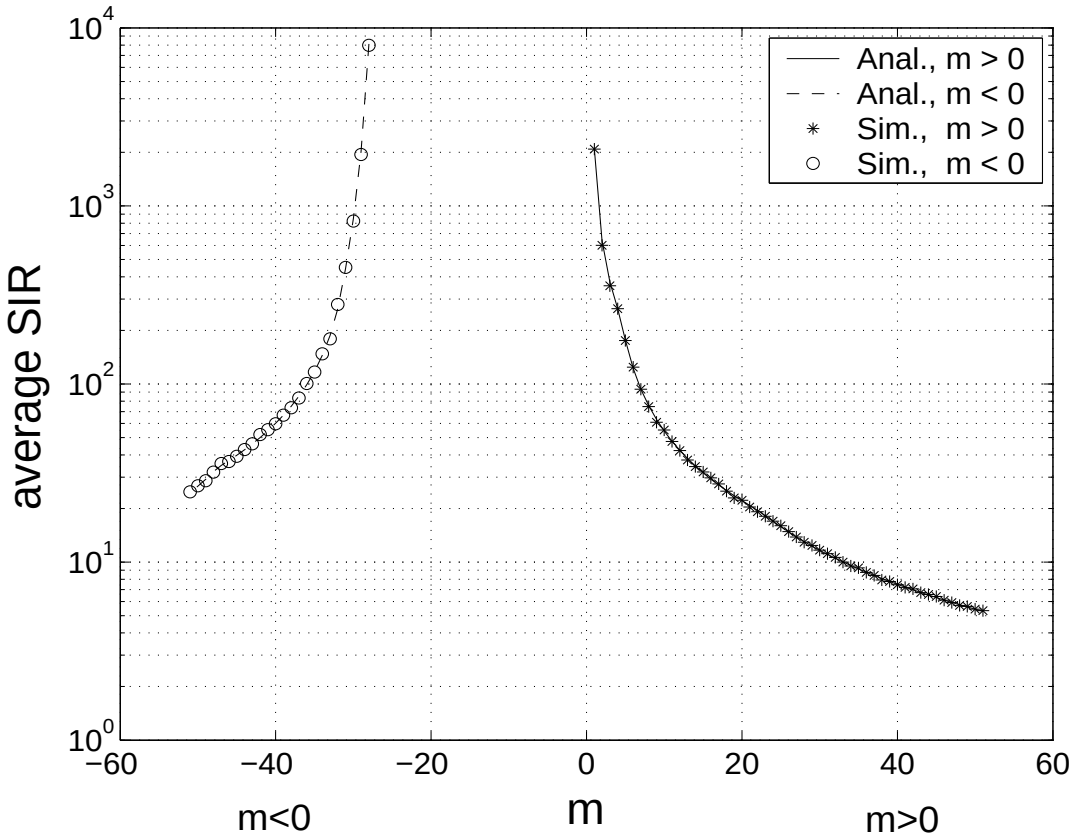

Figure 5.3: Average SIR vs. m (analysis and simulation) for channel c5.2

5.2.4 Effect of timing errors on the trigonometric interpolator, case of $m > 0$

In this section we explore the effect of timing errors on the performance of a pilot-aided channel estimator. Consider the case of $m \geq 0$. Let $H_{eq}(i) = \sum_k h_{eq}(k) e^{-\frac{j2\pi ik}{N}}$ represent the relationship between the transmitted data point at the ith sub-carrier, X_i, and the received data point,Y_i^r in this case, (h_{eq} is the IFFT of H_{eq}). Using Eq. 5.2,

$$H_{eq}^r(i) = \frac{\Gamma_0^r}{N} H_i e^{\frac{j2\pi mi}{N}} \tag{5.15}$$

Then,

$$h_{eq}^r(k) = \frac{\Gamma_0^r}{N} h_{((k+m))_N} \tag{5.16}$$

As can be seen from Eq. 5.16, a timing synchronization error of $m > 0$ introduces a rotation of m sampling periods in the base of N in the equivalent channel. This rotation will result in the expansion of the channel beyond its maximum predicted length. Fig. 5.4b shows the equivalent channel for the original channel of length $L-1$ shown in Fig. 5.4a (L is as defined in Chapter 4). As can be seen, a rotation has occurred and resulted in the expansion of the equivalent channel beyond the maximum predicted channel length of ν (ν is defined in Section 4.3). Even one error to the right side will result in an equivalent channel of length $N-1$. This will degrade the performance of the channel estimator, as it assumes an equivalent channel that spans L sampling periods at maximum. To see the effect of timing errors on channel estimation analytically, consider the case that $L \geq \nu+1$ equally-spaced frequency-domain pilot tones, $X_{pilot}(l_i)$ for $0 \leq i \leq L-1$, are inserted among the sub-carriers where $l_i = \frac{i \times N}{L}$. Then,

$$\hat{H}^r_{eq}(l_i) = \frac{Y^r_{l_i}}{X_{pilot}(l_i)} = H^r_{eq}(l_i) + \frac{I^r_{l_i} + S_{l_i} + W^r_{l_i}}{X_{pilot}(l_i)} \quad 0 \leq i \leq L-1 \tag{5.17}$$

Through an IFFT of length L, the estimate of the channel in time-domain would be

$$\hat{h}^r_{eq}(k) = \underbrace{\frac{\Gamma^r_0}{N} h_{((k+m))_L}}_{rotation} + \underbrace{u^r_k}_{Interference} + \underbrace{v^r_k}_{AWGN} \tag{5.18}$$

Define U^r_i and V^r_i as follows:

$$U^r_i = \sum_{z=0}^{L-1} \alpha_{i,z} \frac{I^r_{l_z} + S_{l_z}}{X_{pilot}(l_z)} \quad \& \quad V^r_i = \sum_{z=0}^{L-1} \alpha_{i,z} \frac{W^r_{l_z}}{X_{pilot}(l_z)} \tag{5.19}$$

Then u^r and v^r will be the IFFTs of U^r and V^r respectively and $\alpha_{i,z} = \frac{1}{L}\sum_{g=0}^{L-1} e^{j2\pi g(\frac{z}{L}-\frac{i}{N})}$ as defined in Chapter 4.

As can be seen from Eq. 5.18, there are three factors contributing to channel estimation error: effect of rotation, interference and noise. The first factor occurs because the equivalent channel has a rotation in the base of N while the estimated equivalent channel has a rotation in the base of L. Since L is chosen based on the maximum predicted length of the original channel, ν, it is typically considerably smaller than N. Therefore,

the mismatch between the equivalent channel and the estimated equivalent channel can be considerable, solely due to the first factor. Fig. 5.4c shows the estimated equivalent channel for the equivalent channel of Fig. 5.4b (effect of interference and noise is not shown on the figure). Comparing Fig. 5.4b and 5.4c, a mismatch can be observed in the location of the first m samples of the original channel. Since these samples are typically strong, this can result in a considerable performance degradation of the channel estimator[3]. To analytically assess the contribution of each of the aforementioned factors, an expression for channel estimation error is derived next. Channel estimation error will be,

$$\Delta H^r_{eq}(i) = \underbrace{\sum_{k=0}^{m-1} \beta^r_{i,k} h_k}_{rotation} + \underbrace{U^r_i}_{interference} + \underbrace{V^r_i}_{AWGN} \qquad 0 \leq i \leq N-1 \tag{5.20}$$

where ΔH^r_{eq} represents the frequency-domain channel estimation error for $m > 0$ and $\beta^r_{i,k} = \frac{N-m}{N} \times e^{\frac{-j2\pi i(k-m)}{N}} \times (1 - e^{-\frac{j2\pi iL}{N}})$. First $\overline{U^r_i h^*_k}$ is calculated.

$$\begin{aligned}
\overline{U^r_i h^*_k} &= \sum_{z=0}^{L-1} \alpha_{i,z} \overline{\left[\frac{S_{l_z} h^*_k}{X_{pilot}(l_z)}\right]} \\
&= \sum_{k'=0}^{m-1} \sum_{k''=k'+1}^{C} \overline{h_{k''} h^*_k} \sum_{z=0}^{L-1} \alpha_{i,z} \overline{\left[\frac{x_{N-k''+k'}}{X_{pilot}(l_z)}\right]} e^{-\frac{j2\pi(k'-m)z}{L}} \\
&= \frac{1}{N} \sum_{k'=0}^{m-1} \sum_{k''=k'+1}^{C} \overline{h_{k''} h^*_k} \sum_{z=0}^{L-1} \alpha_{i,z} e^{-\frac{j2\pi[(k'-m)z-(k'-k'')z]}{L}} \\
&= \frac{1}{N} \left[\sum_{k''=1}^{m-1} k'' \overline{h_{k''} h^*_k} + m \sum_{k''=m}^{C} \overline{h_{k''} h^*_k}\right] \sum_{z=0}^{L-1} \alpha_{i,z} e^{-\frac{j2\pi(k''-m)z}{L}}
\end{aligned} \tag{5.21}$$

Since $0 \leq k \leq m-1$, the second term in the bracket is zero. Therefore,

$$\overline{U^r_i h^*_k} = \begin{cases} \frac{k}{N} \sigma^2_{h_k} \sum_{z=0}^{L-1} \alpha_{i,z} e^{-\frac{j2\pi(k-m)z}{L}} & k \geq 1 \\ 0 & k = 0 \end{cases} \tag{5.22}$$

[3]It should be noted that in Fig. 5.4, the estimated equivalent channel is not a rotated version of the equivalent channel. Therefore their Fourier transforms, i.e. H^r_{eq} and $\hat{H}^r_{eq}$, are different in both amplitudes and phases.

and,

$$\begin{aligned}\sum_{k=0}^{m-1}\beta_{i,k}^{*r}\overline{U_i^r h_k^*} &= \frac{1}{N}\sum_{k=1}^{m-1}k\sigma_{h_k}^2\beta_{i,k}^{*r}\sum_{z=0}^{L-1}\alpha_{i,z}e^{-\frac{j2\pi(k-m)z}{L}} \\ &= \frac{1}{NL}\sum_{k=1}^{m-1}k\sigma_{h_k}^2\beta_{i,k}^{*r}\sum_{z'=0}^{L-1}\sum_{z=0}^{L-1}e^{\frac{j2\pi(z'-k+m)z}{L}}e^{-\frac{j2\pi z'i}{N}} \qquad (5.23)\end{aligned}$$

Since $1 \leq z' - k + m \leq L - 2 + m$, therefore, Eq. 5.23 will be non-zero if $z' - k + m = L$ and $m \geq 2$. Since for any k in the given range of Eq. 5.23, $0 \leq L + k - m \leq L - 1$ for $m \leq L + 1$, there will always be a z' that will make $z' - k + m = L$. Therefore,

$$\sum_{k=0}^{m-1}\beta_{i,k}^{*r}\overline{U_i^r h_k^*} = \frac{1}{N}\sum_{k=1}^{m-1}k\sigma_{h_k}^2\beta_{i,k}^{*r}e^{-\frac{j2\pi(L+k-m)i}{N}} \qquad (5.24)$$

Then,

$$\sum_{k=0}^{m-1}\beta_{i,k}^{*r}\overline{U_i^r h_k^*} = \begin{cases}\frac{(N-m)\times(e^{-\frac{j2\pi Li}{N}}-1)}{N^2}\sum_{k=1}^{m-1}k\sigma_{h_k}^2 & m \geq 2 \\ 0 & m = 1\end{cases} \qquad (5.25)$$

Noting that the Gaussian noise term is independent of the first two terms on the right hand side of Eq. 5.20, the following expression can be derived for channel estimation error:

$$\overline{|\Delta H_{eq}^r(i)|^2} = \sum_{k=0}^{m-1}|\beta_{i,k}^r|^2\sigma_{h_k}^2 + \sigma_{U_i^r}^2 + \sigma_{V_i^r}^2 + 2Real(\sum_{k=0}^{m-1}\beta_{i,k}^{*r}\overline{U_i^r h_k^*}) \qquad (5.26)$$

Using the expression for β^r (β^r is defined for Eq. 5.20), the following expressions can be derived: $|\beta_{i,k}^r|^2 = 4\frac{(N-m)^2}{N^2}sin^2(\frac{\pi iL}{N})$ and $\sigma_{V_i^r}^2 = \frac{\sigma_W^2}{\sigma_X^2}$. An expression for $\sigma_{U_i^r}^2$ is derived next.

$$\sigma_{U_i^r}^2 = \sum_{z=0}^{L-1}\sum_{z'=0,z'\neq z}^{L-1}\alpha_{i,z}\alpha_{i,z'}^*E\left[\frac{(I_{l_z}^r + S_{l_z}) \times (I_{l_{z'}}^{r*} + S_{l_{z'}}^*)}{X_{pilot}(l_z)X_{pilot}^*(l_{z'})}\right] + \sum_{z=0}^{L-1}|\alpha_{i,z}|^2\frac{\overline{|I_{l_z}^r + S_{l_z}|^2}}{\sigma_X^2} \qquad (5.27)$$

It can be shown, using the expression of I^r of Eq. 5.2, that $E\left[\frac{I_{l_z}^r \times I_{l_{z'}}^{r*}}{X_{pilot}(l_z)X_{pilot}^*(l_{z'})}\right] = 0$ for $z \neq z'$. To see this note that for $1 \leq k, k' \leq N-1$ and $z \neq z'$, $E\left[\frac{X_{l_z-k}X_{l_{z'}-k'}^*}{X_{pilot}(l_z)X_{pilot}^*(l_{z'})}\right] = 0$ as $X_{pilot}(g) = X_g$ for an arbitrary g.

For $g \neq g'$, the following expression can be written,

$$\overline{\left[\frac{I_g^r S_{g'}^*}{X_g X_{g'}^*}\right]} = \sum_{k=0}^{m-1} \sum_{k'=k+1}^{C} \sum_{k''=1}^{N-1} \frac{\Gamma_{k''}^r}{N} \overline{H_{((g-k''))_N} h_{k'}^*} \overline{\left[\frac{X_{((g-k''))_N} x_{N-k'+k}^*}{X_g X_{g'}^*}\right]} e^{\frac{j2\pi[g'(k-m)+m(g-k'')]}{N}} \tag{5.28}$$

Since $k'' \geq 1$,

$$\overline{\left[\frac{X_{((g-k''))_N} x_{N-k'+k}^*}{X_g X_{g'}^*}\right]} = \frac{1}{N} \sum_{k'''=0}^{N-1} \overline{\left[\frac{X_{k'''}^* X_{((g-k''))_N}}{X_g X_{g'}^*}\right]} e^{\frac{-j2\pi k'''(k-k')}{N}} = 0 \quad g \neq g' \tag{5.29}$$

Therefore,

$$E\left[\frac{I_g^r S_{g'}^*}{X_g X_{g'}^*}\right] = 0 \quad g \neq g' \tag{5.30}$$

Using Eq. 5.30, Eq. 5.27 can be written as follows:

$$\sigma_{U_i^r}^2 = \sum_{z=0}^{L-1} \sum_{z'=0, z' \neq z}^{L-1} \alpha_{i,z} \alpha_{i,z'}^* E\left[\frac{S_{l_z} S_{l_{z'}}^*}{X_{pilot}(l_z) X_{pilot}^*(l_{z'})}\right] + \sum_{z=0}^{L-1} |\alpha_{i,z}|^2 \frac{\overline{|I_{l_z}^r + S_{l_z}|^2}}{\sigma_X^2} \tag{5.31}$$

For an arbitrary k'' and g'' where $k'' \neq g''$, the following expression can be written,

$$E\left[\frac{S_{k''} S_{g''}^*}{X_{k''} X_{g''}^*}\right] = E\left[\frac{\sum_{k=0}^{m-1} s_{N-m+k} e^{\frac{-j2\pi k''(k-m)}{N}} \sum_{g=0}^{m-1} s_{N-m+g}^* e^{\frac{j2\pi g''(g-m)}{N}}}{X_{k''} X_{g''}^*}\right] \tag{5.32}$$

Using the expression for s from Eq. 5.4 and noting that the ICI and ISI terms of Eq. 5.4 are independent,

$$\begin{aligned} E\left[\frac{S_{k''} S_{g''}^*}{X_{k''} X_{g''}^*}\right] &= \sum_{k=0}^{m-1} \sum_{g=0}^{m-1} \sum_{k'=k+1}^{C} \sum_{g'=g+1}^{C} \overline{h_{k'} h_{g'}^*} \overline{\left[\frac{x_{N-k'+k} x_{N-g'+g}^*}{X_{k''} X_{g''}^*}\right]} e^{\frac{-j2\pi[(k-m)k''-(g-m)g'']}{N}} \\ &= \frac{1}{N^2} \sum_{k=0}^{m-1} \sum_{g=0}^{m-1} \sum_{k'=max(k,g)+1}^{C} \sigma_{h_{k'}}^2 e^{-\frac{j2\pi(k'-m)(k''-g'')}{N}} \quad k'' \neq g'' \end{aligned} \tag{5.33}$$

Therefore, the first term on the right hand side of Eq. 5.31 can be written as follows:

$$\begin{aligned}
&\textstyle\sum_{z=0}^{L-1}\sum_{z'=0,z'\neq z}^{L-1}\alpha_{i,z}\alpha_{i,z'}^{*}E\left[\frac{S_{l_z}S_{l_{z'}}^{*}}{X_{pilot}(l_z)X_{pilot}^{*}(l_{z'})}\right]= \\
&\textstyle\frac{1}{N^2L^2}\sum_{k=0}^{m-1}\sum_{g=0}^{m-1}\sum_{k'=max(k,g)+1}^{C}\sigma_{h_{k'}}^{2}\times \\
&\textstyle\sum_{z=0}^{L-1}\sum_{z'=0,z'\neq z}^{L-1}\sum_{g'=0}^{L-1}\sum_{g''=0}^{L-1}e^{j2\pi\left[g'(\frac{z}{L}-\frac{i}{N})-g''(\frac{z'}{L}-\frac{i}{N})-\frac{(k'-m)(z-z')}{L}\right]}= \\
&\textstyle\frac{1}{N^2L^2}\sum_{k=0}^{m-1}\sum_{g=0}^{m-1}\sum_{k'=max(k,g)+1}^{C}\sigma_{h_{k'}}^{2}\sum_{g'=0}^{L-1}\sum_{g''=0}^{L-1}e^{-\frac{j2\pi i(g'-g'')}{N}}\times \\
&\left[\textstyle\sum_{z=0}^{L-1}e^{\frac{j2\pi z(g'-k'+m)}{L}}\sum_{z'=0}^{L-1}e^{-\frac{j2\pi z'(g''-k'+m)}{L}}-\sum_{z=0}^{L-1}e^{\frac{j2\pi z(g'-g'')}{L}}\right]
\end{aligned} \tag{5.34}$$

Since $-L < -C+m \leq g'-k'+m \leq L-2+m$, for $m \leq L+1$ then $-L < -C+m \leq g'-k'+m \leq 2L-1$. Therefore, the first two sums inside the bracket of Eq. 5.34 will have non-zero values only for $g'-k'+m = L$ and 0. To have $g'-k'+m = 0$ and $g'-k'+m = L$, then $0 \leq k'-m \leq L-1$ and $-L \leq k'-m \leq -1$ should hold respectively. Therefore, for $-L \leq k'-m \leq L-1$, there will always be a g' in the range of $0 \leq g' \leq L-1$. In Eq. 5.34, $1 \leq k' \leq C$. For any k' in this range, $-L \leq k'-m \leq L-1$ (assuming that $m \leq L+1$, which is a reasonable assumption). Then for any k' of Eq. 5.34, there will be one and only one g' that would result in $g'-k'+m$ being a multiple of L (here only 0 or L). Therefore,

$$\begin{aligned}
&\sum_{z=0}^{L-1}\sum_{z'=0,z'\neq z}^{L-1}\alpha_{i,z}\alpha_{i,z'}^{*}E\left[\frac{S_{l_z}S_{l_{z'}}^{*}}{X_{pilot}(l_z)X_{pilot}^{*}(l_{z'})}\right]= \\
&\frac{1}{N^2}\sum_{k=0}^{m-1}\sum_{g=0}^{m-1}\sum_{k'=max(k,g)+1}^{C}\sigma_{h_{k'}}^{2}-\frac{1}{N^2}\sum_{k=0}^{m-1}\sum_{g=0}^{m-1}\sum_{k'=max(k,g)+1}^{C}\sigma_{h_{k'}}^{2}=0
\end{aligned} \tag{5.35}$$

Then,

$$\sigma_{U_i^r}^{2}=\sum_{z=0}^{L-1}|\alpha_{i,z}|^2\frac{\overline{|I_{l_z}^{r}+S_{l_z}|^2}}{\sigma_X^2} \tag{5.36}$$

Using Eq. 5.25, 5.26 and 5.8, the normalized channel estimation error at i^{th} sub-carrier

,$Ch^r_{error,norm}(i)$, can be written as follows:

$$Ch^r_{error,norm}(i) = \frac{\overline{|\Delta H^r_{eq}(i)|^2}}{\overline{|H^r_{eq}(i)|^2}} =$$
$$\underbrace{4\frac{\sum_{k=0}^{m-1}\sigma^2_{h_k} - \frac{\sum_{k=1}^{m-1} k\sigma^2_{h_k}}{N-m}\varpi(m-2)}{\sum_{k=0}^{C}\sigma^2_{h_k}} sin^2(\frac{\pi i L}{N})}_{factor\#1:rotation} + \underbrace{\frac{1}{SIR^r_{ave}(m)}}_{interference} + \underbrace{\frac{1}{SNR^r_{ave}(m)}}_{noise} \tag{5.37}$$

where $SNR^r_{ave}(m) = \frac{(N-m)^2\sigma^2_X\sigma^2_H}{N^2\sigma^2_W}$ and $\varpi(z) = 1$ for $z \geq 0$ and zero otherwise. Since, with high probability, m is much smaller than N, Eq. 5.37 can be tightly approximated as long as $\frac{k}{N-m} << 1$ for $1 \leq k \leq m-1$. For $m << \frac{N+1}{2}$, $\frac{m-1}{N-m} << 1$. Therefore, Eq. 5.37 can be tightly approximated as follows:

$$Ch^r_{error,norm}(i) \approx \underbrace{4\Upsilon^r_{\%}(m) sin^2(\frac{\pi i L}{N})}_{factor\#1:rotation} + \underbrace{\frac{1}{SIR^r_{ave}(m)}}_{interference} + \underbrace{\frac{1}{SNR^r_{ave}(m)}}_{noise} \tag{5.38}$$

where $\Upsilon^r_{\%}(m) = \frac{\sum_{k=0}^{m-1}\sigma^2_{h_k}}{\sum_{k=0}^{C}\sigma^2_{h_k}}$ represents the ratio of the power of the misplaced channel samples to the total power of the channel (see Fig. 5.4b, c). Let *factor#1* represent the effect of rotation (first term on the right-hand side of Eq. 5.38). As can be seen, it does not affect those sub-channels carrying pilot tones. However, it results in a considerable increase of error for other sub-carriers particularly for those at $i = z_{odd} \times ceil(\frac{N}{2L})$, where z_{odd} represents odd integers. In a reasonable SNR^r_{ave} environment, the overall impact of *factor#1* is considerably higher than other terms. Call the ratio of the first term to the sum of the last two terms on the right hand side of Eq. 5.38, $Ch_{error,ratio}$. Examining $Ch_{error,ratio}$ for different values of m and $\Upsilon_{\%}$ in a reasonable SNR environment shows that *factor#1* is the dominant factor with high probability.

5.2.5 Effect of timing errors on the trigonometric interpolator, case of $m < 0$

Similar expressions can be derived for the case of $m < 0$. Using Eq. 5.10,

$$H^l_{eq}(i) = \frac{\Gamma^l_0}{N} H_i e^{\frac{j2\pi mi}{N}} \tag{5.39}$$

Then,

$$h^l_{eq}(k) = \frac{\Gamma^l_0}{N} h_{((k+m))_N} \tag{5.40}$$

To see the effect of rotation in this case, Fig. 5.4d and 5.4e show the equivalent and estimated equivalent channel for the original channel of Fig. 5.4a respectively. In contrast to the case for $m > 0$, where even one error to the right resulted in an equivalent channel of length $N-1$ (see Fig. 5.4b), the equivalent channel length for $m < 0$ varies depending on the length of the channel. For instance, for a channel of length $C \leq \nu$, the equivalent channel length will be $C - m$ for $m \leq -1$. Therefore for $C - \nu \leq m \leq -1$, the equivalent length would still be less than or equal to ν, which poses no problem for the channel estimator. Furthermore, the mismatch is in the location of the last m samples of the original channel and these samples typically have the lowest amplitudes. Depending on the length of the channel, these samples may be solely occupied by noise and/or interference. Therefore, it can be seen again that errors to the left side may not cause any performance degradation, depending on the length of the channel delay spread, guard interval and number of pilots. Following the same procedure, an analytical expression can be found for the case of[4] $m < 0$,

$$\begin{aligned} Ch^l_{error,norm}(i) &= \underbrace{4\frac{\sum_{k=L+m}^{L-1}\sigma^2_{h_k} - \frac{\sum_{k=L+m}^{G+m+d-1}(k-G-m)\sigma^2_{h_k}}{N-d}\varpi(d-2)}{\sum_{k=0}^{C}\sigma^2_{h_k}} sin^2(\frac{\pi i L}{N})}_{factor\#1:rotation} + \\ & \underbrace{\frac{1}{SIR^l_{ave}(m)}}_{interference} + \underbrace{\frac{1}{SNR^l_{ave}(m)}}_{noise} \end{aligned} \tag{5.41}$$

[4]In this derivation $\sum_{z=0}^{L-1}\alpha_{i,z}\overline{\left[\frac{\Psi_{l_z}h^*_k}{X_{pilot}(l_z)}\right]}$ is derived under the assumption that $L \geq G+1$.

Performing a similar approximation, it can be shown that,

$$Ch^{l}_{error,norm}(i) \approx \underbrace{sin^2(\frac{\pi i L}{N})\Upsilon^{l}_{\%}(m)}_{factor\#1:rotation} + \underbrace{\frac{1}{SIR^{l}_{ave}(m)}}_{interference} + \underbrace{\frac{1}{SNR^{l}_{ave}(m)}}_{noise} \tag{5.42}$$

where $SNR^{l}_{ave}(m) = \frac{(N-d)^2\sigma^2_X\sigma^2_H}{N^2\sigma^2_W}$ and $\Upsilon^{l}_{\%}(m) = \frac{\sum_{k=L+m}^{L-1}\sigma^2_{h_k}}{\sum_{k=0}^{C}\sigma^2_{h_k}}$ represents the ratio of the power of the misplaced channel samples to the total power of the channel.

5.2.6 Analytical and Simulation Results of the effect of timing errors on channel estimation

As can be seen from the expressions for channel estimation error, timing errors can degrade the performance of a channel estimator considerably. It was also shown that the major contributor to channel estimation error is *factor#1*, the effect of rotation. Fig. 5.5 shows normalized channel estimation error, from both analysis and simulation results, as a function of sub-carrier for channel c5.3. Channel c5.3 has the following power-delay profile:

Power-delay profile of channel c5.3:

[0.1214 0.1969 0.0987 0.0784 0.1242 0.1969 0.0987 0.0623 0.0197]

System specifications are as follows for this result: $N = 892$ and $G = L = 223$. The channel is estimated from pilot tones at locations 0, 4, 8, ... As can be seen, for both cases of $m > 0$ and $m < 0$, *factor#1* (effect of rotation) contributes essentially all of the channel estimation error. Furthermore, it can seen that in the presence of timing errors, channel estimation error has quite high values. For example $Ch_{error,norm} = 1$ means normalized channel estimation error of 100%. Finally, the agreement of analysis (Eq. 5.38 and 5.42) and simulation results can be clearly seen.

5.3 Timing Synchronization Error Correction

It was shown that the pilot-aided channel estimator is super-sensitive to timing synchronization errors due to the effect of rotation. This sensitivity can be exploited to design a robust synchronization algorithm. After a coarse timing synchronizer has detected a start point for the symbol (different choices for this synchronizer will be discussed later in this section), $\hat{H}_{eq}(k)$ can be obtained using the pilot tones. This channel estimate may be far from $H_{eq}(k)$ in the presence of timing errors . Call $\hat{X}_k = \frac{Y_k}{\hat{H}_{eq}(k)}$, the estimated input. Let $\tilde{X}_k = Dec(\hat{X}_k)$ represent the estimated input after passing through the decision device. Define a decision-directed measure function as $MF = \sum_{k=0}^{N-1} |\hat{X}_k - \tilde{X}_k|^2$. In the presence of *factor#1*, MF becomes very large, as is shown in the previous section. Therefore, synchronization error correction can be obtained through minimizing MF. Note that timing errors are solely detected through the large impact of *factor#1* on the performance. Therefore, as long as *factor#1* is the major cause of performance loss, which is the case with high probability, we can detect timing errors. Due to the presence of *factor#1*, it is possible to perform all the updates neccesary to find the best timing correction solely in the frequency-domain without a need to go back and forth from frequency to time domain. Consider correcting errors to the right. As can be seen from Fig. 5.4c, the position of the last m samples of the estimated channel is different from that of the equivalent channel, where m is unknown. Therefore the estimated channel will be updated through an iterative process, correcting for one mismatched channel sample at a time. This means that at the first iteration, the last channel sample in $\hat{h}^r_{eq}(k)$ should be transferred from position $L-1$ to position $N-1$. Following the same procedure, the update necessary in the ith iteration ($i \geq 1$) for the kth sub-channel for correcting errors to the right will be as follows (a channel sample is moved from position $L-i$ to $N-i$):

$$\hat{H}^{(i+1),r}_{eq}(k) = \hat{H}^{(i),r}_{eq}(k) + \varsigma \times \hat{h}^r_{eq}(L-i) \times e^{\frac{j2\pi ik}{N}} \tag{5.43}$$

Similarly for detecting errors to the left, we will have,

$$\hat{H}^{(i+1),l}_{eq}(k) = \hat{H}^{(i),l}_{eq}(k) - \varsigma \times \hat{h}^l_{eq}(i-1) \times e^{-\frac{j2\pi(i-1)k}{N}} \tag{5.44}$$

Where $\varsigma = 1 - e^{-\frac{j2\pi Lk}{N}}$ and $\hat{H}_{eq}^{(1),r}(k) = \hat{H}_{eq}^{r}(k)$ and $\hat{H}_{eq}^{(1),l}(k) = \hat{H}_{eq}^{l}(k)$. In each iteration, the measure function, $MF^{(i)}$, will be evaluated. Finally the iteration that results in the minimum MF is chosen. Call this iteration $i_{corr,z}$. $z = 1$ denotes that a timing error to the right has been detected. Similarly $z = -1$ indicates detection of an error to the left. Then it is possible to go back to the time domain and correct the start of the symbol. For $z = 1$, the initial start point of the symbol should be moved to the left by $i_{corr,z}$. The opposite will be the case for $z = -1$. In practice, a coarse synchronizer should be used for the initial timing acquisition. A traditional choice would be a sliding correlator that correlates the data points at the beginning and end of the symbol, looking for a peak. After that, fine synchronization can be achieved as described.

Note that the sensitivity of the channel estimator to *factor#1* makes it possible to design a timing synchronizer with performance considerably better than that of the traditional one. If a sub-optimum channel estimator were to be used instead, the same improvement would not be achieved for two reasons. First, due to the lack of *factor#1*, timing synchronization errors do not affect the estimated channel significantly. Therefore correcting the channel in the frequency domain, as was done in the proposed algorithm, would not result in timing error detection anymore. Then to perform a decision-directed correction, there would be a need to go back and forth between time and frequency domains, which would increase the complexity. Second, the high sensitivity of the trigonometric channel estimator allows for robust detection of synchronization errors in the presence of noise and Doppler. However, such sensitivity does not exist for other sub-optimum estimators, resulting in a rather high probability of false correction in the fine synchronization stage.

5.4 Simulation Results

An OFDM system is simulated in a high delay spread environment as is the case for Single Frequency Networks[5] (SFN). The following parameters are chosen for simulations[6]. Input modulation is 8PSK. Useful bit rate is 7.3Mbps. N=892, $L = G$=223 and $T_s = .26\mu s$.

[5]Similar (or more) improvement is also obtained with non-SFN channels.

[6]System parameters are based on the Sirius Radio second generation system specification proposal.

The simulated channels have two main clusters each with 9 non-zero delay-profile samples, to represent an SFN channel. Two power-delay profiles are considered, channels c5.4 and c5.5. The delay spread of channel c5.4 is $36.5\mu s$ spanning 64% of the guard interval. Channel c5.4 is shown in Fig. 5.6. Channel c5.5 has a similar profile, but the delay between its two clusters has increased such that the total length spans 100% of the guard interval (worst case channel) to make the impact of errors to the left side more pronounced. In both channels two main clusters are equal power as is seen in Fig. 5.6. Each channel delay-profile sample is generated as a random variable with Rayleigh distributed amplitude and uniformly distributed phase. Three methods are simulated. The first two methods utilize only the traditional correlation-based timing synchronizer. The first method picks the maximum correlation point. The second method picks the point from which the sum of the next L correlation points are maximized, hence reducing the chance of an error to the right side (which is more serious) at the price of increasing the probability of errors to the left side. The third method utilizes method I for initial coarse synchronization followed by the proposed decision-directed synchronization error correction method of the previous section. To evaluate the performance of these methods, $P_{error}(m)$, the probability of making a timing error of m sampling periods, is measured. To measure the cost of making an erroneous offset, $P_b(m)$, the average BER (bit error rate) in case of an offset of m, is used (this is the pre-decoding BER).

The first and third curves of Fig. 5.7 show $P_{error}(m)$ of the three methods, for channel c5.4 in the absence of noise. The second and fourth curves of Fig. 5.7 show $P_b(m)$ for the three methods[7]. Note that the delay of channel c5.4 spans 64% of the guard interval. This allows for timing offsets of up to 36% of the guard interval (which becomes 82 sampling points) to the left to occur without any loss of performance. This thesis refers to this region as the "*safe zone*" which can be seen in Fig. 5.7. The proposed method has considerably lower probability of synchronization error in the places that BER is high and mainly has timing offsets in the *safe zone*. From $P_{error}(m)$ and $P_b(m)$, the average BER due to

[7]Note that $P_b(m)$ of method III is different from that of method I and II. To obtain $P_b(m)$ at a specific timing synchronization offset, bit error rate should be averaged over different input, noise and channel realizations at that synchronization offset. For a given offset of m, channel realizations that would lead to that offset are different for method III than for methods I and II. This is due to the fact that method III uses channel estimation to correct timing errors.

timing synchronization errors, $\bar{P}_b$, can be found: $\bar{P}_b = \sum_m P_b(m)P_{error}(m)$. For channel c5.4, $\bar{P}_b$ would be as follows for the three methods: $\bar{P}_{b,method\ I} = .398, \bar{P}_{b,method\ II} = .0079, \bar{P}_{b,proposed\ method} = 4.4 \times 10^{-4}$. Fig. 5.8 shows similar curves for channel c5.5. In this case, there will be more sensitivity to $m \leq -1$, since the delay spread spans 100% of the guard interval. This can be seen from P_b curves in Fig. 5.8, where there is no *safe zone*. This affects the shape of $P_{error}(m)$ of method III as can be seen. However, method II still makes a considerable number of timing errors to the left which has a heavy cost for this channel. To see the effect of noise, Fig. 5.9 shows average bit error rate vs. average received SNR for channel c5.4. The dashed line shows the BER of a perfect synchronizer for comparison. As can be seen, the proposed method has performance very close to that of the perfect synchronizer.

Overall, the proposed method is robust in mitigating timing synchronization errors and can be a promising candidate to accompany a pilot-aided channel estimator in OFDM systems.

5.5 Summary

This chapter started by deriving the exact expressions of interference terms (ICI and ISI) and their corresponding average powers in the presence of timing errors. The effect of timing errors on the performance of the trigonometric interpolator was then analyzed. Pilot-aided channel estimators were shown to be super-sensitive to timing synchronization errors. This was confirmed by deriving expressions for channel estimation errors in the presence of timing errors. Based on the analysis, a robust timing synchronization algorithm was proposed that does not need additional training overhead. Simulation results showed the performance of the proposed algorithm in high delay spread environments, indicating that it can reduce the error profile to be close to that of the no synchronization error case.

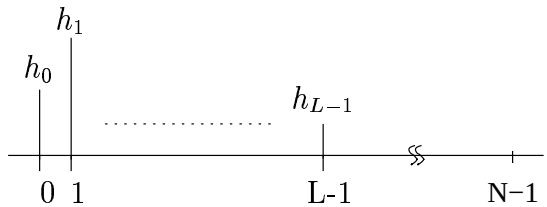

Fig. 5.4a Original channel of normalized length of $L-1$

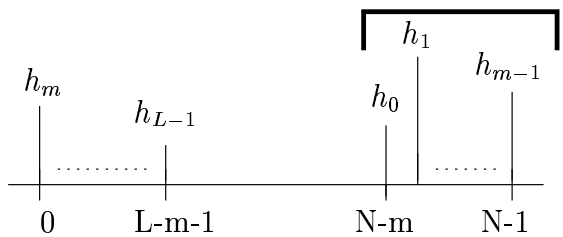

Fig. 5.4b Equivalent channel for $m \geq 1$

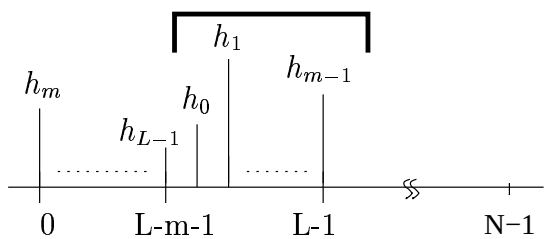

Fig. 5.4c Estimated channel for $m \geq 1$

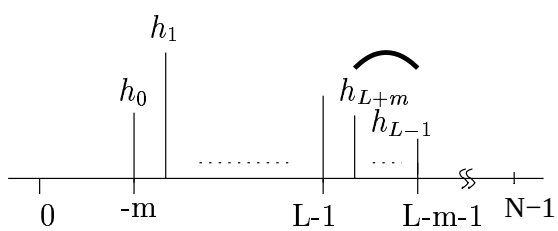

Fig. 5.4d Equivalent channel for $m \leq -1$

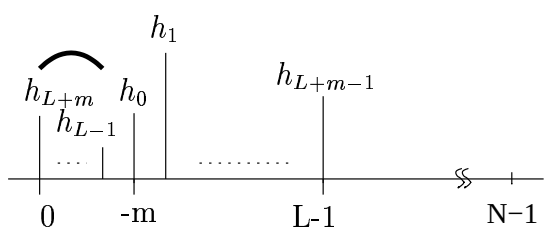

Fig. 5.4e Estimated channel for $m \leq -1$

Figure 5.4: Effect of rotation

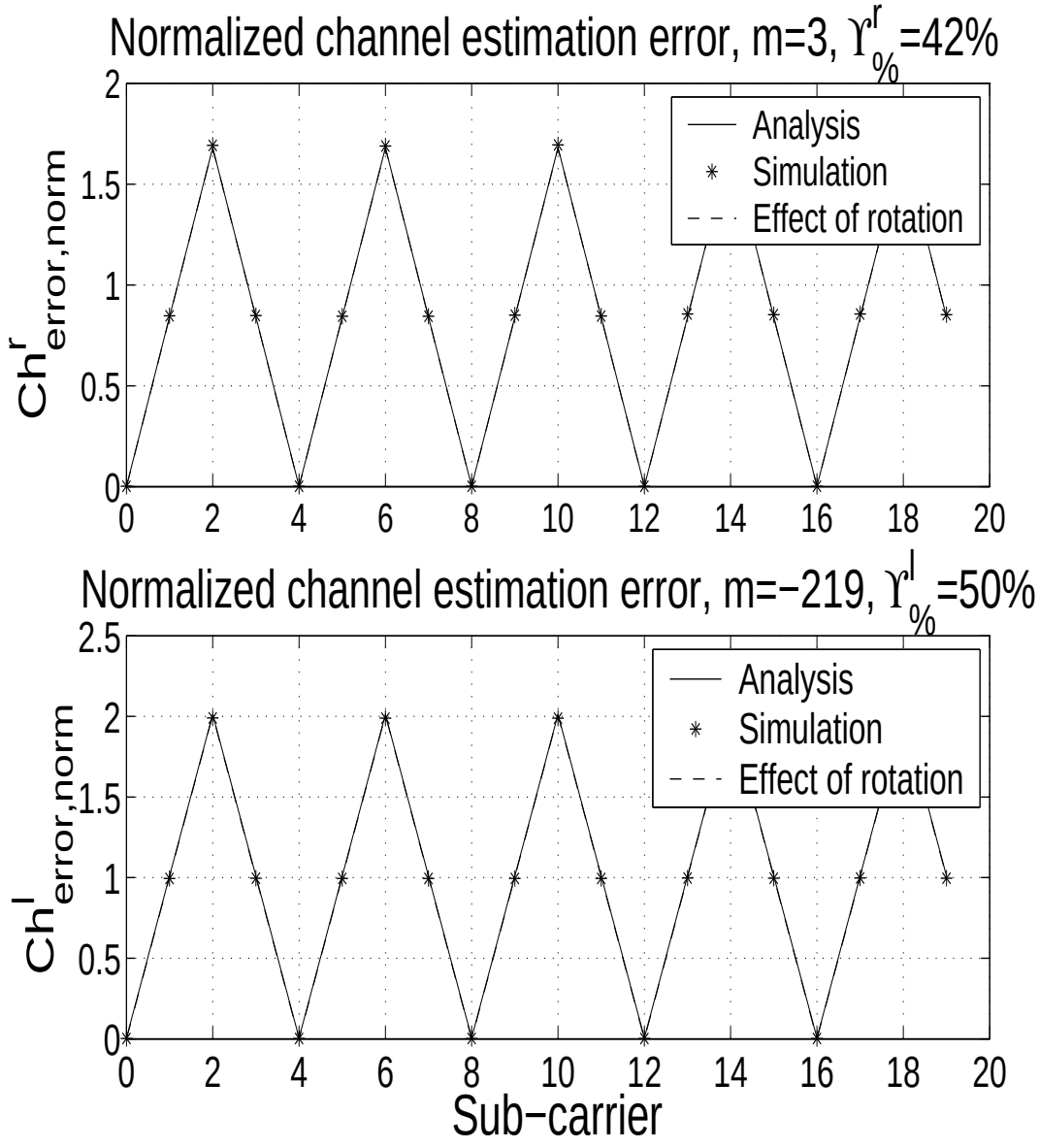

Figure 5.5: Normalized channel estimation error vs. sub-carrier for channel c5.3

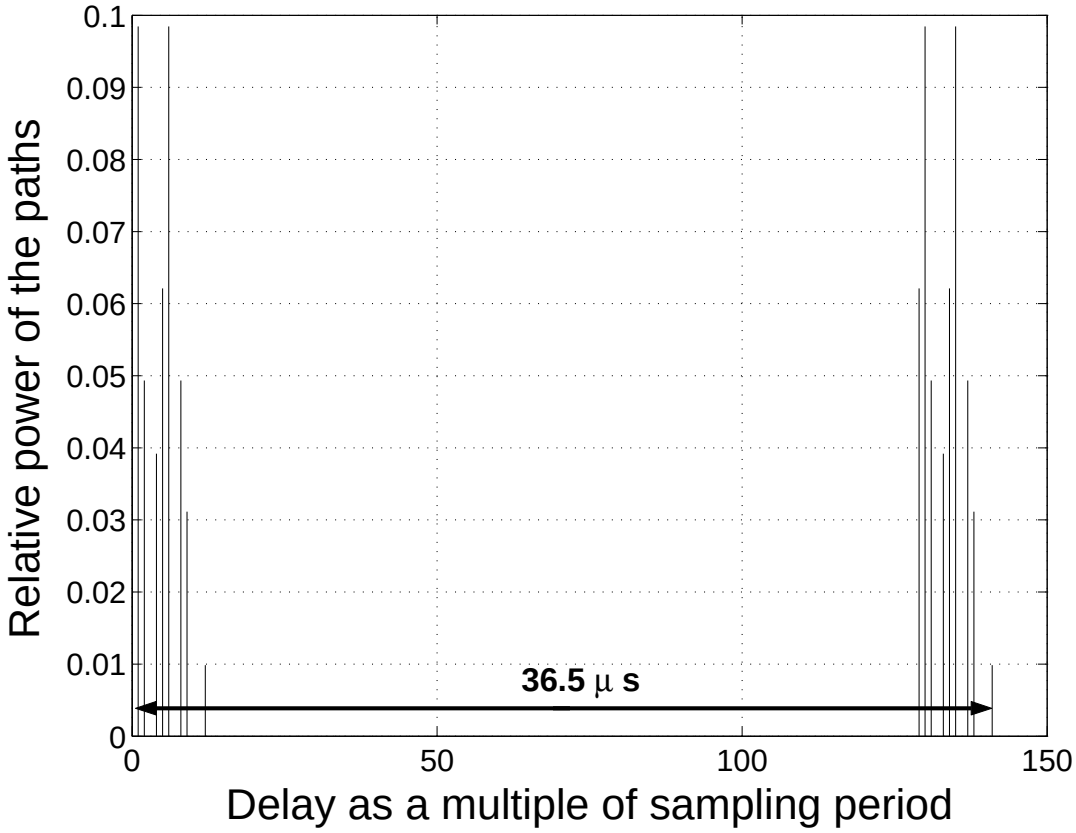

Figure 5.6: Power-Delay profile of channel c5.4

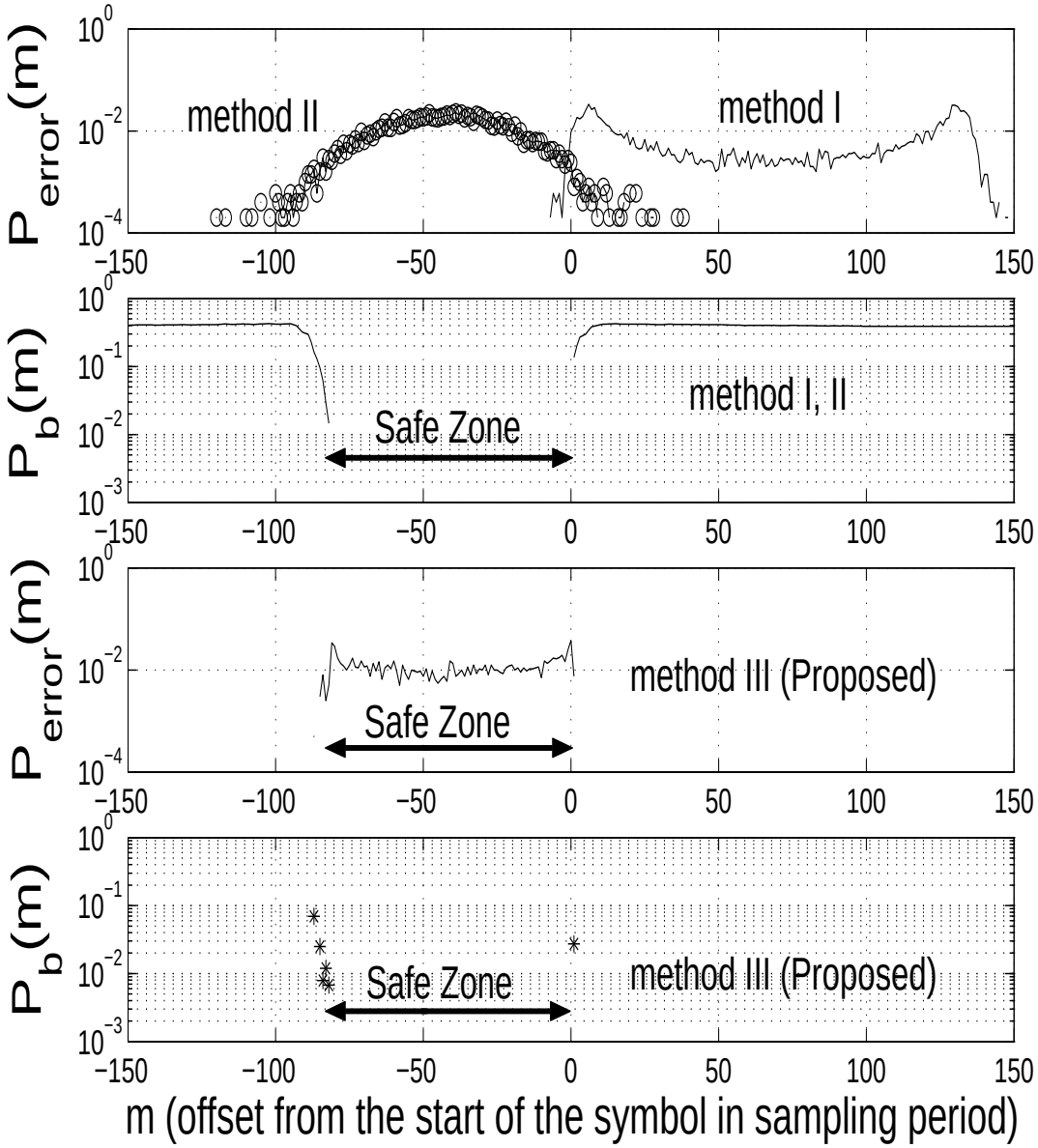

Figure 5.7: Performance for channel c5.4 in the absence of noise

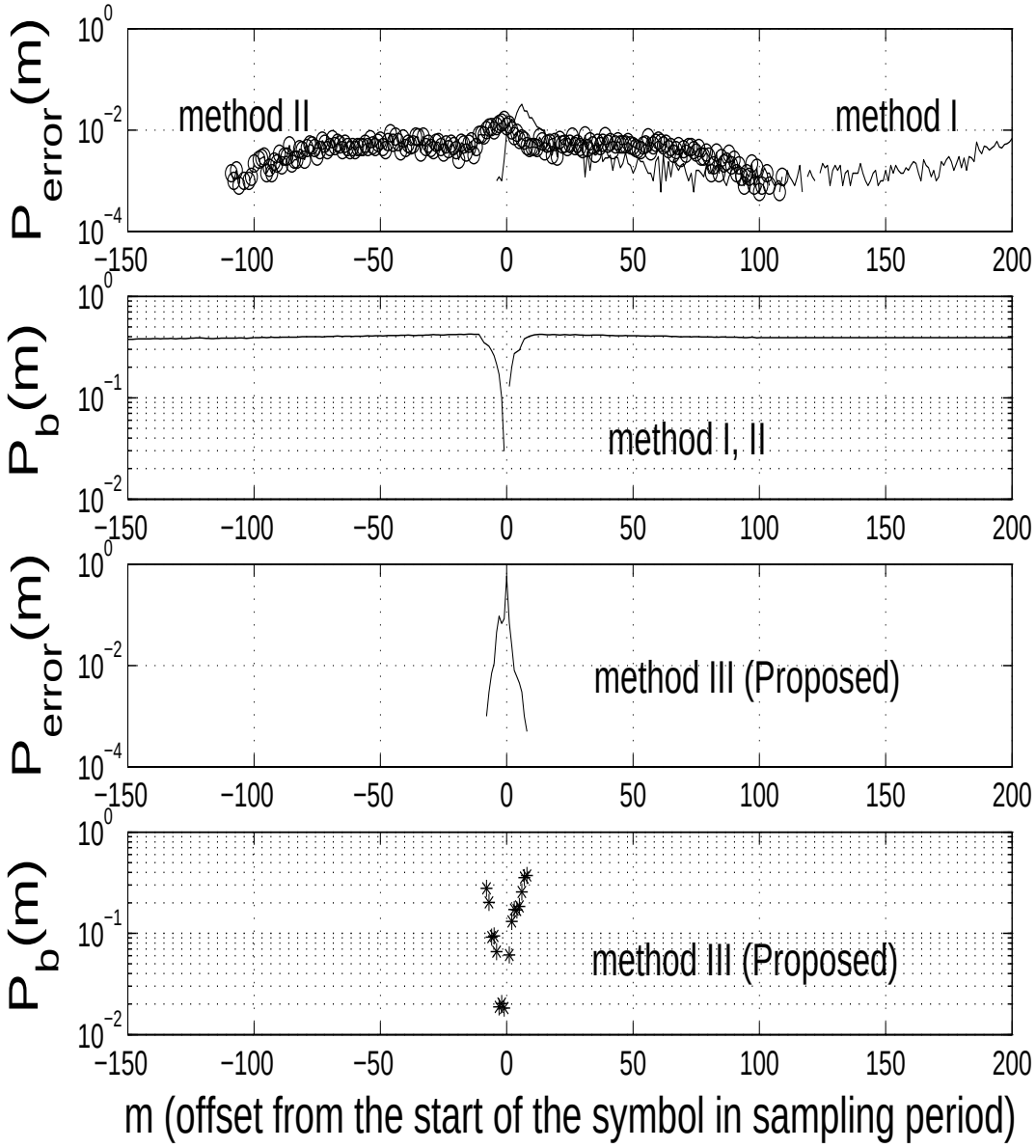

Figure 5.8: Performance for channel c5.5 in the absence of noise

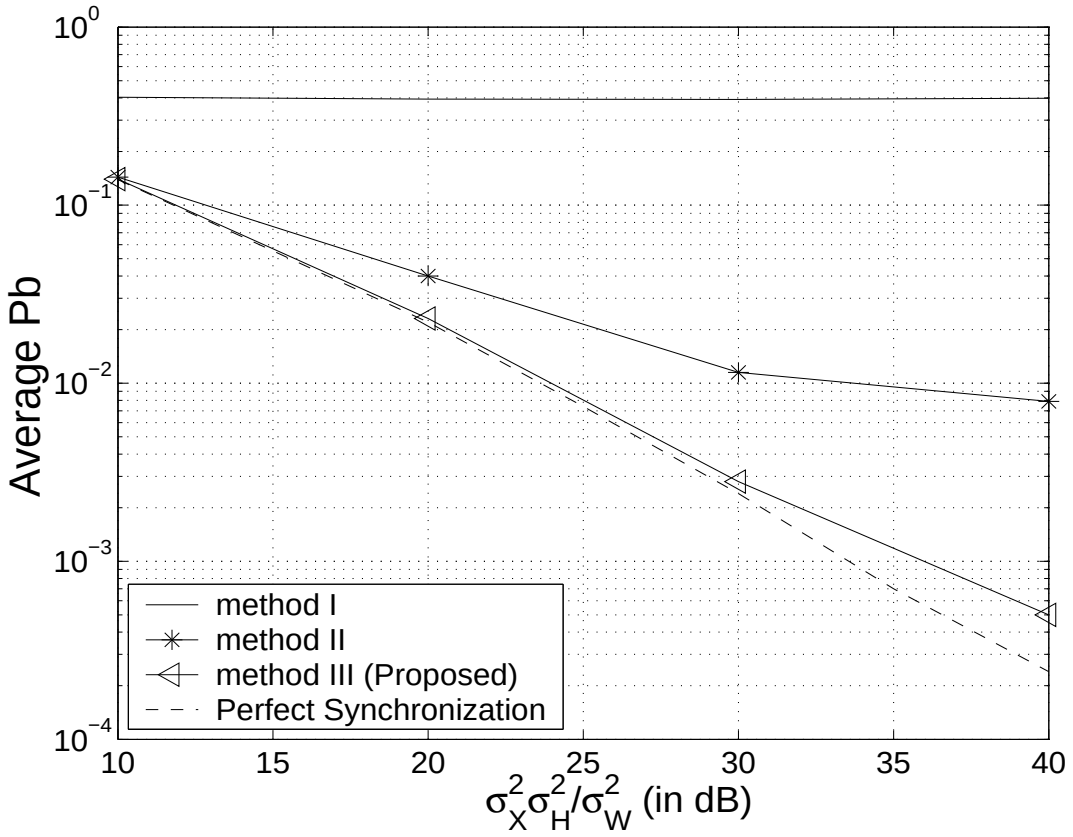

Figure 5.9: Average P_b for channel c5.4 in the presence of noise

Chapter 6

Timing Synchronization for High-Mobility Cases

Chapter 5 showed that OFDM systems are sensitive to timing synchronization errors. It also indicated that utilizing trigonometric interpolators can further increase this sensitivity. Based on the analysis, a timing synchronization algorithm was proposed that exploited this sensitivity to improve timing synchronization without additional training overhead. The analysis of Chapter 5 was carried out under low-mobility assumption. This chapter extends the analysis to high-mobility environments. High mobility refers to the cases where channel can not be considered constant over one OFDM symbol. Timing synchronization becomes more challenging for high-mobility applications. The power-delay profile of the channel may change rapidly due to the sporadic birth and death of paths in high-mobility environments which would necessitate more frequent timing synchronization. Therefore, utilizing timing synchronization algorithms that do not require training information can increase bandwidth efficiency considerably for high-mobility applications.

The effects of timing errors on an OFDM system in a mobile environment are investigated in this chapter . Expressions are derived for average SIR in the presence of mobility and timing errors. The effects of these errors on channel estimation in a high-mobility environment are then investigated. Analytical expressions for channel estimation error in the presence of timing synchronization errors and mobility are found. The analysis shows

that the sensitivity of the channel estimator can still be exploited to improve timing synchronization in high-mobility environments. The algorithm proposed in the previous chapter is then extended to high-mobility applications. Finally simulation results show the performance of the algorithm in high delay spread and Doppler spread environments.

6.1 Introduction

As shown in the previous chapter, the performance of OFDM systems is sensitive to the performance of the timing synchronizer and channel estimator. Furthermore, high mobility can introduce time-variations within one OFDM symbol which ruins the performance. Each of these issues has been explored separately in the communications literature. To understand the effect of timing synchronization errors on channel estimation, Chapter 5 considered both issues. The super-sensitivity of the pilot-aided channel estimator to timing synchronization errors was shown. Based on the analysis, a robust timing synchronization algorithm was proposed that utilizes this sensitivity to correct for timing synchronization errors without requiring additional training overhead.

Timing synchronization becomes more challenging in high-mobility environments since the power-delay profile of the channel may change rapidly due to the sporadic and frequent birth and death of paths. For such applications, applying training-based algorithms for timing synchronization can increase the training overhead considerably. Furthermore, utilizing correlation-based methods would result in performance degradation due to high delay spread. Therefore the method proposed in Chapter 5 is a good candidate for such applications. It is the goal of this chapter to include high mobility in the analysis of the previous chapter.

6.2 Effect of timing Synchronization Errors in a high-mobility environment

In high-mobility environments, channel time-variations within one OFDM symbol can not be neglected. Let $h_k^{(i)}$ represent the kth sample of the channel delay profile at time instant $t = i \times T_s$. A constant channel is assumed over the time interval $i \times T_s \leq t < (i+1) \times T_s$ with $t = 0$ indicating the start of the data part of the symbol. Let $\vartheta_{mob,i}$ represent the channel output in the absence of noise and in a mobile environment. Then,

$$\vartheta_{mob,i} = \sum_{k=0}^{G} h_k^{(i)} x_{((i-k))_N} \quad 0 \leq i \leq N-1 \tag{6.1}$$

Case of $m > 0$ in the presence of high mobility

In this case, an error of m sampling periods to the right side has occurred as described in Section 5.2.1. Then, the terms $\vartheta_{mob,0}, \vartheta_{mob,1}, \ldots, \vartheta_{mob,m-1}$ are missed and instead m data points of the next OFDM symbol are erroneously selected. The received signal can thus be written as follows:

$$y_{mob,i}^r = \vartheta_{mob,((i+m))_N} \times \gamma_i^r + s_{mob,i} + w_{mob,i}^r \quad 0 \leq i \leq N-1 \tag{6.2}$$

where the superscript r denotes the case of $m > 0$. $w_{mob,i}^r$ is a sample of AWGN, γ_i^r is as defined in Chapter 5 and $s_{mob,i} = \begin{cases} 0 & 0 \leq i \leq N-m-1 \\ y_{mob,pf}^{next}(i-N+m) & else \end{cases}$.
$y_{mob,pf}^{next}(i)$ represents the ith sample of the output cyclic prefix of the next OFDM symbol (excluding the effect of AWGN) in the presence of mobility. Using the FFT of $\vartheta_{mob,i}$, it can be easily shown that the FFT of $y_{mob,i}^r$ will be as follows:

$$Y_{mob,i}^r = \underbrace{e^{\frac{j2\pi mi}{N}} H_i^{norot,r}}_{H_{mob,eq}^r(i)} X_i + \underbrace{\frac{\Gamma_0^r}{N} e^{\frac{j2\pi mi}{N}} ICI_{mob}(i)}_{ICI \quad due \quad to \quad mobility} + \tag{6.3}$$

$$\underbrace{\overbrace{\underbrace{\sum_{k=1}^{N-1}\sum_{k'=0}^{N-1}}_{k+k'\neq N}\frac{\Gamma_k^r}{N}H_{((i-k))_N,k'}X_{((i-k-k'))_N}e^{\frac{j2\pi m(i-k)}{N}}}^{I^r_{mob,i}}+S_{mob,i}+W^r_{mob,i}}_{ICI \quad \& \quad ISI \quad due \quad to \quad timing \quad errors} \quad 0\leq i\leq N-1$$

where $H_i^{norot,r}=\sum_{z=0}^{N-1}e^{-j\frac{2\pi mz}{N}}\frac{\Gamma_z^r}{N}H_{((i-z))_N,N-z}$ with $H_{i,z}=\frac{1}{N}\sum_{g=0}^{C}\sum_{g'=0}^{N-1}h_g^{(g')}e^{-\frac{j2\pi}{N}(z\times(g'-g)+g\times i)}$. Γ^r is as defined in Chapter 5, S_{mob} and W^r_{mob} are the FFTs of s_{mob} and w^r_{mob} respectively and C is as defined in Chapter 5. ICI_{mob} is the ICI term introduced solely by mobility and is defined as follows:

$$ICI_{mob}(i)=\sum_{z=1}^{N-1}H_{i,z}X_{((i-z))_N} \tag{6.4}$$

Next the power of interference terms is derived. Let the auto-correlation function of the gth channel power-delay profile sample be defined as follows: $R_g(z)=E(h_g^{(g')}h_g^{(g'-z)*})$. Then the normalized auto-correlation function will be: $R_{g,norm}(z)=\frac{R_g(z)}{\sigma_g^2}$. To make the analysis tractable, without loss of generality, the assumption is made throughout this analysis that $R_{g,norm}(z)$ is the same for all the channel delay-profile samples (hence the subscript g will be dropped, i.e. $R_{norm}(z)$). This assumption does not affect final results and conclusions of this chapter. Also for the ease of derivation, R_g is considered real in the following analysis. A complex R_g can easily be incorporated into the derivation.
The power of the second term on the right hand side of Eq. 6.3 will be as follows:

$$\begin{aligned}E(|\frac{\Gamma_0^r}{N}e^{\frac{j2\pi mi}{N}}ICI_{mob}(i)|^2) &= \frac{|\Gamma_0^r|^2}{N^2}E(|ICI_{mob}(i)|^2)\\ &= \frac{(N-m)^2\sigma_X^2}{N^2}\sum_{z=1}^{N-1}\overline{|H_{i,z}|^2}\\ &= \frac{(N-m)^2\sigma_X^2\sigma_H^2}{N^4}(N^2-\sum_{g=0}^{N-1}\sum_{g'=0}^{N-1}R_{norm}(g-g'))\end{aligned} \tag{6.5}$$

Next the average power of $I^r_{mob,i}$ is derived:

$$\sigma^2_{I^r_{mob}} = \frac{\sigma^2_X}{N^2} \underbrace{\sum_{k=1}^{N-1}\sum_{k'=0}^{N-1}}_{k+k'\neq N} \underbrace{\sum_{k''=1}^{N-1}\sum_{k'''=0}^{N-1}}_{k''+k'''\neq N} \Gamma^r_k \Gamma^{r*}_{k''} \overline{H_{((i-k))_N,k'} H^*_{((i-k''))_N,k'''}} e^{-j\frac{2\pi m(k-k'')}{N}}$$
$$for \quad k+k' = k''+k''' \quad or \quad k+k' = k''+k'''+N \quad or \quad k+k'+N = k''+k''' \tag{6.6}$$

For arbitrary z, z', n and n',

$$\begin{aligned}\overline{H_{z,z'}H^*_{n,n'}} &= \frac{1}{N^2}\sum_{g=0}^{N-1}\sum_{g'=0}^{N-1}\sum_{g''=0}^{N-1} R_g(g'-g'')e^{-\frac{j2\pi(z'(g'-g)+gz-n'(g''-g)-gn)}{N}} \\ &= \frac{1}{N^2}\sum_{g'=0}^{N-1}\sum_{g''=0}^{N-1} R_{norm}(g'-g'')\sum_{g=0}^{C}\sigma^2_g e^{-\frac{j2\pi(g(z-z'+n'-n)+z'g'-n'g'')}{N}} \end{aligned} \tag{6.7}$$

Therefore,

$$\overline{H_{((i-k))_N,k'}H^*_{((i-k''))_N,k'''}} = \frac{\sigma^2_H}{N^2}\sum_{g'=0}^{N-1}\sum_{g''=0}^{N-1} R_{norm}(g'-g'')e^{-\frac{j2\pi(k'g'-k'''g'')}{N}}$$
$$for \quad k+k' = k''+k''' \quad or \quad k+k' = k''+k'''+N \quad or \quad k+k'+N = k''+k''' \tag{6.8}$$

Next the conditions of Eq. 6.8 are checked. To have $k+k' = k''+k'''$, for every k, k' there should exist a k'' such that $0 \leq k''' = k+k'-k'' \leq N-1$. This means that there should exist a k'' in the range of $k+k'-N+1 \leq k'' \leq k+k'$. Also, for this case, if $k+k' \neq N$, then $k''+k''' \neq N$ either. To have $k+k' = k''+k'''+N$, for every k, k', there should be a k'' such that $k+k'-2N+1 \leq k'' \leq k+k'-N$. In this scenario $k''+k'''$ can not be N. To have $k+k'+N = k''+k'''$, for every k, k', there should be a k'' such that $k+k'+1 \leq k'' \leq k+k'+N$. Similarly, $k+k'$ can not be N in this case. Therefore since $k+k'-2N+1 < 1$ and $k+k'+N > N-1$, for every k, k', there always exists a set of

k'' and k''' in one of the regions of Eq. 6.6. Therefore,

$$\sigma^2_{I^r_{mob}} =$$
$$\frac{\sigma_X^2\sigma_H^2}{N^4}\underbrace{\sum_{k=1}^{N-1}\sum_{k'=0}^{N-1}}_{k+k'\neq N}\sum_{k''=1}^{N-1}\Gamma^r_k\Gamma^{r*}_{k''}\sum_{g'=0}^{N-1}\sum_{g''=0}^{N-1}R_{norm}(g'-g'')e^{-\frac{j2\pi(k'g'-(k+k'-k'')g'')}{N}}e^{-j\frac{2\pi m(k-k'')}{N}} =$$
$$\frac{\sigma_X^2\sigma_H^2}{N^4}\sum_{k=1}^{N-1}\sum_{k''=1}^{N-1}\Gamma^r_k\Gamma^{r*}_{k''}\sum_{g'=0}^{N-1}\sum_{g''=0}^{N-1}R_{norm}(g'-g'')\times$$
$$\sum_{k'=0}^{N-1}e^{-j\frac{2\pi k'(g'-g'')}{N}}e^{j\frac{2\pi g''(k-k'')}{N}}e^{-j\frac{2\pi m(k-k'')}{N}}-$$
$$\frac{\sigma_X^2\sigma_H^2}{N^4}\sum_{k=1}^{N-1}\sum_{k''=1}^{N-1}\Gamma^r_k\Gamma^{r*}_{k''}\sum_{g'=0}^{N-1}\sum_{g''=0}^{N-1}R_{norm}(g'-g'')e^{\frac{-j2\pi(-kg'+g''k'')}{N}}e^{-j\frac{2\pi m(k-k'')}{N}} \tag{6.9}$$

Therefore,

$$\begin{aligned}
\sigma^2_{I^r_{mob}} &= \frac{\sigma_X^2\sigma_H^2}{N^2}\sum_{k=1}^{N-1}|\Gamma_k|^2 - \\
&\quad \frac{\sigma_X^2\sigma_H^2}{N^4}\sum_{g'=0}^{N-1}\sum_{g''=0}^{N-1}R_{norm}(g'-g'')\sum_{k=1}^{N-1}\Gamma^r_k e^{j\frac{2\pi k(g'-m)}{N}}\sum_{k''=1}^{N-1}\Gamma^{r*}_{k''}e^{-j\frac{2\pi k''(g''-m)}{N}} \\
&= \frac{\sigma_X^2\sigma_H^2}{N^2}\sum_{k=1}^{N-1}|\Gamma_k|^2 - \frac{\sigma_X^2\sigma_H^2\Gamma_0^2}{N^4}\sum_{g'=0}^{N-1}\sum_{g''=0}^{N-1}R_{norm}(g'-g'') - \\
&\quad \frac{\sigma_X^2\sigma_H^2}{N^2}\sum_{g'=m}^{N-1}\sum_{g''=m}^{N-1}R_{norm}(g'-g'') + \\
&\quad 2\frac{\sigma_X^2\sigma_H^2(N-m)}{N^3}\sum_{g'=m}^{N-1}\sum_{g''=0}^{N-1}R_{norm}(g'-g'')
\end{aligned} \tag{6.10}$$

Next the power of $S_{mob,i}$ is calculated. $S_{mob,i} = \sum_{k=0}^{m-1} s_{mob,N-m+k}e^{-\frac{j2\pi i(k-m)}{N}}$, where $s_{mob,N-m+k}$ can be written as follows:

$$\begin{aligned}
s_{mob,N-m+k} &= y^{next}_{mob,pf}(k) \qquad 0 \le k \le m-1 \\
&= \overbrace{\sum_{k'=k+1}^{C} h^{(N-m+k)}_{k'} x_{N-k'+k}}^{ICI} + \overbrace{\sum_{k'=0}^{k} h^{(N-m+k)}_{k'} x^{next}_{N-G+k-k'}}^{ISI}
\end{aligned} \tag{6.11}$$

Similar to the case of low-mobility,

$$\sigma^2_{S_{mob}} = \frac{m\sigma^2_X\sigma^2_H}{N} \tag{6.12}$$

Next,

$$\begin{aligned}\overline{\frac{\Gamma^r_0}{N}e^{\frac{j2\pi mi}{N}}ICI_{mob}(i)S^*_{mob,i}} &= \frac{\Gamma^r_0}{N}\sum_{z=1}^{N-1}\sum_{k=0}^{m-1}\sum_{k'=k+1}^{C}\overline{h^{*(N-m+k)}_{k'}H_{i,z}}\,\overline{X_{((i-z))_N}x^*_{N-k'+k}}e^{\frac{j2\pi ik}{N}} \\ &= \frac{\sigma^2_X\Gamma^r_0}{N^2}\sum_{z=1}^{N-1}\sum_{k=0}^{m-1}\sum_{k'=k+1}^{C}\overline{h^{*(N-m+k)}_{k'}H_{i,z}}e^{-\frac{j2\pi((k-k')(i-z)-ik)}{N}}\end{aligned} \tag{6.13}$$

Since,

$$\overline{h^{*(N-m+k)}_{k'}H_{i,z}} = \frac{1}{N}\sum_{g'=0}^{N-1}R^*_{k'}(N-m+k-g')e^{-\frac{j2\pi(z(g'-k')+k'i)}{N}} \tag{6.14}$$

Therefore,

$$\begin{gathered}\overline{\frac{\Gamma^r_0}{N}e^{\frac{j2\pi mi}{N}}ICI_{mob}(i)S^*_{mob,i}} = \\ \frac{\sigma^2_X\Gamma^r_0}{N^3}\sum_{g'=0}^{N-1}\sum_{k=0}^{m-1}\sum_{k'=k+1}^{C}\sigma^2_{k'}R_{norm}(N-m+k-g')\sum_{z=1}^{N-1}e^{-\frac{j2\pi z(g'-k)}{N}} = \\ \frac{\sigma^2_X\Gamma^r_0}{N^2}\sum_{g'=0}^{m-1}\sum_{k'=g'+1}^{C}\sigma^2_{k'}R_{norm}(N-m)- \\ \frac{\sigma^2_X\Gamma^r_0}{N^3}\sum_{g'=0}^{N-1}\sum_{k=0}^{m-1}\sum_{k'=k+1}^{C}\sigma^2_{k'}R_{norm}(N-m+k-g')\end{gathered} \tag{6.15}$$

Next,

$$\overline{I^r_{mob,i}S^*_{mob,i}} =$$
$$\sum_{z=0}^{m-1}\sum_{z'=z+1}^{C}\underbrace{\sum_{k=1}^{N-1}\sum_{k'=0}^{N-1}}_{k+k'\neq N}\frac{\Gamma^r_k}{N}\overline{H_{((i-k))_N,k'}h^{*(N-m+z)}_{z'}X_{((i-k-k'))_N}x^*_{N-z'+z}}e^{\frac{j2\pi(m(i-k)+i(z-m))}{N}} =$$
$$\frac{\sigma^2_X}{N^3}\sum_{z=0}^{m-1}\sum_{z'=z+1}^{C}\underbrace{\sum_{k=1}^{N-1}\sum_{k'=0}^{N-1}}_{k+k'\neq N}\Gamma^r_k\sum_{g'=0}^{N-1}R_{z'}(N-m+z-g')e^{\frac{-j2\pi k'(g'-z)}{N}}e^{\frac{-j2\pi k(m-z)}{N}} =$$
$$\frac{\sigma^2_X}{N^3}\sum_{z=0}^{m-1}\sum_{z'=z+1}^{C}\sum_{k=1}^{N-1}\Gamma^r_k\sum_{g'=0}^{N-1}R_{z'}(N-m+z-g')\sum_{k'=0}^{N-1}e^{\frac{-j2\pi k'(g'-z)}{N}}e^{\frac{-j2\pi k(m-z)}{N}}-$$
$$\frac{\sigma^2_X}{N^3}\sum_{z=0}^{m-1}\sum_{z'=z+1}^{C}\sum_{k=1}^{N-1}\Gamma^r_k\sum_{g'=0}^{N-1}R_{z'}(N-m+z-g')e^{\frac{-j2\pi k(m-g')}{N}} =$$
$$\frac{\sigma^2_X}{N^2}\sum_{z=0}^{m-1}\sum_{z'=z+1}^{C}R_{z'}(N-m)\sum_{k=1}^{N-1}\Gamma^r_k e^{\frac{-j2\pi k(m-z)}{N}}-$$
$$\frac{\sigma^2_X}{N^3}\sum_{z=0}^{m-1}\sum_{z'=z+1}^{C}\sum_{k=1}^{N-1}\Gamma^r_k\sum_{g'=0}^{N-1}R_{z'}(N-m+z-g')e^{\frac{-j2\pi k(m-g')}{N}} =$$
$$-\frac{\sigma^2_X\Gamma^r_0}{N^2}\sum_{z=0}^{m-1}\sum_{z'=z+1}^{C}\sigma^2_{z'}R_{norm}(N-m)-$$
$$\frac{\sigma^2_X}{N^3}\sum_{z=0}^{m-1}\sum_{z'=z+1}^{C}\sum_{k=1}^{N-1}\Gamma^r_k\sum_{g'=0}^{N-1}R_{z'}(N-m+z-g')e^{\frac{-j2\pi k(m-g')}{N}} =$$
$$-\frac{\sigma^2_X\Gamma^r_0}{N^2}\sum_{z=0}^{m-1}\sum_{z'=z+1}^{C}\sigma^2_{z'}R_{norm}(N-m)-$$
$$\frac{\sigma^2_X}{N^3}\sum_{z=0}^{m-1}\sum_{z'=z+1}^{C}\sum_{g'=0}^{N-1}\sigma^2_{z'}R_{norm}(N-m+z-g')\sum_{k=1}^{N-1}\Gamma^r_k e^{\frac{-j2\pi k(m-g')}{N}} =$$
$$-\frac{\sigma^2_X\Gamma^r_0}{N^2}\sum_{z=0}^{m-1}\sum_{z'=z+1}^{C}\sigma^2_{z'}R_{norm}(N-m)+$$
$$\frac{\sigma^2_X\Gamma^r_0}{N^3}\sum_{z=0}^{m-1}\sum_{z'=z+1}^{C}\sum_{g'=0}^{N-1}\sigma^2_{z'}R_{norm}(N-m+z-g')-$$
$$\frac{\sigma^2_X}{N^2}\sum_{z=0}^{m-1}\sum_{z'=z+1}^{C}\sigma^2_{z'}\sum_{g'=m}^{N-1}R_{norm}(N-m+z-g') \tag{6.16}$$

Therefore,

$$\overline{I^r_{mob,i}S^*_{mob,i}+\frac{\Gamma^r_0}{N}e^{\frac{j2\pi mi}{N}}ICI_{mob}(i)S^*_{mob,i}} =$$
$$-\frac{\sigma^2_X}{N^2}\sum_{z=0}^{m-1}\sum_{z'=z+1}^{C}\sigma^2_{z'}\sum_{g'=m}^{N-1}R_{norm}(N-m+z-g') \tag{6.17}$$

Finally $\overline{\frac{\Gamma^r_0}{N}e^{-\frac{j2\pi mi}{N}}ICI^*_{mob}(i)I^r_{mob,i}}$ is calculated:

$$\overline{\frac{\Gamma^r_0}{N}e^{-\frac{j2\pi mi}{N}}ICI^*_{mob}(i)I^r_{mob,i}} =$$
$$\frac{\Gamma^r_0}{N^2}\sum_{z=1}^{N-1}\underbrace{\sum_{k=1}^{N-1}\sum_{k'=0}^{N-1}}_{k+k'\neq N}\Gamma^r_k\overline{H_{((i-k))_N,k'}H^*_{i,z}X_{((i-k-k'))_N}X^*_{((i-z))_N}}e^{-\frac{j2\pi mk}{N}} \tag{6.18}$$

Eq. 6.18 has non-zero values for $k+k'=z$ or $k+k'=N+z$. In both cases, $k+k'$ can not be N. Therefore,

$$\begin{gathered}\overline{\frac{\Gamma_0^r}{N}e^{-\frac{j2\pi mi}{N}}ICI^*_{mob}(i)I^r_{mob,i}} = \\ \frac{\Gamma_0^r\sigma_X^2\sigma_H^2}{N^4}\sum_{z=1}^{N-1}\sum_{k=1}^{N-1}\sum_{k'=0}^{N-1}\Gamma_k^r e^{-\frac{j2\pi mk}{N}}\sum_{g'=0}^{N-1}\sum_{g''=0}^{N-1}R_{norm}(g'-g'')e^{-\frac{j2\pi(k'g'-zg'')}{N}} \\ for \quad k+k'=z \quad or \quad k+k'=N+z\end{gathered} \tag{6.19}$$

$$\begin{gathered}\overline{\frac{\Gamma_0^r}{N}e^{-\frac{j2\pi mi}{N}}ICI^*_{mob}(i)I^r_{mob,i}} = \\ \frac{\Gamma_0^r\sigma_X^2\sigma_H^2}{N^4}\sum_{k=1}^{N-1}\Gamma_k^r e^{-\frac{j2\pi mk}{N}}\sum_{g'=0}^{N-1}\sum_{g''=0}^{N-1}R_{norm}(g'-g'')\sum_{k'=0}^{N-1-k}e^{-\frac{j2\pi k'(g'-g'')}{N}}e^{\frac{j2\pi kg''}{N}}+ \\ \frac{\Gamma_0^r\sigma_X^2\sigma_H^2}{N^4}\sum_{k=1}^{N-1}\Gamma_k^r e^{-\frac{j2\pi mk}{N}}\sum_{g'=0}^{N-1}\sum_{g''=0}^{N-1}R_{norm}(g'-g'')\sum_{k'=N+1-k}^{N-1}e^{-\frac{j2\pi k'(g'-g'')}{N}}e^{\frac{j2\pi kg''}{N}} = \\ \frac{\Gamma_0^r\sigma_X^2\sigma_H^2}{N^4}\sum_{k=1}^{N-1}\Gamma_k^r e^{-\frac{j2\pi mk}{N}}\sum_{g'=0}^{N-1}\sum_{g''=0}^{N-1}R_{norm}(g'-g'')\sum_{k'=0}^{N-1}e^{-\frac{j2\pi k'(g'-g'')}{N}}e^{\frac{j2\pi kg''}{N}}- \\ \frac{\Gamma_0^r\sigma_X^2\sigma_H^2}{N^4}\sum_{g'=0}^{N-1}\sum_{g''=0}^{N-1}R_{norm}(g'-g'')\sum_{k=1}^{N-1}\Gamma_k^r e^{\frac{j2\pi(g'-m)k}{N}} = \\ 0-\frac{\Gamma_0^r\sigma_X^2\sigma_H^2}{N^4}\sum_{g'=0}^{N-1}\sum_{g''=0}^{N-1}R_{norm}(g'-g'')\sum_{k=1}^{N-1}\Gamma_k^r e^{\frac{j2\pi(g'-m)k}{N}} = \\ \frac{\Gamma_0^{r2}\sigma_X^2\sigma_H^2}{N^4}\sum_{g'=0}^{N-1}\sum_{g''=0}^{N-1}R_{norm}(g'-g'')-\frac{\Gamma_0^r\sigma_X^2\sigma_H^2}{N^3}\sum_{g'=m}^{N-1}\sum_{g''=0}^{N-1}R_{norm}(g'-g'')\end{gathered} \tag{6.20}$$

Finally the total average SIR would be as follows:

$$\begin{aligned}\frac{1}{SIR^r_{mob,ave}} &= \frac{N^2}{\sum_{g=m}^{N-1}\sum_{g'=m}^{N-1}R_{norm}(g-g')}- \\ &\quad 2\frac{\sum_{z=0}^{m-1}\sum_{z'=z+1}^{C}\sum_{g'=m}^{N-1}\sigma_{z'}^2R_{norm}(N-m+z-g')}{\sigma_H^2\sum_{g=m}^{N-1}\sum_{g'=m}^{N-1}R_{norm}(g-g')}-1\end{aligned} \tag{6.21}$$

Case of $m<0$ in the presence of high mobility

In this case, an error of m sampling periods to the left side has occurred. Then only d data points are corrupted due to the interference from the previous symbol, as described in Chapter 5. The received signal can thus be written as follows:

$$y^l_{mob,i} = \vartheta_{mob,((i+m))_N}\times\gamma_i^l+\psi_{mob,i}+w^l_{mob,i} \quad 0\le i\le N-1 \tag{6.22}$$

$w^l_{mob,i}$ is a sample of AWGN, γ_i^l is as defined in Chapter 5 and

$$\psi_{mob,i} = \begin{cases} y_{mob,pf}(G+m+i) & 0\le i\le d-1 \\ 0 & else\end{cases}.$$

$y_{mob,pf}(i)$ represents the ith sample of the output cyclic prefix of the current OFDM symbol (excluding the effect of AWGN) in the presence of high mobility. Similar to the case of $m > 0$, the FFT of $y^l_{mob,i}$ will be as follows:

$$Y^l_{mob,i} = \underbrace{e^{\frac{j2\pi mi}{N}} H_i^{norot,l}}_{H^l_{mob,eq}(i)} X_i + \underbrace{\frac{\Gamma^l_0}{N} e^{\frac{j2\pi mi}{N}} ICI_{mob}(i)}_{ICI \quad due \quad to \quad mobility} +$$

$$\underbrace{\overbrace{\sum_{\underbrace{k=1}_{k+k'\neq N}}^{N-1} \sum_{k'=0}^{N-1} \frac{\Gamma^l_k}{N} H_{((i-k))_N,k'} X_{((i-k-k'))_N} e^{\frac{j2\pi m(i-k)}{N}}}^{I^l_{mob,i}} + \Psi_{mob,i}}_{ICI \quad \& \quad ISI \quad due \quad to \quad timing \quad errors} + W^l_{mob,i} \quad 0 \leq i \leq N-1 \tag{6.23}$$

where $H_i^{norot,l} = \sum_{z=0}^{N-1} e^{-j\frac{2\pi mz}{N}} \frac{\Gamma^r_z}{N} H_{((i-z))_N,N-z}$. Γ^l is as defined in Chapter 5, Ψ_{mob} and W^l_{mob} are the FFTs of ψ_{mob} and w^l_{mob} respectively. $\Psi_{mob,i} = \sum_{k=0}^{d-1} \psi_{mob,k} e^{-\frac{j2\pi ki}{N}}$ where $\psi_{mob,k}$ can be written as follows:

$$\psi_{mob,k} = \sum_{k'=0}^{G+m+k} h_{k'}^{(m+k)} x_{N+m+k-k'} + \sum_{k'=G+m+k+1}^{C} h_{k'}^{(m+k)} x^{prev}_{N-k'+G+m+k} \quad 0 \leq k \leq d-1 \tag{6.24}$$

$\sigma^2_{\Psi_{mob}}$ is the same as σ^2_Ψ calculated in Chapter 5. The other terms can be calculated following the same procedure as for the $m > 0$ case. The average SIR will be as follows for this case:

$$\frac{1}{SIR^l_{mob,ave}} = \frac{N^2}{\sum_{g\in R_{m<0}} \sum_{g'\in R_{m<0}} R_{norm}(g-g')} - 2\frac{\sum_{z=0}^{d-1} \sum_{z'=0}^{z+G+m} \sum_{g'\in R_{m<0}} \sigma^2_{z'} R_{norm}(m+z-g')}{\sigma^2_H \sum_{g\in R_{m<0}} \sum_{g'\in R_{m<0}} R_{norm}(g-g')} - 1 \tag{6.25}$$

where $g' \in R_{m<0}$ refers to the set of g' such that $N+d+m \leq g' \leq N-1$ or $0 \leq g' \leq N+m-1$.

6.3 Effect of timing errors on the triogonometric interpolator in the presence of high mobility, case of $m > 0$

In this section we explore the effect of timing errors on the performance of a pilot-aided channel estimator. Consider the case of $m \geq 0$. Through an IFFT of $H^r_{mob,eq}$ of Eq. 6.3, the time-domain equivalent channel will be:

$$h^r_{mob,eq}(k) = h^{norot,r}_{((k+m))_N} \tag{6.26}$$

where $h^{norot,r}$ represents the IFFT of $H^{norot,r}$. Timing synchronization error introduces a rotation of m sampling periods in the base of N in the equivalent channel. It will be next proved that $h^{norot,r}$ has the same delay spread length as h.

$$\begin{aligned}
h^{norot,r}(k) &= \frac{1}{N}\sum_{i=0}^{N-1} H^{norot,r}(i)e^{\frac{j2\pi ki}{N}} \\
&= \frac{1}{N^2}\sum_{i=0}^{N-1} e^{\frac{j2\pi ki}{N}} \sum_{z=0}^{N-1} e^{\frac{-j2\pi mz}{N}}\Gamma^r_z H_{((i-z))_N,N-z} \\
&= \frac{1}{N^3}\sum_{z=0}^{N-1} e^{\frac{-j2\pi mz}{N}}\Gamma^r_z \sum_{i=0}^{N-1} e^{\frac{j2\pi ki}{N}} \sum_{g=0}^{C}\sum_{g'=0}^{N-1} h^{(g')}_g e^{\frac{-j2\pi(gi-g'z)}{N}} \\
&= \frac{1}{N^2}\sum_{g'=0}^{N-1} h^{(g')}_k \sum_{z=0}^{N-1} e^{\frac{j2\pi z(g'-m)}{N}}\Gamma^r_z = \frac{1}{N}\sum_{g'=m}^{N-1} h^{(g')}_k \quad 0 \leq k \leq C
\end{aligned} \tag{6.27}$$

As can be seen from Eq. 6.27, $h^{norot,r}$ has the same length as channel delay spread. Therefore, the rotation introduced by timing errors will result in the expansion of $h^{norot,r}$ beyond its maximum predicted length as was the case in Chapter 5. To see the effect of timing errors on channel estimation analytically, consider the case that L equally-spaced pilot tones are inserted among the sub-carriers. Similar to Eq. 5.18, the time-domain channel estimate can be expressed as follows:

$$\hat{h}^r_{mob,eq}(k) = \underbrace{h^{norot,r}_{((k+m))_L}}_{rotation} + \underbrace{u^{mob,r}_k}_{Interference} + \underbrace{v^{mob,r}_k}_{AWGN} \tag{6.28}$$

Defined $U_i^{mob,r}$ and $V_i^{mob,r}$ as follows:

$$\begin{aligned} U_i^{mob,r} &= \sum_{z=0}^{L-1} \alpha_{i,z} \frac{\frac{\Gamma_0^r}{N} e^{\frac{j2\pi m l_z}{N}} ICI_{mob}(l_z) + I_{mob,l_z}^r + S_{mob,l_z}}{X_{pilot}(l_z)} \\ V_i^{mob,r} &= \sum_{z=0}^{L-1} \alpha_{i,z} \frac{W_{mob,l_z}^r}{X_{pilot}(l_z)} \end{aligned} \tag{6.29}$$

where $l_z = \frac{N}{L}z$. Then $u^{mob,r}$ and $v^{mob,r}$ will be the IFFTs of $U^{mob,r}$ and $V^{mob,r}$ respectively and $\alpha_{i,z}$ is as defined in Chapter 4. Similar to Chapter 5 there are three factors contributing to channel estimation error: effect of rotation, interference and noise. The first factor is a result of the equivalent channel having a rotation in the base of N while the estimated equivalent channel has a rotation in the base of L, as discussed in Chapter 5. Similarly, there will be a mismatch in the location of the first m taps of $h^{norot,r}$ which will result in a significant performance degradation. The presence of high mobility changes the expressions of the interference terms as can be seen by comparing Eq. 6.29 with Eq. 5.19. To assess analytically the contribution of each of the aforementioned factors, an expression for channel estimation error is derived next. We will have,

$$\Delta H_{mob,eq}^r(i) = \sum_{k=0}^{m-1} \beta_{i,k}^{mob} h_k^{norot,r} + U_i^{mob,r} + V_i^{mob,r} \quad 0 \le i \le N-1 \tag{6.30}$$

where $\Delta H_{mob,eq}^r$ represents the frequency-domain channel estimation error, similar to Eq. 5.20, in the presence of high mobility, and $\beta_{i,k}^{mob} = e^{-\frac{j2\pi i(k-m)}{N} \times (1-e^{-j\frac{2\pi i L}{N}})}$.
First $\overline{U_i^{mob,r} h_k^{*norot,r}}$ is calculated. It can be easily seen that $\overline{\left[\frac{ICI_{mob}(l_z) h_k^{*norot,r}}{X_{pilot}(l_z)}\right]} = 0$ and $\overline{\left[\frac{I_{mob,l_z}^r h_k^{*norot,r}}{X_{pilot}(l_z)}\right]} = 0$, therefore,

$$\begin{aligned} \overline{U_i^{mob,r} h_k^{*norot,r}} &= \sum_{z=0}^{L-1} \alpha_{i,z} \overline{\left[\frac{S_{mob,l_z} h_k^{*norot,r}}{X_{pilot}(l_z)}\right]} \\ &= \frac{1}{N} \sum_{g=m}^{N-1} \sum_{k'=0}^{m-1} \sum_{k''=k'+1}^{C} \overline{h_{k''}^{(N-m+k')} h_k^{(g)*}} \sum_{z=0}^{L-1} \alpha_{i,z} \overline{\left[\frac{x_{N-k''+k'}}{X_{pilot}(l_z)}\right]} e^{-\frac{j2\pi(k'-m)z}{L}} \\ &= \frac{1}{N^2} \sum_{g=m}^{N-1} \sum_{k'=0}^{m-1} \sum_{k''=k'+1}^{C} \overline{h_{k''}^{(N-m+k')} h_k^{(g)*}} \sum_{z=0}^{L-1} \alpha_{i,z} e^{-\frac{j2\pi(k''-m)z}{L}} \\ &= \frac{1}{N^2} \sum_{g=m}^{N-1} \sum_{k'=0,k>k'}^{m-1} R_k(N-m+k'-g) \sum_{z=0}^{L-1} \alpha_{i,z} e^{-\frac{j2\pi(k-m)z}{L}} \end{aligned} \tag{6.31}$$

Since $0 \leq k \leq m-1$, then,

$$\overline{U_i^{mob,r} h_k^{*norot,r}} = \frac{\sigma_k^2}{N^2} \sum_{g=m}^{N-1} \sum_{k'=0}^{k-1} R_{norm}(N-m+k'-g) e^{-\frac{j2\pi(L+k-m)i}{N}} \quad k \geq 1 \tag{6.32}$$

and,

$$\begin{gathered} \textstyle\sum_{k=0}^{m-1} \beta_{i,k}^{*mob} \overline{U_i^{mob,r} h_k^{*norot,r}} = \\ \frac{e^{-\frac{j2\pi Li}{N}}-1}{N^2} \textstyle\sum_{k=1}^{m-1} \sigma_{h_k}^2 \sum_{g=m}^{N-1} \sum_{k'=0}^{k-1} R_{norm}(N-m+k'-g) \quad m \geq 2 \end{gathered} \tag{6.33}$$

Similar to Chapter 5, it can be easily shown that[1] for $z \neq z'$, then $E\left[\frac{I_{mob,l_z}^r \times I_{mob,l_{z'}}^{r*}}{X_{pilot}(l_z) X_{pilot}^*(l_{z'})}\right] = 0$, $E\left[\frac{ICI_{mob}(l_z) \times ICI_{mob}^*(l_{z'})}{X_{pilot}(l_z) X_{pilot}^*(l_{z'})}\right] = 0$, $E\left[\frac{I_{mob,l_z}^r \times ICI_{mob}^*(l_{z'})}{X_{pilot}(l_z) X_{pilot}^*(l_{z'})}\right] = 0$, $E\left[\frac{ICI_{mob}(l_z) \times S_{mob,l_{z'}}^*}{X_{pilot}(l_z) X_{pilot}^*(l_{z'})}\right] = 0$ and $E\left[\frac{I_{mob,l_z}^r \times S_{mob,l_{z'}}^*}{X_{pilot}(l_z) X_{pilot}^*(l_{z'})}\right] = 0$. For an arbitrary n and n' where $n \neq n'$,

$$\begin{gathered} E\left[\frac{S_{mob,n} S_{mob,n'}^*}{X_n X_{n'}^*}\right] = \\ \textstyle\sum_{k=0}^{m-1} \sum_{g=0}^{m-1} \sum_{k'=k+1}^{C} \sum_{g'=g+1}^{C} \overline{h_{k'}^{(N-m+k)} h_{g'}^{(N-m+g)*}} \left[\frac{x_{N-k'+k} x_{N-g'+g}^*}{X_n X_{n'}^*}\right] e^{\frac{-j2\pi[(k-m)n-(g-m)n']}{N}} = \\ \textstyle\frac{1}{N^2} \sum_{k=0}^{m-1} \sum_{g=0}^{m-1} \sum_{k'=max(k,g)+1}^{C} \sigma_{h_{k'}}^2 R_{norm}(k-g) e^{-\frac{j2\pi(k'-m)(n-n')}{N}} \end{gathered} \tag{6.34}$$

Therefore,

$$\begin{gathered} \textstyle\sum_{z=0}^{L-1} \sum_{z'=0, z' \neq z}^{L-1} \alpha_{i,z} \alpha_{i,z'}^* E\left[\frac{S_{mob,l_z} S_{mob,l_{z'}}^*}{X_{pilot}(l_z) X_{pilot}^*(l_{z'})}\right] = \\ \textstyle\frac{1}{N^2 L^2} \sum_{k=0}^{m-1} \sum_{g=0}^{m-1} \sum_{k'=max(k,g)+1}^{C} \sigma_{h_{k'}}^2 R_{norm}(k-g) \times \\ \textstyle\sum_{z=0}^{L-1} \sum_{z'=0, z' \neq z}^{L-1} \sum_{n=0}^{L-1} \sum_{n'=0}^{L-1} e^{j2\pi\left[n(\frac{z}{L}-\frac{i}{N}) - n'(\frac{z'}{L}-\frac{i}{N}) - \frac{(k'-m)(z-z')}{L}\right]} = \\ \textstyle\frac{1}{N^2 L^2} \sum_{k=0}^{m-1} \sum_{g=0}^{m-1} \sum_{k'=max(k,g)+1}^{C} \sigma_{h_{k'}}^2 R_{norm}(k-g) \sum_{n=0}^{L-1} \sum_{n'=0}^{L-1} e^{-\frac{j2\pi i(n-n')}{N}} \times \\ \left[\textstyle\sum_{z=0}^{L-1} e^{\frac{j2\pi z(n-k'+m)}{L}} \sum_{z'=0}^{L-1} e^{-\frac{j2\pi z'(n'-k'+m)}{L}} - \sum_{z=0}^{L-1} e^{\frac{j2\pi z(n-n')}{L}}\right] \end{gathered}$$

Similar to Eq. 5.34,

$$\textstyle\sum_{z=0}^{L-1} \sum_{z'=0, z' \neq z}^{L-1} \alpha_{i,z} \alpha_{i,z'}^* E\left[\frac{S_{mob,l_z} S_{mob,l_{z'}}^*}{X_{pilot}(l_z) X_{pilot}^*(l_{z'})}\right] = 0 \tag{6.35}$$

[1] All these expressions will result in $E\left[\frac{X_g X_{g'}^*}{X_k X_{k'}^*}\right]$ for arbitrary g, g', k and k' where $k \neq k'$ and $g \neq g'$ and therefore will be zero.

Therefore,

$$\sigma^2_{U_i^{mob,r}} = \sum_{z=0}^{L-1} |\alpha_{i,z}|^2 \frac{\overline{|\frac{\Gamma_0^r}{N} e^{\frac{j2\pi mz}{L}} ICI_{mob}(l_z) + I^r_{mob,l_z} + S_{mob,l_z}|^2}}{\sigma^2_X} \tag{6.36}$$

and,

$$\overline{|\Delta H^r_{mob,eq}(i)|^2} = \sum_{k=0}^{m-1} |\beta^{mob}_{i,k}|^2 \sigma^2_{h_k^{norot,r}} + \sigma^2_{U_i^{mob,r}} + \sigma^2_{V_i^{mob,r}} + 2Real(\sum_{k=0}^{m-1} \beta^{mob*}_{i,k} \overline{U_i^{mob,r} h_k^{*norot,r}}) \tag{6.37}$$

Using Eq. 6.27,

$$\overline{|H^{norot,r}(k)|^2} = \frac{\sigma^2_H}{N^2} \sum_{g'=m}^{N-1} \sum_{g''=m}^{N-1} R_{norm}(g' - g'') \tag{6.38}$$

Similar to the derivation of Chapter 5, $\overline{U_i^{mob,r} h_k^{norot,r*}}$ is dropped as its value is considerably smaller than the other terms. Therefore,

$$Ch^{mob,r}_{error,norm}(i) = \frac{\overline{|\Delta H^r_{mob,eq}(i)|^2}}{\overline{|H^r_{mob,eq}(i)|^2}} \approx \underbrace{4\Upsilon^r_{\%}(m) sin^2(\frac{\pi i L}{N})}_{factor\#1:rotation} + \underbrace{\frac{1}{SIR^r_{mob,ave}(m)}}_{interference} + \underbrace{\frac{1}{SNR^r_{mob,ave}(m)}}_{noise} \tag{6.39}$$

where $SIR^r_{mob,ave}(m) = \frac{\sigma^2_X \sigma^2_H \sum_{g'=m}^{N-1} \sum_{g''=m}^{N-1} R_{norm}(g'-g'')}{N^2 |\frac{\Gamma_0^r}{N} e^{\frac{j2\pi mi}{N}} ICI_{mob}(i) + I^r_{mob,i} + S_{mob,i}|^2}$, as defined previously, $\Upsilon^r_{\%}(m)$ is as defined in Chapter 5 and $SNR^r_{mob,ave}(m) = \frac{\sigma^2_X \sigma^2_H \sum_{g'=m}^{N-1} \sum_{g''=m}^{N-1} R_{norm}(g'-g'')}{N^2 \sigma^2_W}$. Compared with the channel estimation error derived in Eq. 5.38 for the low-mobility case, rotation has the same contribution as it had before. The second and third terms on the right hand side of Eq. 6.39, however, have slightly higher values compared to their corresponding terms in the low-mobility case. As the first term takes on high values, the effect of rotation is expected still to be the major contributor to channel estimation error.

Fig. 6.1 shows $Ch^{mob,r}_{error,norm}$ for those sub-carriers at mid-points between every two consecutive pilot tones and for different levels of mobility for channel c5.3 of Chapter 5. $f_{d,norm}$ refers to the ratio of the maximum Doppler spread divided by sub-carrier spacing and each channel delay-profile sample has a Jakes power-spectrum [10]. To see the contribution of the rotation factor, the solid line shows the effect of the first term on the right-hand side of Eq. 6.39. Comparing that with the $Ch^{mob,r}_{error,norm}$ for the no Doppler case, it can be seen

that $factor\#1$ contributes almost all of the channel estimation error at low m. As m approaches the length of the guard interval (G), ICI and ISI introduced by timing synchronization error increase. Still, $factor\#1$ contributes to more than 80% of the channel estimation error at $m = G$ for the no Doppler case. Comparing the channel estimation error for the no Doppler case with the error in the presence of mobility, it can be seen that mobility does not have a distinguishable impact on channel estimation error for $f_{d,norm}$ as high as 20% since the effect of rotation is already very high. To examine a case where Doppler has a distinguishable impact on channel estimation error, $f_{d,norm}$ is increased to 50%. It should be noted that even in case of perfect timing synchronization, such a high Doppler spread would ruin the performance of an OFDM system and therefore is not a realistic scenario. Even for such a high Doppler spread, Fig. 6.1 shows that *factor#1* contributes to more than 70% of channel estimation error. The timing synchronization method proposed in Chapter 5 is effective as long as *factor#1* is the major contributor to channel estimation error. The analysis of this section suggested that in the presence of timing errors, mobility has a negligible impact on channel estimation. Therefore, extending the method proposed in Chapter 5 will also provide robust timing synchronization for high mobility applications as will be shown later in this chapter.

6.4 Effect of timing errors on the triogonometric interpolator in the presence of high mobility, case of $m < 0$

Similar expressions can be derived for the case of $m < 0$:

$$h^{l}_{mob,eq}(k) = h^{norot,l}_{((k+m))_N} \tag{6.40}$$

Similar to Eq. 6.27,

$$h^{norot,l}(k) = \frac{1}{N} \sum_{g' \in R_{m<0}} h_k^{(g')} \tag{6.41}$$

Since the length of $h^{norot,l}$ is the same as the length of the original channel delay spread, rotation has the same impact as it had for the low-mobility case, as discussed in Section 5.2.5. Following the same procedure as the case of $m > 0$, the following expressions can be derived:

$$\begin{aligned}
\hat{h}^l_{mob,eq}(k) &= \underbrace{h^{norot,l}_{((k+m))_L}}_{rotation} + \underbrace{u^{mob,l}_k}_{Interference} + \underbrace{v^{mob,l}_k}_{AWGN} \\
\Delta H^l_{mob,eq}(i) &= \sum_{k=0}^{m-1} \beta^{mob}_{i,k} h^{norot,l}_k + U^{mob,l}_i + V^{mob,l}_i \quad 0 \le i \le N-1 \\
Ch^{mob,l}_{error,norm}(i) &= \frac{\overline{|\Delta H^l_{mob,eq}(i)|^2}}{\overline{|H^l_{mob,eq}(i)|^2}} \approx \\
&\underbrace{4\Upsilon^l_{\%}(m) sin^2(\frac{\pi i L}{N})}_{factor\#1:rotation} + \underbrace{\frac{1}{SIR^l_{mob,ave}(m)}}_{interference} + \underbrace{\frac{1}{SNR^l_{mob,ave}(m)}}_{noise} \qquad (6.42)
\end{aligned}$$

where $SIR^l_{mob,ave}(m)$ and $\Upsilon^l_{\%}(m)$ are as defined previously and $SNR^l_{mob,ave}(m) = \frac{\sigma^2_X \sigma^2_H \sum_{g' \in R_{m<0}} \sum_{g'' \in R_{m<0}} R_{norm}(g'-g'')}{N^2 \sigma^2_W}$. It can be seen that the effect of rotation is the same as before. Mobility resulted in a slight increase of the second and third terms on the right hand side of Eq. 6.42. However, as the effect of rotation is significantly higher, it is still the main contributor to channel estimation error.

6.5 Timing synchronization error correction

In Chapter 5 it was shown that pilot-aided channel estimators are super-sensitive to timing synchronization errors due to the effect of rotation. In Chapter 6 it has been shown that in a mobile environment, the effect of rotation is still the dominant cause of channel estimation performance degradation. Therefore, this sensitivity can still be exploited to design a synchronization algorithm that works robustly in high mobility environments. After a coarse timing synchronizer has detected a start point for the symbol (a correlation-based synchronizer can be used for this as discussed in the previous chapter), $\hat{H}_{mob,eq}$ can be obtained using pilot tones. In the presence of timing errors, this channel estimate may be far from $H_{mob,eq}$. Call $\hat{X}_i = \frac{Y_{mob,i}}{\hat{H}_{mob,eq}(i)}$, the estimated input at the ith sub-channel. Let

$\tilde{X}_i = Dec(\hat{X}_i)$ represent the estimated input after passing through the decision device. Define a decision-directed measure function as $MF = \sum_{i=0}^{N-1} |\hat{X}_i - \tilde{X}_i|^2$, similar to Chapter 5. In the presence of channel rotation, MF can become very large. Therefore, timing synchronization error correction can be obtained iteratively by minimizing MF. As long as *factor#1* is the major cause of performance loss, which is the case with high probability, timing errors can be detected. Through an iterative process, the estimated channel is updated, correcting for one mismatched tap at a time. Following the same procedure as in Chapter 5, the update necessary for correcting errors to the right at the ith iteration and k^{th} sub-channel will be as follows:

$$\hat{H}_{mob,eq}^{(i+1),r}(k) = \hat{H}_{mob,eq}^{(i),r}(k) + \varsigma \times \hat{h}_{mob,eq}^{r}(L-k) \times e^{\frac{j2\pi ik}{N}} \tag{6.43}$$

Similarly, for detecting errors to the left
$\hat{H}_{mob,eq}^{(i+1),l}(k) = \hat{H}_{mob,eq}^{(i),l}(k) - \varsigma \times \hat{h}_{mob,eq}^{l}(i-1) \times e^{-j2\pi(i-1)k/N}$, where ς is as defined in Chapter 5 and $\hat{H}_{mob,eq}^{(1),r}(k) = \hat{H}_{mob,eq}^{(1),l}(k) = \hat{H}_{mob,eq}(k)$. In each iteration, the measure function, $MF^{(i)}$, will be evaluated. Finally the iteration that results in the minimum MF is selected and the correction necessary is applied to the start of the symbol in the time domain.

6.6 Simulation Results

An OFDM system is simulated in a high delay spread and Doppler spread environment. System parameters are the same as in Section 5.4. The power-delay profile of the simulated channel is the same as channel c5.4 (shown in Fig. 5.6). Each channel delay-profile sample is generated as a random process with Rayleigh distributed amplitude and uniformly distributed phase using the Jakes Doppler spectrum [10]. The time-domain auto-correlation of each sample is a zero-order Bessel function. Fig. 5.7 and 5.9 showed the performance of the proposed algorithm in a low-mobility environment. Fig. 6.2 shows the performance for high-mobility applications and at $\frac{\sigma_X^2 \sigma_H^2}{\sigma_W^2} = 20dB$. To see the impact of mobility, Fig. 6.2 shows the performance for different levels of mobility: $f_{d,norm}$ =10%, 20% and 50%. Compared with the no Doppler case, it can be observed that the error profile is not affected by high mobility. This is due to the considerable impact of $factor\#1$

on channel estimation error as was shown in the previous section. This shows that the proposed algorithm can be used for robust timing synchronization in high delay spread and Doppler spread environments.

6.7 Summary

This chapter started by deriving the expressions of interference terms in the presence of timing synchronization errors and mobility. The effects of timing errors and mobility on the performance of the trigonometric interpolator were then analyzed. Expressions for channel estimation error in the presence of mobility and timing synchronization errors were derived. The effect of rotation was shown to be still the main contributor to channel estimation error in high mobility environments. Based on this observation, the timing synchronization algorithm proposed in Chapter 5 was extended to high mobility applications. Simulation results showed the performance of the proposed algorithm in high delay spread and Doppler spread environments. The simulation results show that the proposed algorithm is robust in the presence of high mobility.

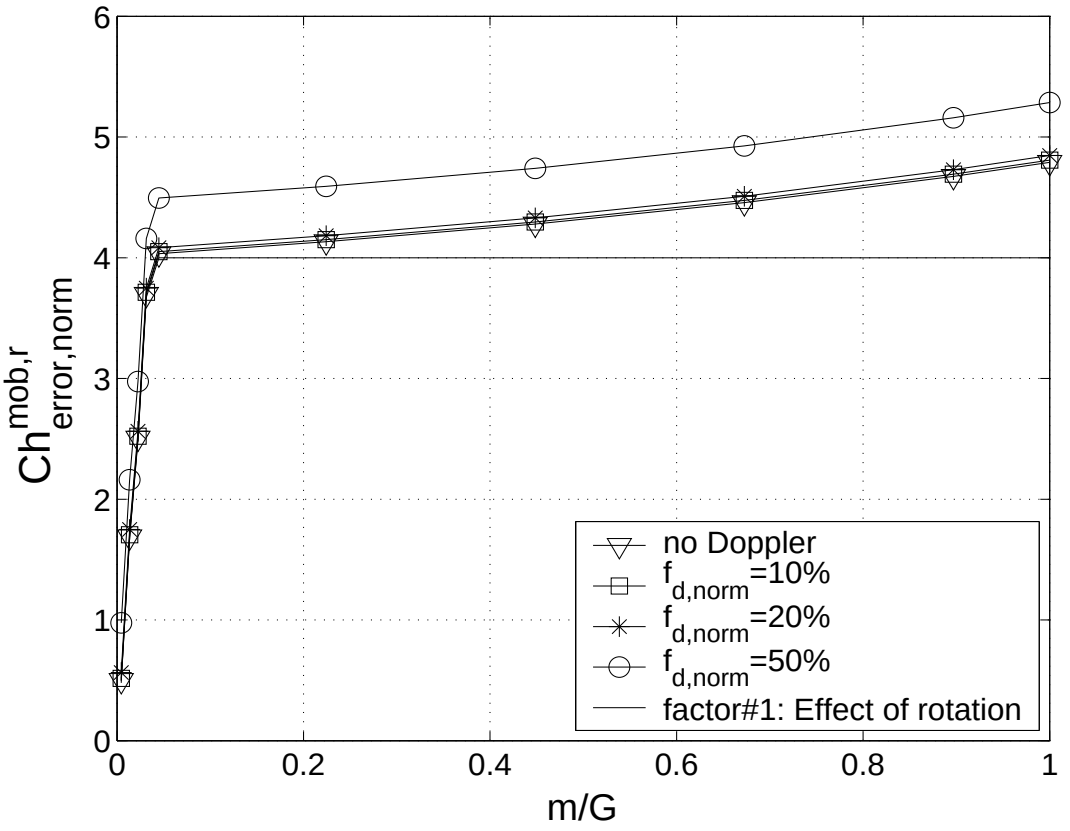

Figure 6.1: Normalized channel estimation error vs. normalized m for channel c5.3 (G is as defined in Section 3.2)

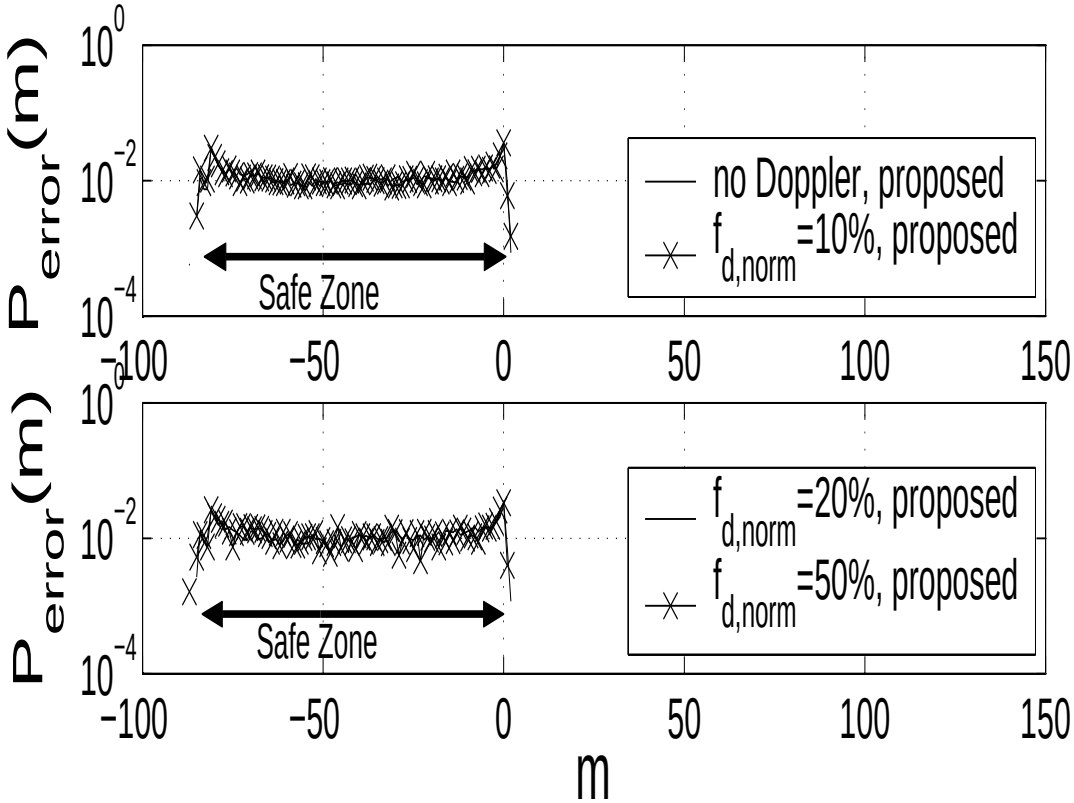

Figure 6.2: Performance in the presence of mobility for channel c5.4 at $\frac{\sigma_X^2 \sigma_H^2}{\sigma_W^2} = 20dB$

Chapter 7

Mobility Mitigation

7.1 Introduction

Once robust timing synchronization is achieved in high mobility environments, as proposed in Chapter 6, the effects of mobility need to be mitigated. Doppler spread, resulting from mobility and angular spread of arriving paths, ruins the orthogonality of sub-carriers and introduces ICI, which degrades the performance. This becomes more severe as mobile speed, carrier frequency or OFDM symbol duration increases. As delay spread increases, symbol duration should also increase for two reasons. First, most receivers require a near-constant channel in each frequency sub-band. As delay spread increases, this can be achieved by an increase of the symbol length. Second, to prevent Inter-OFDM Symbol-Interference, the length of the guard interval should increase as well. Therefore, to reduce the overhead of the cyclic prefix, the symbol length should increase [26]. OFDM systems become more susceptible to time-variations as symbol length increases. Also, due to the high demand for bandwidth, there is a trend towards higher carrier frequencies. Therefore, to have an acceptable reception quality in high delay spread and Doppler spread environments, there is a need for ICI mitigation. In References [22], [21], authors analyzed the effect of ICI by modeling it as Gaussian noise. A simplified bound on ICI power has also been derived [13] . To mitigate the introduced ICI, techniques using receiver antenna diversity have been proposed [22], [27]. However, sensitivity analysis has shown that as normalized Doppler spread (defined as the maximum Doppler spread divided by

the sub-carrier spacing) increases, antenna diversity becomes less effective in mitigating ICI in OFDM mobile systems [9].

Jeon and Chang have proposed another method for ICI mitigation which assumes a linear model for channel variations [11] . However, they assumed that some of the coefficients of the channel matrix are negligible, which is only the case under low Doppler and delay spread conditions. For instance, their results showed performance improvement under normalized Doppler spread of up to 2.72% and delay spread of $2\mu s$ (normalized delay spread of 1) for a channel that had two non-zero power-delay profile samples. In high mobility applications that require ICI mitigation, however, delay spread can be much longer. For instance, the delay spread can be as high as $40\mu s$ for SFN channels (defined in Chapter 5) and $20\mu s$ for cellular applications[1]. Furthermore, normalized Doppler can be as high as 10% depending on the carrier frequency. Their method also relies on information from adjacent OFDM symbols for channel estimation, which increases processing delay.

To improve the performance in high delay spread and Doppler spread environments, two new ICI mitigation methods are presented in this chapter. Compared to the method of Jeon et al., the proposed methods can mitigate ICI in considerably higher delay and Doppler spread applications such as those found in SFN and cellular networks. Furthermore, in one of the methods ICI is mitigated without relying on the adjacent symbols. Both of the methods are based on a piece-wise linear approximation for channel time-variations.

In the absence of Doppler spread, frequency-domain pilot tones or differential modulation (either across sub-carriers or across adjacent symbols) should be used to remove the effect of channel frequency-selective fading. As the delay spread increases, differential modulation across adjacent sub-bands degrades performance. As Doppler spread and/or the length of the OFDM symbol increase, differential modulation across adjacent symbols leads to performance degradation as well. Therefore, frequency-domain pilot tones with trigonometric interpolation between them is used in this chapter, as explained in

[1]For a high rate application that requires total bandwidth of 4MHz, delay spread of $40\mu s$ would result in the normalized delay spread of 160.

Chapter 4. In the presence of Doppler spread, however, these pilot tones can not estimate channel time-variations. This chapter shows how to estimate these variations utilizing either the cyclic prefix or the next symbol. Finally, analysis and simulation results show performance improvement in high delay spread and Doppler spread environments.

7.2 System Model in a mobile environment

In the case of perfect timing synchronization and in the presence of mobility, the channel output y can be expressed as follows:

$$y_i = \sum_{k=0}^{G} h_k^{(i)} x_{((i-k))_N} + w_i \quad 0 \leq i \leq N-1 \tag{7.1}$$

where $h_k^{(i)}$ represents the kth sample of the channel delay profile at time instant $t = i \times T_s$ and w and x are as defined in Chapter 4. A constant channel is assumed over the time interval $i \times T_s \leq t < (i+1) \times T_s$ with $t = 0$ indicating the start of the data part of the symbol. $h_k^{(i)}$ for $-G \leq i \leq -1$ and $0 \leq i \leq N-1$ represents the kth sample of the channel delay profile in the guard and data interval respectively. G, N and T_s are as defined in Chapter 4.

Then Y, the FFT of sequence y, will be as follows:

$$Y_i = H_{i,0} X_i + \underbrace{\sum_{z=1}^{N-1} H_{i,z} X_{((i-z))_N}}_{ICI_{mob}(i)} + W_i \quad 0 \leq i \leq N-1 \tag{7.2}$$

W denotes the FFT of w and the second term on the right hand side of Eq. 7.2 represents ICI. Define $F_{g'}$ as the FFT of the time variations of the g'^{th} channel delay-profile sample:

$$F_{g'}(z) = \sum_{g=0}^{N-1} h_{g'}^{(g)} e^{-\frac{j2\pi gz}{N}} \quad 0 \leq g' \leq G \quad \& \quad 0 \leq z \leq N-1 \tag{7.3}$$

Then $H_{i,z}$ can be defined as

$$H_{i,z} = \frac{1}{N}\sum_{g'=0}^{G} F_{g'}(z)e^{-\frac{j2\pi g'(i-z)}{N}} \quad 0 \leq i, z \leq N-1 \tag{7.4}$$

Furthermore, $H_{i,0} = \sum_{g'=0}^{G} h_{g'}^{ave} e^{-\frac{j2\pi g' i}{N}}$ where $h_{g'}^{ave} = \frac{1}{N}\sum_{g=0}^{N-1} h_{g'}^{(g)}$ is the average of the g'^{th} channel delay-profile sample over the time duration of $0 \leq t < N \times T_s$. Therefore $H_{i,0}$ represents the FFT of this average[2].

As was noted by previous work, the ICI term on the right hand side of Eq. 7.2 can not be neglected as the maximum Doppler shift, $f_{d,norm}$, increases (eg. [22]).

7.3 Pilot Extraction

$L \geq \nu + 1$ equally spaced pilots, $X_{pilot}(l_i)$, are inserted at sub-channels $l_i = \frac{i \times N}{L}$ for $0 \leq i \leq L-1$, as discussed in Chapter 4. An estimate of $H_{i,0}$ can then be acquired at pilot tones as follows:

$$\hat{H}_{l_{i,0}} = \frac{Y_{l_i}}{X_{pilot}(l_i)} = H_{l_{i,0}} + \frac{ICI_{mob}(l_i) + W_{l_i}}{X_{pilot}(l_i)} \quad 0 \leq i \leq L-1 \tag{7.5}$$

In Eq. 7.5, $ICI_{mob}(l_i)$ denotes ICI (marked in Eq. 7.2) at l_i^{th} sub-carrier. Through an IFFT of length L, the estimate of h_k^{ave} would be

$$\hat{h}_k^{ave} = \frac{1}{L}\sum_{i=0}^{L-1} \hat{H}_{l_{i,0}} e^{\frac{j2\pi ik}{L}} \quad 0 \leq k \leq L-1 \tag{7.6}$$

In the absence of mobility, L pilots would have been enough to estimate the channel. However in the presence of Doppler spread, due to the ICI term of Eq. 7.2, using the estimate of $\hat{h}_k^{ave}$ for data detection results in poor performance. This motivates the need to mitigate the resultant ICI.

[2]note that $h_{g'}^{ave}$ refers to a time averaging over the data part of the OFDM symbol and represents a short-term averaging. Therefore, it is different from a long-term averaging as the length of the data part of the OFDM symbol is not long enough with respect to the channel coherence time to include enough sampling realizations.

7.4 Piece-wise Linear Approximation

This chapter approximates channel time-variations with a piece-wise linear model with a constant slope over the time duration T (Fig. 7.1). For normalized Doppler spread of up to 20%, the linear approximation is a good estimate of channel time-variations and the effect on correlation characteristics is negligible. To see this, Appendix A shows how this approximation affects the correlation function as normalized Doppler spread increases.

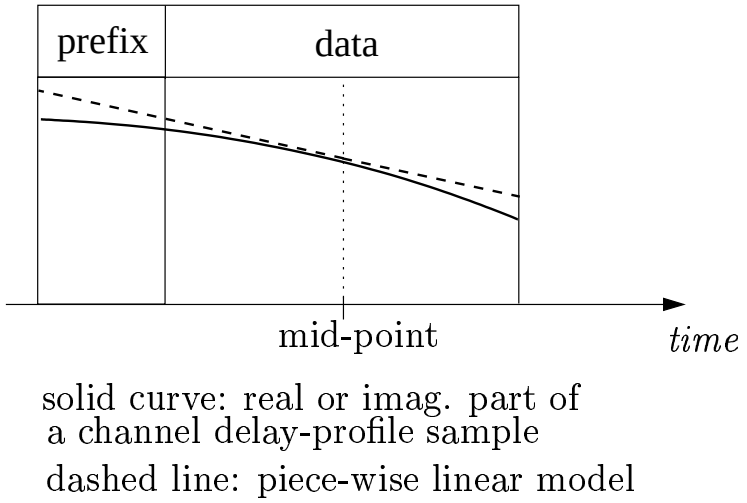

Figure 7.1: Piece-wise linear model in one received OFDM symbol

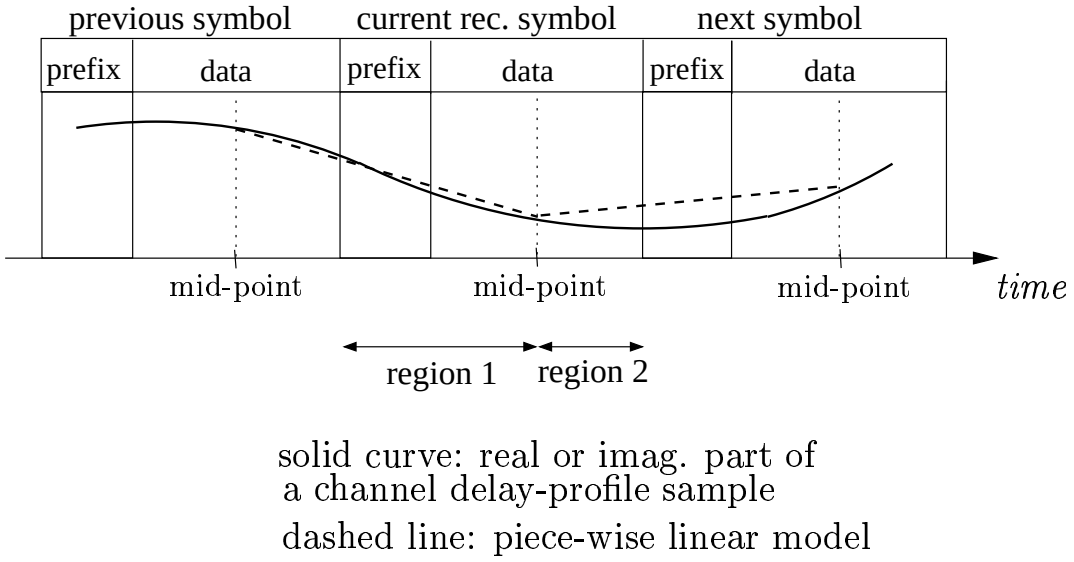

Figure 7.2: Piece-wise linear model for method II

In this section the frequency-domain relationship, similar to Eq. 7.2, is derived when the linear approximation is applied. Let cs_k denote the slope of the kth channel delay-profile sample in the current OFDM symbol. To perform the linearization, knowledge of the channel at one time instant in the symbol is necessary. Let $E(z)$ represent the average of z. Then for the kth channel delay-profile sample, $E(|h_k^{ave} - h_k^{(g)}|^2)$ is minimized for $g = \frac{N}{2} - 1$ as is shown next. Let CF_k be defined as follows: $CF_k(g) = E(|h_k^{ave} - h_k^{(g)}|^2)$. The goal is to minimize CF_k over $0 \leq g \leq N-1$. CF_k can be written as follows:

$$\begin{aligned} CF_k(g) &= \frac{1}{N^2}\sum_{z=0}^{N-1}\sum_{z'=0}^{N-1} E(h_k^{(z)} h_k^{*(z')}) + E(|h_k^{(g)}|^2) - \frac{1}{N}\sum_{z=0}^{N-1} E(h_k^{(z)} h_k^{*(g)}) - \\ &\quad \frac{1}{N}\sum_{z=0}^{N-1} E(h_k^{*(z)} h_k^{(g)}) \\ &= \frac{1}{N^2}\sum_{z=0}^{N-1}\sum_{z'=0}^{N-1} R_k(z-z') + R_k(0) - \frac{2}{N}\underbrace{\sum_{z=0}^{N-1} Re\{R_k(z-g)\}}_{CF_k'(g)} \end{aligned} \tag{7.7}$$

$Re\{\}$ stands for the real part of the argument and $R_k(z') = E(h_k^{(z)} h_k^{*(z-z')})$. From Eq. 7.7, minimization of CF_k is equivalent to maximization of $CF_k'(g) = \sum_{z=0}^{N-1} Re\{R_k(z-g)\}$ over g. Assume $R_k(z') = \sigma_k^2 J_0(2\pi f_d z' T_s)$ where J_0 represents zero-order Bessel function. Since $NT_s \leq \frac{1}{f_d}$ (which means that the length of the data part of the symbol is less than channel coherence time), it can be easily seen that CF_k' is maximized for $g = \frac{N}{2} - 1$ and $g = \frac{N}{2}$ (N is assumed even). Therefore, $h_k^{(\frac{N}{2}-1)}$ is approximated with the estimate of h_k^{ave}. Then,

$$\hat{h}_k^{(\frac{N}{2}-1)} = \hat{h}_k^{ave} \tag{7.8}$$

Consider linearization around $h_k^{(\frac{N}{2}-1)}$. Then $h_k^{(i)}$ can be approximated as follows:

$$h_k^{(i)} \approx h_k^{(\frac{N}{2}-1)} + (i + 1 - \frac{N}{2}) \times cs_k \times T_s \quad 0 \leq i \leq N-1 \tag{7.9}$$

Inserting Eq. 7.9 in Eq. 7.1 will result in the following:

$$\vec{y} \approx (\mathbf{h}_{mid} + \mathbf{M} \times \mathbf{A}) \times \vec{x} + \vec{w} \tag{7.10}$$

$\vec{y}$, $\vec{x}$ and $\vec{w}$ are $N \times 1$ vectors containing samples of y_i, x_i and w_i for $0 \leq i \leq N-1$. Furthermore, $\mathbf{h}_{mid}$ and $\mathbf{A}$ will be as follows for $1 \leq k, k' \leq N$:

$$\mathbf{h}_{mid}(k,k') = \begin{cases} h^{(\frac{N}{2}-1)}_{((k-k'))_N} & 0 \leq k-k' \leq G \quad \& \quad -(N-1) \leq k-k' \leq -(N-G) \\ 0 & else \end{cases} \tag{7.11}$$

$$\mathbf{A}(k,k') = \begin{cases} cs_{((k-k'))_N} & 0 \leq k-k' \leq G \quad \& \quad -(N-1) \leq k-k' \leq -(N-G) \\ 0 & else \end{cases} \tag{7.12}$$

$\mathbf{M}$ is a diagonal matrix with diagonal elements of $\mathbf{M}(k,k) = \varphi_{k-1} = T_s \times (k - \frac{N}{2})$ for $1 \leq k \leq N$. Let $\vec{y}_1 = \mathbf{A}\vec{x}$. Since $\mathbf{A}$ is a circular toeplitz matrix, taking an FFT of $\vec{y}_1$ will result in a multiplication by a diagonal matrix in the frequency domain. Therefore, $\vec{Y}_1 = \mathbf{H}_{slope}\vec{X}$ with Y_1 representing the FFT of y_1 and $\mathbf{H}_{slope} = diag\{FFT([\ cs_0 \quad cs_1 \quad \cdots \quad cs_G \quad 0 \quad \cdots \quad 0\ ])\}$. Let $\vec{y}_2 = \mathbf{M}\vec{y}_1$. Taking an FFT of $\vec{y}_2$, $Y_2(k) = \frac{\chi_k \otimes_N Y_1(k)}{N}$ where χ is the FFT of φ and $\otimes_N$ represents circular convolution in the base of N. Taking an FFT of φ, it can be easily shown that χ is as follows [17]:

$$\chi_k = T_s \times N \times \begin{cases} -\frac{1}{1-e^{-\frac{j2\pi k}{N}}} & k \neq 0 \\ 0.5 & k = 0 \end{cases} \tag{7.13}$$

Therefore,

$$\vec{Y} \approx \mathbf{H}_{mid}\vec{X} + \vec{Y}_2 = \mathbf{H}_{mid}\vec{X} + \mathbf{COF} \times \mathbf{H}_{slope}\vec{X} + \vec{W} \tag{7.14}$$

where

$$\mathbf{H}_{mid} = diag\{FFT([\ h_0^{(\frac{N}{2}-1)} \quad h_1^{(\frac{N}{2}-1)} \quad \cdots \quad h_G^{(\frac{N}{2}-1)} \quad 0 \quad \cdots \quad 0\ ])\} \tag{7.15}$$

$FFT(\vec{z})$ represents the FFT of the vector $\vec{z}$. $\vec{W}$ is a vector containing the FFT of noise samples and $\mathbf{COF}_{n,n'} = \frac{\chi_{n-n'}}{N}$. To solve Eq. 7.14 for $\vec{X}$, both $\mathbf{H}_{mid}$ and $\mathbf{H}_{slope}$ need to be estimated. Matrix $\mathbf{COF}$ is a fixed matrix that is pre-calculated and stored in the receiver. An estimate of $\mathbf{H}_{mid}$ is readily available from Eq. 7.5, 7.6 and 7.15. The

following sub-sections will show two methods to estimate $\mathbf{H}_{slope}$. In Method I this is done by utilizing the redundancy of the cyclic prefix while in Method II the information of the next symbol is used.

7.4.1 Method I: ICI mitigation using cyclic prefix

The output prefix vector, $\vec{y}_{pf}$ of Fig. 3.1, can be written as follows:

$$\vec{y}_{pf} = \mathbf{Q} \times \vec{c}_{pf} + \vec{w}_p \tag{7.16}$$

In Eq. 7.16 $\vec{c}_{pf} = \begin{bmatrix} \vec{x}_{pf}^{pre} \\ \vec{x}_{pf} \end{bmatrix}$, $\vec{w}_p$ contains AWGN samples and

$$\mathbf{Q}(i,j) = h^{(-G+i-1)}_{((i-j+G))_{2\times G}} \quad 1 \leq i \leq G \quad 1 \leq j \leq 2 \times G \tag{7.17}$$

Since $\nu \leq G$, $h_k^{(i)} = 0$ for $k > G$ in matrix $\mathbf{Q}$. $\vec{x}_{pf}$ is the transmitted cyclic prefix vector, as defined in Chapter 3. $\vec{x}_{pf}^{pre}$ is similarly defined for the transmitted cyclic prefix of the previous OFDM symbol and is already known to the receiver. Define $\vec{\zeta}$ as a vector containing slopes of all the samples of the channel delay profile:

$$\vec{\zeta} = \begin{bmatrix} cs_0 & cs_1 & \cdots & cs_G \end{bmatrix}^t \tag{7.18}$$

Inserting $h_k^{(i)}$ from Eq. 7.9 in $\mathbf{Q}$, it can be easily shown that Eq. 7.16 can be written as follows:

$$\vec{y}_{pf} - \mathbf{RH} \times \vec{c}_{pf} \approx \mathbf{D} \times \mathbf{X}_{p_{mat}} \times \vec{\zeta} + \vec{w}_p \tag{7.19}$$

In Eq. 7.19 $\mathbf{RH}(i,j) = h^{(\frac{N}{2}-1)}_{((i-j+G))_{2\times G}}$ for $1 \leq i \leq G$ and $1 \leq j \leq 2\times G$ and can be estimated from Eq. 7.5, 7.6. $\mathbf{D}$ is a pre-determined diagonal matrix with $\mathbf{D}(i,i) = T_s \times (-\frac{N}{2} + i - G)$

Table 7.1: Procedure for Method I

Step	*Command*
1	Set the initial estimate of $\mathbf{H}_{slope}$ to zero
2	Use Eq. 7.5, 7.6 & 7.15 to estimate $\mathbf{H}_{mid}$ from pilots
3	Solve Eq. 7.14 for $\vec{X}$
4	Solve Eq. 7.19 for $\vec{\zeta}$
5	Estimate $\mathbf{H}_{slope}$ from estimated $\vec{\zeta}$
6	If not converged or timed out, go to step 3

for $1 \leq i \leq G$ and is stored in the receiver. $\mathbf{X}_{p_{mat}}$ is defined as follows:

$$\mathbf{X}_{p_{mat}} = \begin{bmatrix} Rev(\vec{c}_{pf}^{\,t}\,[1:G+1]) \\ Rev(\vec{c}_{pf}^{\,t}\,[2:G+2]) \\ \vdots \\ Rev(\vec{c}_{pf}^{\,t}\,[G:2\times G] \end{bmatrix} \tag{7.20}$$

In Eq. 7.20, $Rev(\vec{z}[i:j])$ represents the vector produced by reversing the order of elements i through j of vector $\vec{z}$ and $\vec{z}^t$ denotes transpose of $\vec{z}$. Eq. 7.14 and 7.19 provide enough information to solve for $\vec{X}$. There are two sets of unknowns, $\vec{X}$ and $\vec{\zeta}$. $\mathbf{H}_{slope}$ is formed from the FFT of $\vec{\zeta}$. It is possible to combine both equations to form a new one that is only a function of $\vec{X}$. However, the complexity of solving such an equation would be high. Therefore, a simpler iterative approach is used to solve for $\vec{X}$. This starts with an initial estimate for $\vec{X}$ and $\vec{\zeta}$. In each iteration the estimate of $\vec{X}$ is improved using Eq. 7.14 followed by updating the estimate of $\vec{\zeta}$ using Eq. 7.19. This procedure is summarized in Table 7.1.

7.4.2 Method II: ICI mitigation utilizing adjacent symbols

It is possible to acquire channel slopes without using the redundancy of the cyclic prefix. This can be done by utilizing either the previous symbol or both adjacent symbols. A

constant slope is assumed over the time duration of $T + \frac{N}{2} \times T_s$ for the former and T for the latter. Use of the previous symbol can handle lower Doppler spread values without adding processing delay. On the other hand, use of both adjacent symbols would yield better performance at the price of delay of the reception of the next symbol. Since ICI mitigation in high mobility environments is of interest, both adjacent symbols are utilized to acquire channel slopes. This is shown in Fig. 7.2. Pilots of the current symbol provide an estimate of the channel at the mid-point of the current symbol, $\hat{h}_k^{(\frac{N}{2}-1)}$. This estimate is stored in the system. Upon processing of the next symbol, an estimate of the channel at mid-point of the next symbol, $\hat{h}_k^{(\frac{N}{2}-1),next}$, becomes available. Estimate of the slopes in region 2 (see Fig. 7.2) can then be obtained as follows:

$$\hat{cs}_k^{r_2} = \frac{\hat{h}_k^{(\frac{N}{2}-1),next} - \hat{h}_k^{(\frac{N}{2}-1)}}{T} \quad 0 \leq k \leq G \tag{7.21}$$

$cs_k^{r_2}$ represents the slope of the kth channel delay-profile sample in region 2. Similarly, $cs_k^{r_1}$, the slope in region 1, is estimated while processing the previous OFDM symbol and is stored in the receiver. Utilizing two slopes introduces a minor change in Eq. 7.10. It can be shown that,

$$\vec{y}_{method_{II}} \approx (\mathbf{h}_{mid} + \mathbf{M}^{r_1} \times \mathbf{A}^{r_1} + \mathbf{M}^{r_2} \times \mathbf{A}^{r_2}) \times \vec{x} + \vec{w} \tag{7.22}$$

$\mathbf{A}^{r_z}$ represents the channel slope matrix of Eq. 7.12 in the zth region ($1 \leq z \leq 2$) with $\mathbf{M}^{r_1}$ and $\mathbf{M}^{r_2}$ defined as follows:

$$\mathbf{M}^{r_1}(i,j) = \begin{cases} \mathbf{M}(i,j) & i = j \quad \& \quad 1 \leq i \leq \frac{N}{2} \\ 0 & else \end{cases}$$
$$\mathbf{M}^{r_2}(i,j) = \begin{cases} \mathbf{M}(i,j) & i = j \quad \& \quad \frac{N}{2} + 1 \leq i \leq N \\ 0 & else \end{cases} \tag{7.23}$$

Following the same procedure of Section 7.4, it can be easily shown that the frequency-domain relationship will be:

$$\vec{Y}_{method_{II}} \approx \mathbf{H}_{mid}\vec{X} + (\mathbf{COF}^{r_1} \times \mathbf{H}^{r_1}_{slope} + \mathbf{COF}^{r_2} \times \mathbf{H}^{r_2}_{slope}) \times \vec{X} + \vec{W} \tag{7.24}$$

In Eq. 7.24, $\mathbf{H}^{r_z}_{slope}$ is the diagonal matrix defined in Section 7.4 for the slopes of the zth region and can be formed from $\hat{cs}^{r_z}_k$. $\mathbf{COF}^{r_1}$ and $\mathbf{COF}^{r_2}$ are fixed matrices. It can be easily shown that

$$\mathbf{COF}^{r_1}(n,n') = T_s \times \begin{cases} \frac{-.5}{1-e^{\frac{-j2\pi(n-n')}{N}}} + \frac{1-(-1)^{n-n'}}{N\times(1-e^{\frac{-j2\pi(n-n')}{N}})^2} & n \neq n' \\ \frac{1}{4} - \frac{N}{8} & n = n' \end{cases}$$

$$\mathbf{COF}^{r_2}(n,n') = T_s \times \begin{cases} \frac{-.5}{1-e^{\frac{-j2\pi(n-n')}{N}}} - \frac{1-(-1)^{n-n'}}{N\times(1-e^{\frac{-j2\pi(n-n')}{N}})^2} & n \neq n' \\ \frac{1}{4} + \frac{N}{8} & n = n' \end{cases} \tag{7.25}$$

An estimate of X can then be obtained from Eq. 7.24.

7.4.3 Complexity Analysis

In general, solving Eq. 7.14 and 7.19 in case of Method I and Eq. 7.24 or 7.22 in case of Method II requires matrix inversion which could increase receiver complexity. For Method I, since the size of Eq. 7.19 is smaller, the main complexity is in solving Eq. 7.14. This requires an $N \times N$ matrix inversion. In general, any matrix inversion algorithm can be used. Also, Eq. 7.14 and 7.24 show a special structure. For instance, in Eq. 7.14 a sum of $diagonal + (toeplitz \times diagonal)$ needs to be inverted. The special structure can be used to reduce the complexity in iterative methods. Compared with the method proposed in [11], Methods I and II can handle considerably higher delay spread and Doppler spread (see Section 7.1) at the price of higher computational complexity (by neglecting some of the channel coefficients, the complexity of the method proposed in [11] is reduced to $N-q$ inversions of a matrix of size $q \times q$, where q is smaller than N). However, depending on the computational power of the receiver, other less complex methods like conjugate

gradient can be used for matrix inversion. A good survey of such methods and their complexity analysis can be found in [3], [12]. Furthermore, Section 7.6 shows how adding a noise/interference reduction mechanism can further reduce the complexity.

Another important issue is the convergence property of Method I. In general, for the range of normalized Doppler spread values that the piece-wise linear approximation can be applied, channel slopes are small enough that the initial estimate of zero in the first step of Method I results in convergence of the method after a few iterations. A more detailed analysis of convergence properties of such iterative methods is beyond the scope of this thesis but can be found in [12], [18].

7.5 Mathematical Analysis of the effect of linearization

In this section a mathematical analysis is provided for the effect of piece-wise linear approximation in mitigating ICI. A narrowband time-varying channel is assumed to make the analysis tractable. Wideband channels will be considered in the next section. $SIR_{mob,ave}$ is defined as the ratio of average received signal power to the average received interference power. The goal is to calculate $SIR_{mob,ave}$ when ICI is mitigated and compare it to that of the "no mitigation" case. Consider a narrowband time-varying channel, $h^{(i)}$. Note that the index k of $h_k^{(i)}$ is dropped in this section under the narrowband channel assumption. Then in the absence of noise, Eq. 7.1 can be simplified as follows:

$$y_i = h^{(i)} \times x_i \tag{7.26}$$

The estimate of x_i will be

$$\hat{x}_i = \frac{y_i}{\hat{h}^{(i)}} = x_i + \frac{e_i}{\hat{h}^{(i)}} \times x_i \tag{7.27}$$

In Eq. 7.27, $e_i = h^{(i)} - \hat{h}^{(i)}$. Since $\hat{h}^{(i)}$ is the sum of a considerable number of uncorrelated random variables as estimated from pilot tones, its distribution is approximated with a complex Gaussian. In practice if $\hat{h}^{(i)}$ has values near zero, the received signal will not be

divided by those small numbers. From a theoretical standpoint, if the cases of near zero $\hat{h}^{(i)}$ are not excluded, the variance of $\hat{x}_i$ will be infinite (this can be seen from the results of this section). Therefore, the probability of a near zero $\hat{h}^{(i)}$ should be excluded to make the analysis meaningful. This can be done by introducing a slight modification in the pdf of $|\hat{h}^{(i)}|^2$. Let $prob(|\hat{h}^{(i)}|^2 \leq \mu) = \epsilon$. Then for an ϵ near zero, the pdf of $|\hat{h}^{(i)}|^2$ is taken to be zero for $|\hat{h}^{(i)}|^2 \leq \mu$.

Taking an FFT of Eq. 7.27,

$$\hat{X}_i = X_i + NI_i \tag{7.28}$$

where NI_i is the FFT of $\frac{e_i}{\hat{h}^{(i)}} \times x_i$. NI_i is not purely interference and contains a term that depends on X_i as well. However, it can be shown that the power of that term is considerably smaller than the power of the main signal term. Therefore, to reduce the complexity of the analysis NI_i is taken as the interference term which makes the analysis a tight approximation. $SIR_{mob,ave}$ can then be defined as follows:

$$SIR_{mob,ave} = \frac{\sigma_X^2}{\sigma_{NI}^2} \tag{7.29}$$

σ_X^2 is the average power of X and σ_{NI}^2 can be calculated as follows:

$$\sigma_{NI}^2 = E(NI_i NI_i^*) \tag{7.30}$$

Since $E(x_n x_{n'}^*) = \frac{\sigma_X^2}{N}\delta_{n,n'}$ for arbitrary n and n', then

$$\sigma_{NI}^2 = \frac{\sigma_X^2}{N} \times \sum_{i=0}^{N-1} E(|\frac{e_i}{\hat{h}^{(i)}}|^2) \tag{7.31}$$

and

$$SIR_{mob,ave} = \frac{N}{\sum_{i=0}^{N-1} E(\frac{|e_i|^2}{|\hat{h}^{(i)}|^2})} \tag{7.32}$$

Both e_i and $\hat{h}^{(i)}$ have complex Gaussian distributions. Furthermore, they are jointly Gaussian (since a linear combination of them is the sum of a considerable number of

uncorrelated random variables) and correlated. Then $E(|\frac{e_i}{\hat{h}^{(i)}}|^2)$ will be as follows:

$$\begin{aligned} E(|\frac{e_i}{\hat{h}^{(i)}}|^2) &= E(\frac{[Re\{e_i\}]^2 + [Im\{e_i\}]^2}{\left[Re\{\hat{h}^{(i)}\}\right]^2 + \left[Im\{\hat{h}^{(i)}\}\right]^2}) \\ &= E(\frac{E([Re\{e_i\}]^2 + [Im\{e_i\}]^2)|_{\hat{h}^{(i)}}}{\left[Re\{\hat{h}^{(i)}\}\right]^2 + \left[Im\{\hat{h}^{(i)}\}\right]^2}) \\ &= E(\frac{E([Re\{e_i\}]^2)|_{Re\{\hat{h}^{(i)}\}} + E([Im\{e_i\}]^2)|_{Im\{\hat{h}^{(i)}\}}}{\left[Re\{\hat{h}^{(i)}\}\right]^2 + \left[Im\{\hat{h}^{(i)}\}\right]^2}) \end{aligned} \tag{7.33}$$

where $e_i = Re\{e_i\} + jIm\{e_i\}$ and $\hat{h}^{(i)} = Re\{\hat{h}^{(i)}\} + jIm\{\hat{h}^{(i)}\}$. $Re\{e_i\}$, $Im\{e_i\}$, $Re\{\hat{h}^{(i)}\}$ and $Im\{\hat{h}^{(i)}\}$ are zero mean Gaussian variables with independent inphase and quadrature parts. It can be easily shown [19] that $E([Re\{e_i\}]^2)|_{Re\{\hat{h}^{(i)}\}} = \sigma^2_{Re\{e_i\}}(1 - \rho^2_{Re\{e_i\},Re\{\hat{h}^{(i)}\}}) + \frac{\rho^2_{Re\{e_i\},Re\{\hat{h}^{(i)}\}}\sigma^2_{Re\{e_i\}}}{\sigma^2_{Re\{\hat{h}^{(i)}\}}}\left[Re\{\hat{h}^{(i)}\}\right]^2$ with $\sigma^2_{Re\{e_i\}} = E([Re\{e_i\}]^2) = .5\sigma^2_{e_i}$, $\sigma^2_{Re\{\hat{h}^{(i)}\}} = E(\left[Re\{\hat{h}^{(i)}\}\right]^2) = .5\sigma^2_{\hat{h}^{(i)}}$ and the correlation coefficient ρ defined as follows: $\rho_{z,z'} = \frac{E(zz'^*)}{\sigma_z\sigma_{z'}}$ for arbitrary z and z'. $E([Im\{e_i\}]^2)|_{Im\{\hat{h}^{(i)}\}}$ can be similarly calculated. Therefore,

$$E(|\frac{e_i}{\hat{h}^{(i)}}|^2)) = \frac{\rho^2_{e_i,\hat{h}^{(i)}}\sigma^2_{e_i}}{\sigma^2_{\hat{h}^{(i)}}} + \sigma_{e_i^2}(1 - \rho^2_{e_i,\hat{h}^{(i)}})E(\frac{1}{|\hat{h}^{(i)}|^2}) \tag{7.34}$$

where $\sigma^2_{\hat{h}^{(i)}} = E(|\hat{h}^{(i)}|^2)$, $\sigma^2_{e_i} = E(|e_i|^2)$ and ρ is as defined earlier. These parameters are functions of channel correlation characteristics (or Doppler spectrum) and are derived in Appendix B for both the cases of ICI mitigation and no mitigation. Also, it can be easily shown that $E(\frac{1}{|\hat{h}^{(i)}|^2}) = \frac{Ei(-ln(1-\epsilon))}{\sigma^2_{\hat{h}^{(i)}}}$ where Ei and ln stand for the exponential integral and logarithm in the base e respectively. Inserting Eq. 7.34 in Eq. 7.31 results in the following $SIR_{mob,ave}$:

$$SIR_{mob,ave} = \frac{N}{\sum_{i=0}^{N-1}\frac{\sigma^2_{e_i}\times\rho^2_{e_i,\hat{h}^{(i)}} + Ei(-ln(1-\epsilon))\times(1-\rho^2_{e_i,\hat{h}^{(i)}})\times\sigma^2_{e_i}}{\sigma^2_{\hat{h}^{(i)}}}} \tag{7.35}$$

Fig. 7.3 shows $SIR_{mob,ave}$ of Eq. 7.35 for both the cases of "ICI mitigation" and "no mitigation", as a function of $f_{d,norm}$ at $\epsilon = 10^{-6}$. The derivations of Appendix B are used to plot the theoretical results. $f_{d,norm}$ is defined as f_d (maximum Doppler) divided by the

sub-carrier spacing. The channel power spectrum is the Jakes spectrum [10] for this result. This means that function R of Appendix B is $R_h(t) = J_0(2\pi f_d t)$ with J_0 representing the zero-order Bessel function. The analytic results match the corresponding simulations as can be seen. The figure shows how ICI mitigation through linearization improves $SIR_{mob,ave}$.

7.6 Noise/Interference Reduction

In Section 7.3, an estimate of h_k^{ave} was acquired using equally-spaced pilots. In most cases, the number of active (non-zero) channel delay spread samples will be less than $\nu + 1$, especially in an SFN environment. In such cases, some of the estimated samples would be noise/interference samples after the IFFT in Eq. 7.6. Therefore, if they can be removed, the effect of noise/interference will be reduced. To do so, estimated channel delay spread samples are compared with a *Threshold*. If the value of a sample is below the *Threshold*, it will be set to zero:

$$if \quad |\hat{h}_k^{ave}| \leq Threshold \quad => \quad \hat{h}_k^{ave} = 0, \quad 0 \leq k \leq L-1 \tag{7.36}$$

The optimum way to define the *Threshold* is to relate it to the received $SNIR$ (Signal to Noise plus Interference Ratio) such that the channel delay-profile samples comparable to or below the noise/interference level are zeroed. However, this requires estimation of the power of noise/interference which may not be feasible in a high mobility environment. Instead, a simple but effective *Threshold* is defined. Upon estimation of $\hat{h}_k^{ave}$ from Eq. 7.6, the estimated sample with the maximum absolute value is detected. Let MAV represent this maximum. Then all the estimated samples with absolute values smaller than $\frac{MAV}{z}$ for some $z \geq 1$ will be zeroed. Choosing small z increases the chance of losing channel samples with significant values and only improves the performance if the noise and/or interference level is high. On the other hand, choosing a high z will reduce the risk of losing samples with considerable values at the price of less efficiency in high noise and/or interference cases. In general, in the absence of knowledge of $SNIR$, it is

better to choose z such that losing the estimates below the *Threshold* does not introduce significant performance loss. Following this criterion, $z = 10$ is used in simulations in the next section. In the case of losing a channel sample, the power of such a sample is less than 1% of the power of the strongest channel sample. This will lead to a slight performance loss at very high $SNIR$ which should not be a problem since these cases already have a very low error rate.

Furthermore, the number of non-zero channel delay-profile samples can be estimated from $\hat{h}_k^{ave}$ after Eq. 7.36 is applied. Let $N_p \leq L$ represent this estimate in the current OFDM symbol. Therefore, only N_p slopes need to be estimated. This will reduce the complexity of both algorithms. For instance it will reduce the number of unknowns from G to N_p in step 4 of Method I. This reduction can be considerable for SFN channels.

7.7 Simulation Results

An OFDM system is simulated in a time-varying environment with high delay spread. System parameters[3] are as follows. Input Modulation is 8PSK. Bit rate (excluding the redundancy) is 7.3Mbps, $N = 892$ and $L = 223$. Length of the guard interval (T_g) is $44.4\mu s$ and length of one OFDM symbol (T) is $273.5\mu s$. The sampling period, T_s, is $.26\mu s$ and $G = \frac{T_g}{T_s} = 173$. Two power-delay profiles are simulated. The power-delay profile of channel c7.1 has non-zero values at two channel delay-profile samples which are separated by $20\mu s$. Power-delay profile of channel c7.2 is the same as channel c5.4 of Chapter 5 and is shown again in Fig. 7.4. Each channel delay-profile sample is generated as a random process with Rayleigh distributed amplitude and uniformly distributed phase using Jakes model [10]. Therefore, the time-domain auto-correlation of each channel delay-profile sample is a zero-order Bessel function. For both channels, the power of channel delay-profile samples is normalized to result in a total power of one. To see how ICI mitigation methods reduce the error floor, Fig. 7.5 shows the average bit error rate, P_b (before decoding), in the absence of noise for both channels. In the "no mitigation" case, pilots

[3]Parameters are based on Sirius Radio second generation system specification proposal for an SFN environment.

are used to estimate h_k^{ave} which is then used to detect the transmitted data without any estimation of time-variations. As can be seen from Fig. 7.5, average P_b increases for the "no mitigation" case. Both of the proposed methods reduce the error floor considerably. Method II shows slightly better performance than Method I. This is due to the iterative way of solving for unknowns in Method I. Also, channe1 c7.1 results in a lower error floor due to its lower delay spread and smaller number of non-zero power-delay profile samples, as expected. To see the effect of noise, Fig. 7.6 shows average P_b (before decoding) as a function of average received SNR for $f_{d,norm} = 6.5\%$. Average received SNR is defined as the ratio of the average total signal power received through all the channel paths to the average received noise power. Average error rate for the ideal case of no Doppler is also plotted for comparison. It can be seen from Fig. 7.6 that ICI mitigation reduces the error rate considerably for both channels. In particular for channel c7.1, the error rate is almost reduced to that of the case with no Doppler.

To see how ICI mitigation methods reduce the required received SNR for achieving a specific pre-decoding bit error rate, Fig. 7.7 shows the required received SNR for reaching an average $P_b = .02$ before decoding. The graph shows how ICI mitigation can save power. For comparison, the required received SNR for the case of no Doppler is 17.6dB for both channels. It can be seen that both methods reduce the amount of required power to a level close to that of the no Doppler case. For instance, at $f_{d,norm} = 8\%$, the amount of power saving is around 4dB. Compared to the "no mitigation" case, the amount of power saving increases considerably as $f_{d,norm}$ increases.

7.8 Conclusion

Two new methods for ICI mitigation in pilot-aided OFDM mobile systems are proposed in this chapter. Both methods use a piece-wise linear approximation to estimate channel time-variations in each OFDM symbol. Performance improvement was shown analytically by deriving SIR_{ave} formulas in a narrowband mobile environment. In high delay spread and Doppler spread environments, simulation results show considerable performance improvement. They illustrate that applying these methods would reduce average P_b or the

required received SNR to values close to those for the cases with no Doppler. The power savings become considerable as $f_{d,norm}$ increases.

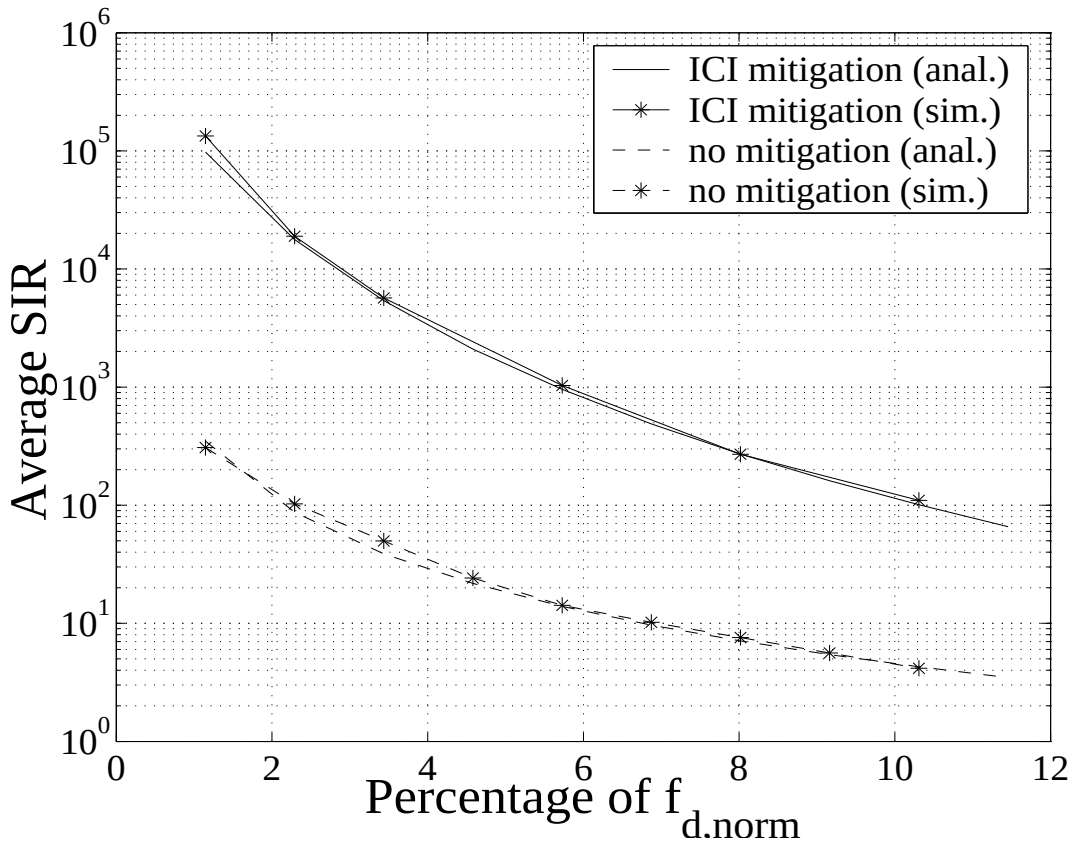

Figure 7.3: Average SIR vs. % of $f_{d,norm}$ for a narrowband channel

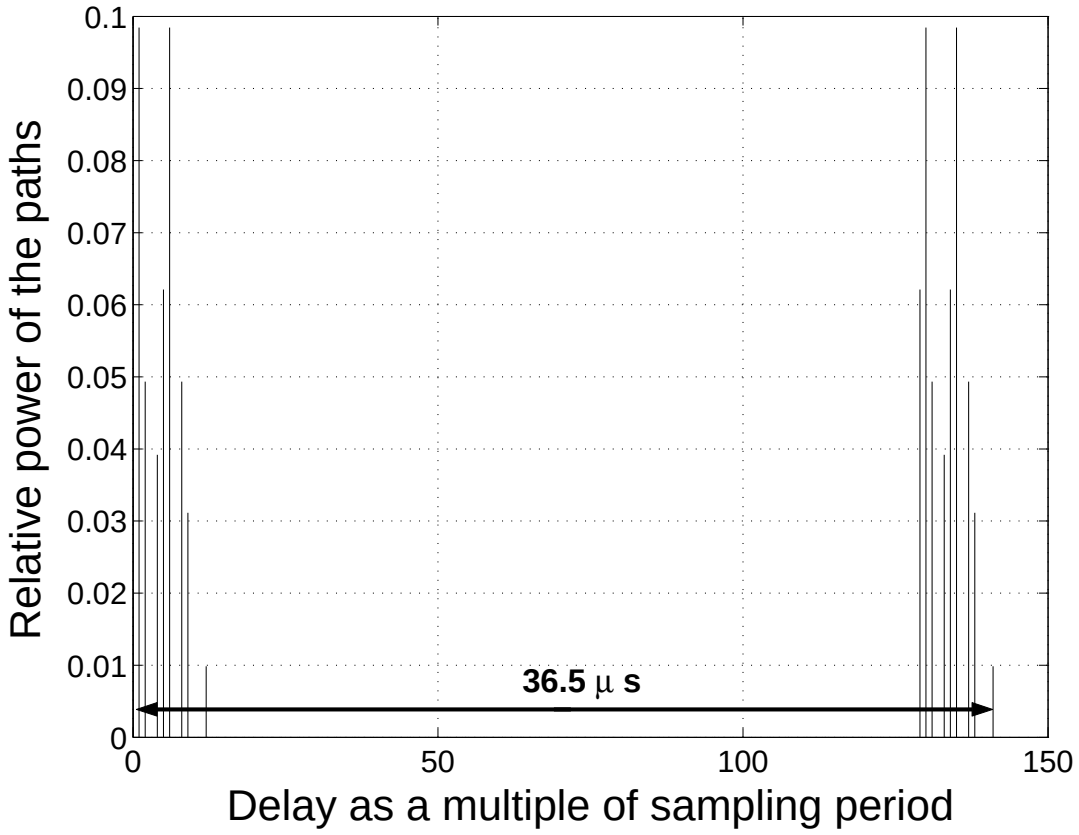

Figure 7.4: Power-Delay profile of channel c7.2 (same as channel c5.4 of Fig. 5.6)

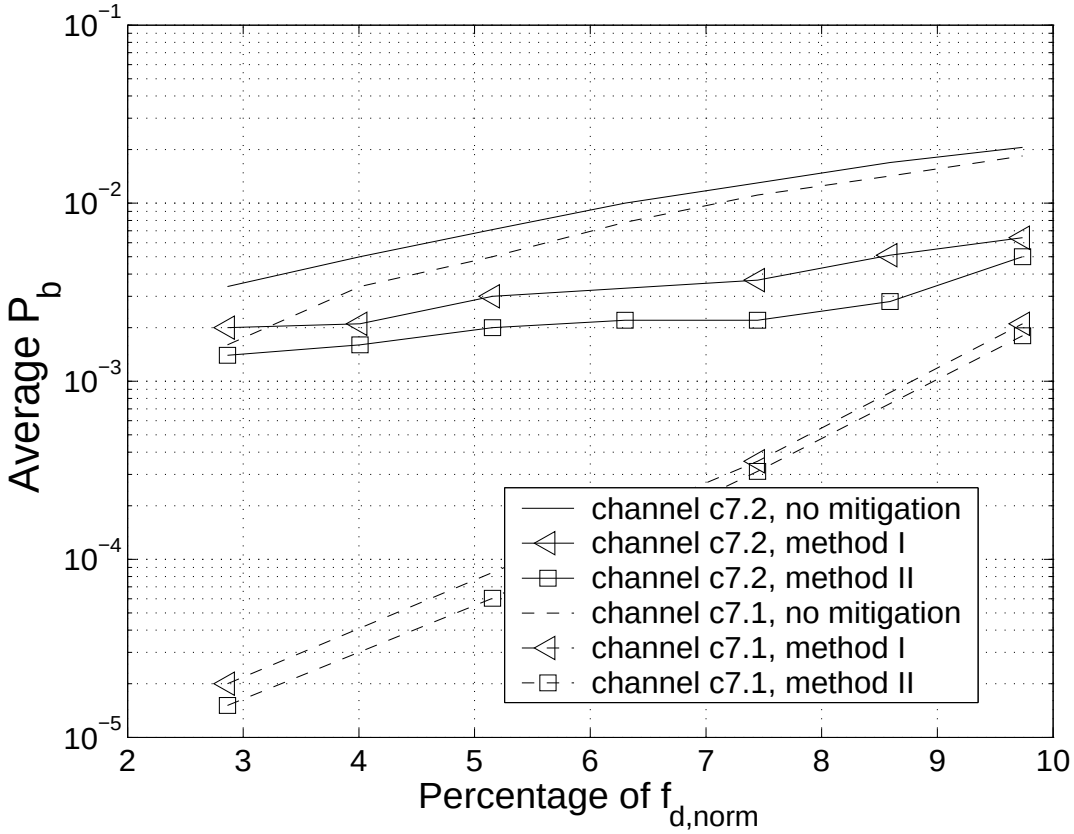

Figure 7.5: Error floor vs. maximum normalized Doppler

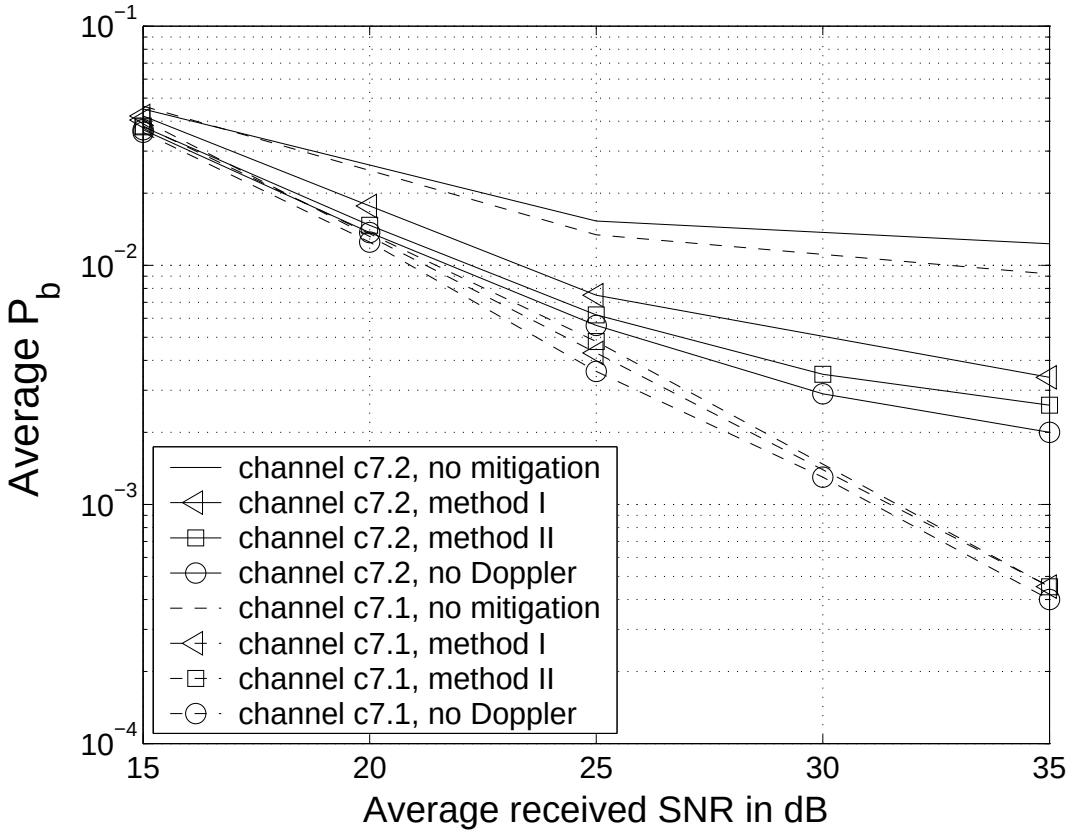

Figure 7.6: Average bit error rate vs. average received SNR for $f_{d,norm} = 6.5\%$

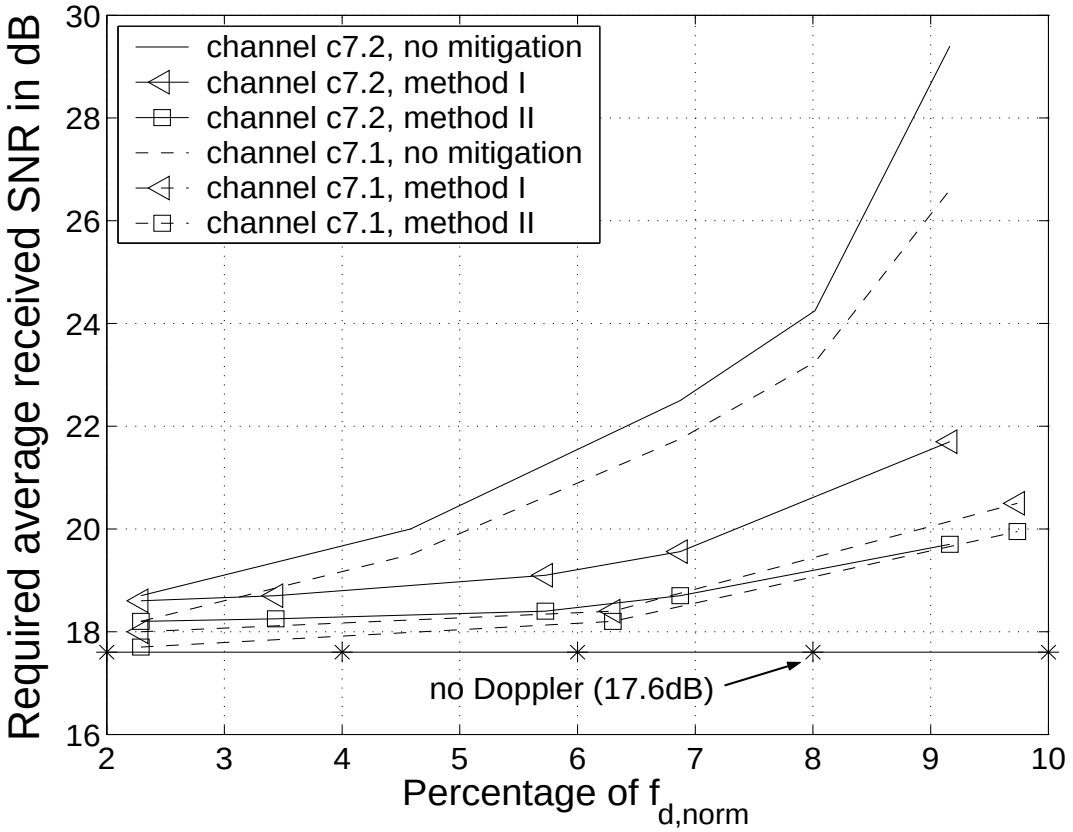

Figure 7.7: Required average received SNR to achieve average $P_b = .02$

Chapter 8

Conclusions

8.1 Thesis Summary

Using OFDM technology for high mobility applications poses several challenges. For instance timing synchronization can become more challenging in high mobility environments as the power-delay profile of the channel may change rapidly. Furthermore, high mobility introduces time-variations within one OFDM symbol, which results in loss of orthogonality among sub-carriers. These issues were addressed in this thesis.

A brief introduction to mobile communications was given in Chapter 2 and basics of an OFDM system were introduced in Chapter 3.

In high delay spread environments, there is a need to transmit frequency-domain pilot tones to estimate channel frequency-selectivity. To estimate the channel at all the sub-carriers using the pilot tones, different interpolators can be used. Average error probability formulas were derived for an OFDM system that uses pilot tones. Using these expressions the performance of a trigonometric interpolator and a linear interpolator was compared. It was shown analytically and through simulations that for those cases where noise is the dominant cause of performance degradation, the linear interpolator outperforms the trigonometric one. It was also shown that as delay spread increases and becomes the dominant cause of performance degradation, the trigonometric interpolator outperforms the linear one considerably and therefore was used in the subsequent chapters for frequency-domain channel estimation.

The effects of timing synchronization errors on an OFDM system in general and on the pilot-aided channel estimator in particular were studied in Chapter 5. Analytical expressions for the average power of the interference terms introduced by timing errors were derived. Analytical expressions for channel estimation error in the presence of timing errors were also found. By considering both the channel estimator and the timing synchronizer, the super-sensitivity of the channel estimator to timing errors was shown. Using this sensitivity, a timing synchronization algorithm was proposed that exploits the super-sensitivity of the channel estimator to achieve robust timing synchronization with no need for additional training overhead. Simulation results showed the performance of the proposed method indicating that it can reduce the probability of error close to that of the perfect synchronization case.

Analysis in Chapter 5 was carried out under the low-mobility assumption. That analysis was extended to high mobility environments in Chapter 6. Expressions for average signal to interference ratio and channel estimation error were derived in the presence of mobility and timing errors. The proposed synchronization algorithm was shown to be robust for high-mobility applications.

Once timing synchronization is achieved, the effects of Doppler spread need to be mitigated. Two new methods were proposed in Chapter 7 for Doppler spread mitigation. Neither method requires additional training overhead. They were based on a piece-wise linear approximation for time-variations of the channel. Performance improvement was shown analytically by deriving average signal to interference ratio formulas in a narrowband mobile environment. Then simulation results showed the performance of the proposed methods for high delay spread and Doppler spread applications. It was shown that applying these methods would reduce average probability of error or the required received SNR to values close to those for the cases with no Doppler spread.

8.2 Future Work

A timing synchronization algorithm was proposed in Chapter 6 that would be robust in the presence of high mobility. The analysis can be extended to show the performance of the proposed timing synchronization algorithm in the presence of fixed frequency offset or phase noise. Furthermore two algorithms were proposed in Chapter 7 for Doppler spread mitigation. Since both algorithms were based on a piece-wise linear approximation for channel time-variations, there would be a limit on the amount of Doppler spread that they can mitigate. As there is a trend towards higher carrier frequencies, it is important to design Doppler mitigation algorithms that would mitigate higher Doppler spread values while minimizing the amount of additional training overhead. One possibility would be to explore higher-order approximations for time-domain channel variations.

OFDM systems are also sensitive to fixed frequency offset and phase noise. Design of robust frequency offset and phase noise estimation algorithms without use of additional training overhead can be a challenge. Work could be conducted to extend the piece-wise linear model (or higher-order models) to estimate frequency offset or phase noise. The effect of both can be modeled as a time-variant equivalent channel. Then in the case of mitigating phase noise, another possibility is to use an estimate of the time-domain correlation characteristics of this time-variant equivalent channel to estimate and mitigate phase noise. In practical scenarios the information on the correlation characteristics may not be available. Such analysis would at least provide an upper bound on the performance improvement and would give insights into design of a better estimator.

In the case of perfect timing synchronization in the absence of mobility but in the presence of delay spread, a multiplication relationship would result in the frequency domain between the transmitted data point and channel for an OFDM system. In the absence of delay spread (i.e. narrowband channel) and in the presence of mobility, a multiplication relationship would result in the time domain making it more computationally efficient to do channel estimation and data detection in the time domain. In the presence of high delay spread and Doppler spread, processing should be done in both time and frequency

domains. Optimization of the amount of processing necessary in each domain and modification of the structure of OFDM systems to reduce computational complexity can be a challenging and important research problem for these cases.

Appendix A

Piecewise Linearization's Impact on Correlation

Consider a wide-sense stationary process h and its piece-wise linear approximation h_{lin} shown in Fig. A.1. h can represent any of the channel paths. $h_{lin}^{(i)}$ represents h_{lin} at time instant $i \times T_s$. It is of interest to compare the auto-correlation function of h_{lin}, $R_{h_{lin}}(t = iT_s, z = nT_s) = E(h_{lin}^{(i)} h_{lin}^{(n)*})$, to that of h. From Fig. A.1, $h_{lin}^{(i)}$ and $h_{lin}^{(n)}$ can be expressed as follows:

$$\begin{aligned} h_{lin}^{(i)} &= h_{lin}^{(i_0)} + \Delta t_1 \times \frac{h_{lin}^{(i_1)} - h_{lin}^{(i_0)}}{T} \quad i_0 \leq i \leq i_1 \\ h_{lin}^{(n)} &= h_{lin}^{(n_0)} + \Delta t_2 \times \frac{h_{lin}^{(n_1)} - h_{lin}^{(n_0)}}{T} \quad n_0 \leq n \leq n_1 \end{aligned} \tag{A.1}$$

For simplicity, it is assumed that $h_{lin}^{(g)} = h^{(g)}$ for[1] $g = i_0$, i_1, n_0 and n_1. Then, $R_{h_{lin}}(t, z)$ will be

$$\begin{aligned} R_{h_{lin}}(t = iT_s, z = nT_s) &= (1 - \frac{\Delta t_1}{T})(1 - \frac{\Delta t_2}{T}) \times E(h^{(i_0)} h^{(n_0)*}) + \\ &\quad (\frac{\Delta t_2}{T} - \frac{\Delta t_1 \Delta t_2}{T^2}) \times E(h^{(i_0)} h^{(n_1)*}) + \\ &\quad (\frac{\Delta t_1}{T} - \frac{\Delta t_1 \Delta t_2}{T^2}) \times E(h^{(i_1)} h^{(n_0)*}) + \end{aligned}$$

[1]Due to the presence of noise and/or interference, $h_{lin}^{(g)}$ may differ from $h^{(g)}$ for $g = i_0$, i_1, n_0 and n_1. Extending the analysis to include this difference should be a straightforward extension of the work in this appendix.

$$\frac{\Delta t_1 \Delta t_2}{T^2} \times E(h^{(i_1)} h^{(n_1)*}) \tag{A.2}$$

Let $R_h(t = iT_s, z = nT_s) = R_h((i-n) \times T_s) = E(h^{(i)} h^{(n)*})$ represent the auto-correlation function of process h. Then,

$$\begin{aligned} R_{h_{lin}}(t,z) &= R_{h_{lin}}(\Delta t_1, \Delta t_2, k) \\ &= (\frac{\Delta t_1}{T} - \frac{\Delta t_1 \Delta t_2}{T^2}) \times R_h((k-1)T) + \\ &\quad (\frac{\Delta t_2}{T} - \frac{\Delta t_1 \Delta t_2}{T^2}) \times R_h((k+1)T) + \\ &\quad (1 - \frac{\Delta t_1}{T} - \frac{\Delta t_2}{T} + 2\frac{\Delta t_1 \Delta t_2}{T^2}) \times R_h(kT) \end{aligned} \tag{A.3}$$

Since h is a wide-sense stationary process, $R_h(t,z) = R_h(t-z) = R_h(\Delta t_1 - \Delta t_2 - kT)$. Define ΔPW as the average power of the difference of $R_h(t,z)$ and $R_{h_{lin}}(t,z)$ over N_{os} OFDM symbols:

$$\Delta PW = \sum_{k=0}^{k=N_{os}-1} \int_0^T \int_0^T (R_{h_{lin}}(\Delta t_1, \Delta t_2, k) - R_h(\Delta t_1 - \Delta t_2 - kT))^2 d\Delta t_1 d\Delta t_2 \tag{A.4}$$

We are interested in $\Delta PW_{normalized}$ which can be defined as follows:

$$\Delta PW_{normalized} = \frac{\Delta PW}{\sum_{k=0}^{k=N_{os}-1} \int_0^T \int_0^T R_h^2(\Delta t_1 - \Delta t_2 - kT) d\Delta t_1 d\Delta t_2} \tag{A.5}$$

Fig. A.2 shows $\Delta PW_{normalized}$ For $R_h(t) = J_0(2\pi f_d t)$ as a function of $f_d \times T$. N_{os} is chosen large enough, i.e. $N_{os} \gg \frac{1}{f_d \times T}$, so that $R_h(N_{os}T)$ becomes negligible. The graph suggests that for $f_d \times T$ of up to 20%, $\Delta PW_{normalized}$ is negligible. For instance, for $f_d \times T = 15\%$, $\Delta PW_{normalized}$ is 1%.

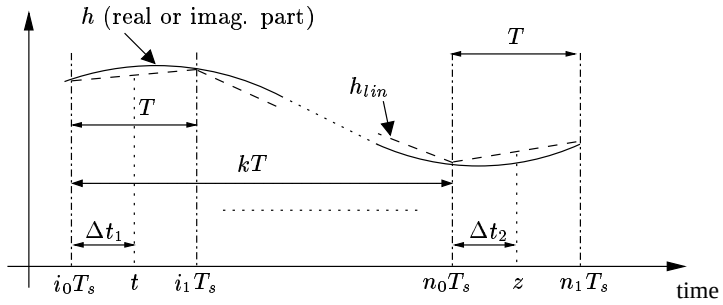

Figure A.1: Piece-wise linear approximation of a random process h

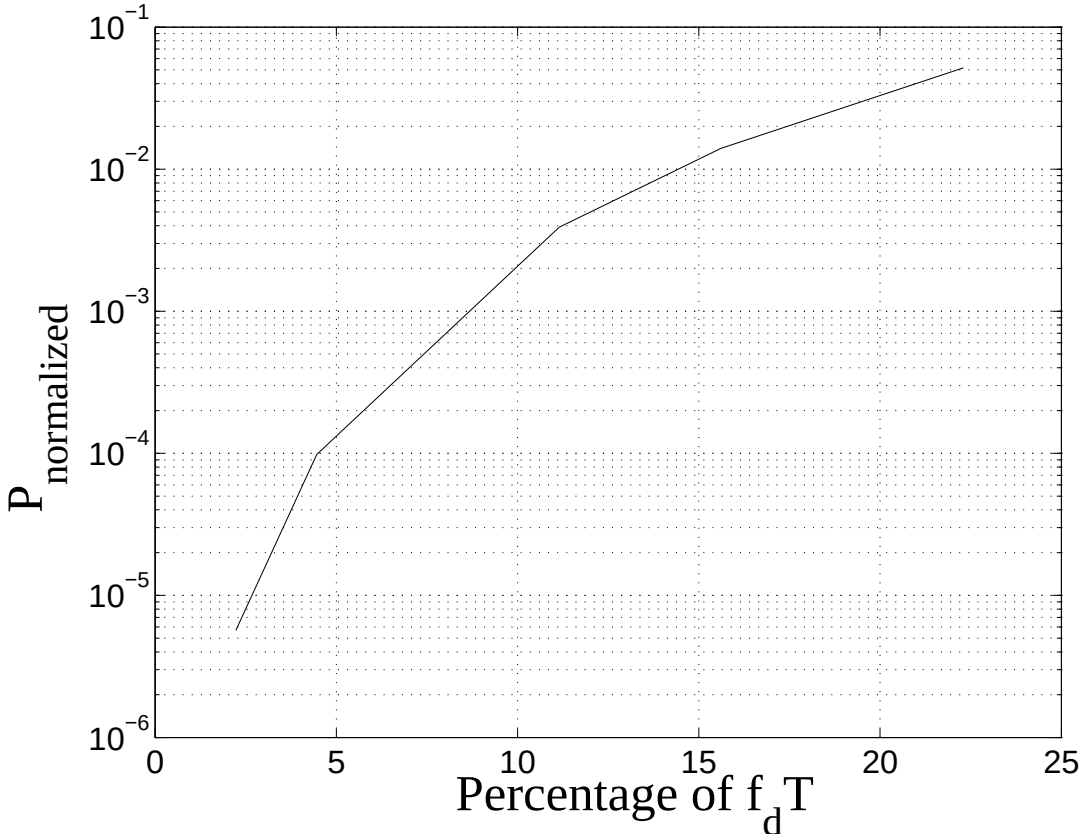

Figure A.2: $\Delta PW_{normalized}$ vs. % of $f_d \times T$

Appendix B

Finding $\sigma^2_{e_i}$, $\sigma^2_{\hat{h}^{(i)}}$ and $\rho_{e_i,\hat{h}^{(i)}}$

B.0.1 The Case of ICI Mitigation

From Eq. 7.6, in the absence of noise and for a narrowband channel, $\hat{h}^{ave} = h^{ave} + \Delta_{h^{ave}}$, where $\Delta_{h^{ave}}$ is the estimation noise with variance of $\sigma^2_{\Delta_{h^{ave}}}$. It can be easily shown, using Eq. 7.5 and 7.6, that $\sigma^2_{\Delta_{h^{ave}}} = \frac{N^2 R_h(0) - N R_h(0) - 2\sum_{k=1}^{N-1}(N-k)R_h(kT_s)}{N^2 L}$. R_h is the autocorrelation function of the narrowband channel as defined in Appendix A. Furthermore, it can be shown that $\mathrm{E}(\Delta_{h^{ave}} \times h^{(i)*}) = 0$ due to the independency of the transmitted data points and channel. Similarly, in the next OFDM symbol, $\hat{h}^{ave,next} = h^{ave,next} + \Delta_{h^{ave,next}}$, where $\Delta_{h^{ave,next}}$ is the estimation noise with $\sigma^2_{\Delta_{h^{ave,next}}} = \sigma^2_{\Delta_{h^{ave}}}$. Define $co_1(i) = (i - .5N + 1)\frac{T_s}{T}$ and $co_2(i) = 1 - co_1(i)$. Using Method II,

$$\hat{h}^{(i)} = co_2(i)\hat{h}^{ave} + co_1(i)\hat{h}^{ave,next} \quad i \in Region2 \tag{B.1}$$

A similar formula can be written for estimation in Region 1. Using these formulas, after some lengthy but straightforward computations, the following formulas can be derived:

$$\begin{aligned}
\sigma^2_{\hat{h}^{(i)}} &= (co_2^2(i) + co_1^2(i)) \times (\frac{N R_h(0) + 2\sum_{k=1}^{N-1} R_h(kT_s)}{N^2} + \sigma^2_{\Delta_{h^{ave}}}) + \\
&\quad 2\frac{co_2(i)co_1(i)}{N^2} \sum_{k=T/T_s-N+1}^{T/T_s+N-1} (N - |k - T/T_s|) \times R_h(kT_s) \\
\sigma^2_{e_i} &= R_h(0) + \sigma^2_{\hat{h}^{(i)}} - \frac{2}{N} \times (co_2(i) \sum_{k=0}^{N-1} R_h((i-k)T_s) + co_1(i) \sum_{k=T/T_s}^{T/T_s+N-1} R_h((i-k)T_s))
\end{aligned}$$

$$\rho_{e_i,\hat{h}^{(i)}} = \frac{\frac{1}{N} \times (co_2(i) \sum_{k=0}^{N-1} R_h((i-k)T_s) + co_1(i) \sum_{k=T/T_s}^{T/T_s+N-1} R_h((i-k)T_s)) - \sigma^2_{\hat{h}^{(i)}}}{\sigma_{\hat{h}^{(i)}} \sigma_{e_i}} \tag{B.2}$$

B.0.2 The Case of No Mitigation

In this case, $\hat{h}^{(i)} = \hat{h}^{ave}$ for $0 \leq i \leq N-1$. Then the parameters can be easily derived as follows:

$$\begin{aligned}
\sigma^2_{\hat{h}^{(i)}} &= \frac{NR_h(0) + 2\sum_{k=1}^{N-1} R_h(kT_s)}{N^2} + \sigma^2_{\Delta_{h^{ave}}} \\
\sigma^2_{e_i} &= R_h(0) + \sigma^2_{\hat{h}^{(i)}} - \frac{2}{N} \sum_{k=0}^{N-1} R_h((i-k)T_s) \\
\rho_{e_i,\hat{h}^{(i)}} &= \frac{\frac{1}{N} \sum_{k=0}^{N-1} R_h((i-k)T_s) - \sigma^2_{\hat{h}^{(i)}}}{\sigma_{\hat{h}^{(i)}} \sigma_{e_i}}
\end{aligned} \tag{B.3}$$

Bibliography

[1] Ahmad R. S. Bahai and Burton R. Saltzberg, *Multi-carrier digital communications - theory and applications of OFDM.* NJ: Kluwer Academic, 1999

[2] J. Bingham, "Multicarrier modulation for data transmission: an idea whose time has come," IEEE Communications Magazine, 28(5):5-14, May 1990

[3] S. Boyd and L. Vandenberghe, *Convex Optimization.* Cambridge University Press, 2003

[4] H. Cheon and D. Hong, "Effect of channel estimation error in OFDM-based WLAN," IEEE Comm. letter, vol. 6, no. 5, May 2002

[5] J. Chow, J. Tu and J. Cioffi, "A discrete multitone transceiver system for HDSL applications," IEEE Journal on Selected Areas in Communications, 9(6):895-908, Aug. 1991

[6] L. Cimini, "Analysis and simulation of a digital mobile channel using orthogonal frequency division multiplexing," IEEE Trans. Commun., vol. COMM-33, pp. 665-675, July 1985

[7] D. Cox, "Universal digital portable radio communications," Proceedings of the IEEE, pp. 436:477, Apr. 1987

[8] B. Le Floch, R. Hallbert-Lasalle and D. Castellain, "Digital audio broadcasting to mobile receivers," IEEE Trans. Consum. Electronics, vol. 35, no. 3, pp. 493-503, Aug. 1989

[9] A. Hutter, E. Carvalho and J. Cioffi, "On the impact of channel estimation for multiple antenna diversity reception in mobile OFDM systems," 34th Asilomar 2000, volume: 2, Page(s): 1820 -1824

[10] William C. Jakes, *Microwave Mobile Communications.* IEEE Press, 1974

[11] W. G. Jeon and K. H. Chang, "An equalization technique for Orthogonal Frequency-Division Multiplexing systems in time-variant multipath channels," IEEE Trans. on Commun., Vol. 47, No. 1, Jan. 1999

[12] C.T. Kelley, *Iterative Methods for Linear and Nonlinear Equations.* Philadelphia, PA: Frontiers in Applied Mathematics, 1995

[13] Ye Li and L. Cimini, "Bounds on the inter-channel interference of OFDM in time-varying impairments," IEEE Trans. Commun., vol. 49, No. 3, March 2001

[14] S. Muller, "On the optimality of metrics for coarse frame synchronization in OFDM: a comparison," Ninth IEEE International Symposium on PIMRC, 1998

[15] R. Negi and J. Cioffi, "Pilot tone selection for channel estimation in a mobile OFDM system," IEEE Trans. on Consumer Electronics, vol. 44, no. 3, Aug. 98

[16] B. O'Hara and A. Petrick, *The IEEE 802.11 Handbook: A Designer's Companion.* Published by Standards Information Network, IEEE Press

[17] A. Oppenheim and R. Schafer, *Discrete-time Signal Processing.* Englewood Cliffs, N J: Prentice-Hall, 1989

[18] J.M. Ortega and W.C. Rheinboldt, *Iterative Solution of Nonlinear Equations in Several Variables.* San Diego, CA: Academic Press Inc., 1970

[19] Athanasios Papoulis, *Probability, Random Variables and Stochastic Processes.* McGrawHill International, 3rd Edition, 1991

[20] Theodore S. Rappaport, *Wireless Communications: Principles and Practice.* Prentice Hall, 1996

[21] P. Robertson and S. Kaiser, "The effects of Doppler spreads in OFDM(A) mobile radio systems," Proc. VTC'99-Fall, 1999, pp. 329-333

[22] M. Russell and G. Stuber, "Interchannel interference analysis of OFDM in a mobile environment," Proc. VTC'95, 1995, pp. 820-824

[23] H. Sari, G. Karam and J. Janclaude, "Transmission techniques for digital TV broadcasting," IEEE Commun. Mag., vol. 36, pp. 100-109, Feb. 1995

[24] T. M. Schmidl, "Synchronization algorithms for wireless data transmission using Orthogonal Frequency Division Multiplexing (OFDM)," PhD Dissertation, Stanford university, June 1997

[25] M. Speth, F. Classen and Meyr, "Frame Synchronization of OFDM systems in frequency selective fading channels," IEEE 47th VTC, 1997

[26] Qinfang Sun and D. C. Cox, "Fundamental limits on symbol rate in frequency selective continuous fading channels," VTC Fall 2001, IEEE VTS 54th, volume 2, page(s) 1205 -1209

[27] S. Sung and D. Brady, "Spectral spatial equalization for OFDM in time-varying frequency-selective multipath channels," IEEE 2000 workshop on Sensor Array and Multichannel Signal Processing, page(s): 434 -438

[28] X. Tang, M. Alouini and A. Goldsmith, "Effect of channel estimation error on M-QAM BER performance in Rayleigh fading," IEEE Trans. on Comm., vol. 47, no. 12, Dec. 1999

[29] J. Van de Beek, M. Sandell and M. Isaksson, "Low-complex frame synchronization in OFDM systems," Fourth IEEE International Conference on Universal Personal Communications, 1995

[30] Richard D.J. van Nee and Ramjee Prasad, *OFDM for wireless multimedia communications.* Boston, MA: Artech House, 1998

[31] S. Weinstein and P. Ebert, "Data transmission by frequency-division multiplexing using the discrete Fourier transform," IEEE Trans. Commun., vol. COMM-19, pp. 628-634, Oct. 1971

[32] B. Yang, K. Letaief and R. Cheng, "Timing recovery for OFDM transmission," JSAC, vol. 18, no. 11, Nov. 2000

[33] W. Zou and Y. Wu, "COFDM: an overview," IEEE Transactions on Broadcasting, 41(1):1-8, Mar. 1995